Jordan Journal of Mechanical and Industrial Engineering (JJMIE)

JJMIE is a high-quality scientific journal devoted to fields of Mechanical and Industrial Engineering. It is published by The Hashemite University in corporation with the Jordanian Scientific Research Support Fund.

SUBMISSION ADDRESS:

Prof. **Mousa S. Mohsen**, Editor-in-Chief
Jordan Journal of Mechanical & Industrial Engineering,
Hashemite University,
PO Box 330127, Zarqa, 13133 , Jordan
E-mail: jjmie@hu.edu.jo

Hashemite Kingdom of Jordan

Hashemite University

Jordan Journal of Mechanical and Industrial Engineering

JJMIE

An International Peer-Reviewed Scientific Journal

http://jjmie.hu.edu.jo/

ISSN 1995-6665

Jordan Journal of Mechanical and Industrial Engineering (JJMIE)

JJMIE is a high-quality scientific journal devoted to fields of Mechanical and Industrial Engineering. It is published by The Jordanian Ministry of Higher Education and Scientific Research in corporation with the Hashemite University.

Introduction: The Editorial Board is very committed to build the Journal as one of the leading international journals in mechanical and industrial engineering sciences in the next few years. With the support of the Ministry of Higher Education and Scientific Research and Jordanian Universities, it is expected that a heavy resource to be channeled into the Journal to establish its international reputation. The Journal's reputation will be enhanced from arrangements with several organizers of international conferences in publishing selected best papers of the conference proceedings.

Aims and Scope: Jordan Journal of Mechanical and Industrial Engineering (JJMIE) is a refereed international journal to be of interest and use to all those concerned with research in various fields of, or closely related to, mechanical and industrial engineering disciplines. Jordan Journal of Mechanical and Industrial Engineering aims to provide a highly readable and valuable addition to the literature which will serve as an indispensable reference tool for years to come. The coverage of the journal includes all new theoretical and experimental findings in the fields of mechanical and industrial engineering or any closely related fields. The journal also encourages the submission of critical review articles covering advances in recent research of such fields as well as technical notes.

Guide for Authors

Manuscript Submission

High-quality submissions to this new journal are welcome now and manuscripts may be either submitted online or mail.

Online: For online submission upload one copy of the full paper including graphics and all figures at the online submission site, accessed via E-mail: jjmie@hu.edu.jo. The manuscript must be written in MS Word Format. All correspondence, including notification of the Editor's decision and requests for revision, takes place by e-mail and via the Author's homepage, removing the need for a hard-copy paper trail.

By Mail: Manuscripts (1 original and 3 copies) accompanied by a covering letter may be sent to the Editor-in-Chief. However, a copy of the original manuscript, including original figures, and the electronic files should be sent to the Editor-in-Chief. Authors should also submit electronic files on disk (one disk for text material and a separate disk for graphics), retaining a backup copy for reference and safety.

Note that contributions may be either submitted online or sent by mail. Please do NOT submit via both routes. This will cause confusion and may lead to delay in article publication. Online submission is preferred.

Submission address and contact:

Prof. **Mousa S. Mohsen**, Editor-in-Chief
Jordan Journal of Mechanical & Industrial Engineering,
Hashemite University,
PO Box 330127, Zarqa, 13115 , Jordan
E-mail: jjmie@hu.edu.jo

Types of contributions: Original research papers

Corresponding author: Clearly indicate who is responsible for correspondence at all stages of refereeing and publication, including post-publication. Ensure that telephone and fax numbers (with country and area code) are provided in addition to the e-mail address and the complete postal address. Full postal addresses must be given for all co-authors.

Original material: Submission of an article implies that the work described has not been published previously (except in the form of an abstract or as part of a published lecture or academic thesis), that it is not under consideration for publication elsewhere, that its publication is approved by all authors and that, if accepted, it will not be published elsewhere in the same form, in English or in any other language, without the written consent of the Publisher. Authors found to be deliberately contravening the submission guidelines on originality and exclusivity shall not be considered for future publication in this journal.

Supplying Final Accepted Text on Disk: If online submission is not possible: Once the paper has been accepted by the editor, an electronic version of the text should be submitted together with the final hardcopy of the manuscript. The electronic version must match the hardcopy exactly. We accept MS Word format only. Always keep a backup copy of the electronic file for reference and safety. Label the disk with your name. Electronic files can be stored on CD.

Notification: Authors will be notified of the acceptance of their paper by the editor. The Publisher will also send a notification of receipt of the paper in production.

Copyright: All authors must sign the Transfer of Copyright agreement before the article can be published. This transfer agreement enables Jordan Journal of Mechanical and Industrial Engineering to protect the copyrighted material for the authors, but does not relinquish the authors' proprietary rights. The copyright transfer covers the exclusive rights to reproduce and distribute the article, including reprints, photographic reproductions, microfilm or any other reproductions of similar nature and translations.

PDF Proofs: One set of page proofs in PDF format will be sent by e-mail to the corresponding author, to be checked for typesetting/editing. The corrections should be returned within 48 hours. No changes in, or additions to, the accepted (and subsequently edited) manuscript will be allowed at this stage. Proofreading is solely the author's responsibility. Any queries should be answered in full. Please correct factual errors only, or errors introduced by typesetting. Please note that once your paper has been proofed we publish the identical paper online as in print.

Author Benefits

Page charge: Publication in this journal is free of charge.
Free off-prints: Three journal issues of which the article appears in along with twenty-five off-prints will be supplied free of charge to the corresponding author. Corresponding authors will be given the choice to buy extra off-prints before printing of the article.

Manuscript Preparation:

General: Editors reserve the right to adjust style to certain standards of uniformity. Original manuscripts are discarded after publication unless the Publisher is asked to return original material after use. If online submission is not possible, an electronic copy of the manuscript on disk should accompany the final accepted hardcopy version. Please use MS Word for the text of your manuscript.

Structure: Follow this order when typing manuscripts: Title, Authors, Affiliations, Abstract, Keywords, Introduction, Main text, Conclusions, Acknowledgements, Appendix, References, Figure Captions, Figures and then Tables. For submission in hardcopy, do not import figures into the text - see Illustrations. For online submission, please supply figures imported into the text AND also separately as original graphics files. Collate acknowledgements in a separate section at the end of the article and do not include them on the title page, as a footnote to the title or otherwise.

Text Layout: Use double spacing and wide (3 cm) margins. Ensure that each new paragraph is clearly indicated. Present tables and figure legends on separate pages at the end of the manuscript. If possible, consult a recent issue of the journal to become familiar with layout and conventions. All footnotes (except for table and corresponding author footnotes) should be identified with superscript Arabic numbers. To conserve space, authors are requested to mark the less important parts of the paper (such as records of experimental results) for printing in smaller type. For long papers (more that 4000 words) sections which could be deleted without destroying either the sense or the continuity of the paper should be indicated as a guide for the editor. Nomenclature should conform to that most frequently used in the scientific field concerned. Number all pages consecutively; use 12 or 10 pt font size and standard fonts. If submitting in hardcopy, print the entire manuscript on one side of the paper only.

Corresponding author: Clearly indicate who is responsible for correspondence at all stages of refereeing and publication, including post-publication. The corresponding author should be identified with an asterisk and footnote. Ensure that telephone and fax numbers (with country and area code) are provided in addition to the e-mail address and the complete postal address. Full postal addresses must be given for all co-authors. Please consult a recent journal paper for style if possible.

Abstract: A self-contained abstract outlining in a single paragraph the aims, scope and conclusions of the paper must be supplied.

Keywords: Immediately after the abstract, provide a maximum of six keywords (avoid, for example, 'and', 'of'). Be sparing with abbreviations: only abbreviations firmly established in the field may be eligible.

Symbols: All Greek letters and unusual symbols should be identified by name in the margin, the first time they are used.

Units: Follow internationally accepted rules and conventions: use the international system of units (SI). If other quantities are mentioned, give their equivalent in SI.

Maths: Number consecutively any equations that have to be displayed separately from the text (if referred to explicitly in the text).

References: All publications cited in the text should be presented in a list of references following the text of the manuscript.

Text: Indicate references by number(s) in square brackets in line with the text. The actual authors can be referred to, but the reference number(s) must always be given.

List: Number the references (numbers in square brackets) in the list in the order in which they appear in the text.

Examples:

Reference to a journal publication:

[1] M.S. Mohsen, B.A. Akash, "Evaluation of domestic solar water heating system in Jordan using analytic hierarchy process". Energy Conversion & Management, Vol. 38, No. 9, 1997, 1815-1822.

Reference to a book:

[2] Strunk Jr W, White EB. The elements of style. 3rd ed. New York: Macmillan; 1979.

Reference to a conference proceeding:

[3] B. Akash, S. Odeh, S. Nijmeh, "Modeling of solar-assisted double-tube evaporator heat pump system under local climate conditions". 5th Jordanian International Mechanical Engineering Conference, Amman, Jordan, 2004.

Reference to a chapter in an edited book:

[4] Mettam GR, Adams LB. How to prepare an electronic version of your article. In: Jones BS, Smith RZ, editors. Introduction to the electronic age, New York: E-Publishing Inc; 1999, p. 281-304

Free Online Color: If, together with your accepted article, you submit usable color and black/white figures then the journal will ensure that these figures will appear in color on the journal website electronic version.

Tables: Tables should be numbered consecutively and given suitable captions and each table should begin on a new page. No vertical rules should be used. Tables should not unnecessarily duplicate results presented elsewhere in the manuscript (for example, in graphs). Footnotes to tables should be typed below the table and should be referred to by superscript lowercase letters.

PAGES	PAPERS
119 – 212	Formation of Machine Cells/ Part Families in Cellular Manufacturing Systems Using an ART-Modified Single Linkage Clustering Approach – A Comparative Study *M. Murugan, V. Selladurai*
213 – 219	Energy Conservation Using a Double-effect Absorption Cycle Driven by Solar Energy and Fossil Fuel *A. Ababneh*
221 – 225	Characteristics of Transient Behavior of Gas Flow in Microchannels *M. Ashhab, A. Muhtaseb*
227 – 234	Computer–Aided Maintenance Planning System for Industrial Companies *A. Mukattas, R. H. Fouad, H. Kitan, and M. Samhouri*
235 – 240	Performance of Pre-heated Cottonseed Oil and Diesel Fuel Blends in a Compression Ignition Engine *M. Martin, D. Prithviraj*
241 – 245	Reasons behind Energy Changes of the Jordanian Industrial Sector *Y. Abdallat, A. Al-Ghandoor, I. Al-Hinti*
247 – 253	Salt Fog Corrosion Behavior of Nanostructured TiAlN and AlCrN Hard Coatings on ASTM-SA213-T-22 Boiler Steel *V. Chawla, D. Puri, S. Prakash, B. Sidhu*
255 – 259	A Two-stage Artifitial Neural Network Model to Predict the Shrinkage of a Polystyrene Matrix Reinforced with Silica Sand and Cement. *I. Jalham*
261 – 265	Performance Analysis and Behaviour Characteristics of CVD (Semi Active) in Quarter Car Model. *K. Kamalakannan, A. ElayaPerumal, S. Mangalaramanan, K. Arunachalam*
267 – 272	Drag Reduction in a Wing Model Using a Bird Feather Like Winglet. *A. Hossain, A. Rahman, J. Hossen, P. Iqba, N. Shaari., G. K Sivaraj*
273 – 280	Design of Photovoltaic Water Pumping System and Compare it with Diesel Powered Pump. *M.Abu-Aligah*
281 – 284	Energy and Exergy Use in the Utility Sector of Jordan during 2007-2010. *A. Al-Ghandoor, J.O. Jaber, I. Al-Hinti*

JJMIE

Volume 5, Number 3, June 2011
ISSN 1995-6665
Pages 199 - 212

Jordan Journal of Mechanical and Industrial Engineering

Formation of Machine Cells/ Part Families in Cellular Manufacturing Systems Using an ART-Modified Single Linkage Clustering Approach – A Comparative Study

M. Murugan*,[a], V. Selladurai [b]

[a]Department of Mechanical Engineering, SNS College of Technology, Coimbatore-641035, Tamilnadu, India
[b]Department of Mechanical Engineering, Coimbatore Institute of Technology, Coimbatore-641014, Tamilnadu, India.

Abstract

This paper proposes an Art Modified Single Linkage Clustering approach (ART-MOD-SLC) to solve cell formation problems in Cellular Manufacturing. In this study, an ART1 network is integrated with Modified Single Linkage Clustering (MOD-SLC) to solve cell formation problems. The Percentage of Exceptional Elements (PE), Machine Utilization (MU), Grouping Efficiency (GE) and Grouping Efficacy (GC) are considered as performance measures. This proposed heuristic ART1 Modified Single Linkage Clustering (ART-MOD-SLC) first constructs a cell formation using an ART1 and then refines the solution using Modified Single Linkage Clustering (MOD-SLC) heuristic. ART1 Modified Single Linkage Clustering has been applied to most popular examples in the literature including a real time manufacturing data. The computational results showed that the proposed heuristic generates the best solutions in most of the examples. The proposed method is compared with the well-known clustering approaches selected from the literature namely ROC2, DCA, SLC and MOD-SLC. Comparison and evaluations are performed using four performance measures. Finally analysis of results is carried out to test and validate the proposed ART-MOD-SLC approach. The MCF methods considered in this comparative and evaluative study belong to the cluster formation approaches and have been coded by using C++ with an Intel P-IV compatible system.

Keywords: Cellular Manufacturing; Group Technology; Cell Formation; Modified Single Linkage Clustering (MOD-SLC); ART-MOD-SLC; Performance Measures

1. Introduction

In the competitive business environment today, many businesses focus attention especially on the rapidity for responding to their customers' needs. For this reason, continuous improvements are needed to increase response times to customer changes. One of the strategies is called Group Technology which focuses on Cellular Manufacturing. Group technology (GT) is a manufacturing philosophy that has attracted a lot of attention because of its positive impacts in the batch-type production. The problems in batch manufacturing are high level of product variety and small manufacturing lot sizes (Singh and Rajamani 1996). In the design of a CM system, similar parts are grouped into families and associated machines into groups so that one or more part families can be processed within a single machine group. The process of determining the part families and machine groups are referred to as the cell formation (CF) problem. Group technology is a tool for organizing and using information about component similarities to improve the production efficiency of manufacturing firm. Successful application of group technology, promises improvement of productivity through the reduction of material handling cost, throughput time etc.

The two major tasks that the company must undertake are (a) Identification of part families: if the plant makes 10,000 different parts, reviewing all the part drawing and grouping the parts into families is a substantial task that consumes a significant amount of time. (b) Rearranging production machines into machine cells: It is time consuming and costly to plan and accomplish this rearrangements and machines are not producing during change over. GT offers a substantial benefit to companies that have the perseverance to implement it. Formation of machine cells is one of first important steps in the development and implementation of GT. New achievement in computer technology and artificial intelligence have provided the opportunity to apply more advanced clustering technique to group technology problem.

The ART1 neural network is a novel method for the cell formation problem in-group technology. ART1 is an unsupervised network where the desired output (desired number of clusters) is not known. Cluster formation is dependent on the vigilance parameter value as well as the number of machines and parts present in an input incidence matrix. Iteration taken by ART1 for cluster

* Corresponding author. e-mail: murugan_srec@yahoo.co.in

formation also depends on size of input of the incidence matrix and group efficiency. After forming a cell or a cluster of machines or parts, Modified Single Linkage Clustering (MOD-SLC) is used to obtain the optimized part family or machine cell according to its maximum use in a cluster.

2. Literature Survay

Detailed survey of literature has been carried out to identify the findings and directions given by the researchers. The contributions and directions of selective research works reported in the literature have been presented below. The literature yields seven array-based clustering heuristics, namely: 1. Bond Energy Analysis (McCormick et al [1]); 2. Rank Order Clustering (King, [2]; King et al. [3]); 3. Modified rank order clustering (Chandrasekharan et al. [4]); 4. Direct clustering analysis (Chan et al. [5]); 5. Occupancy Value Method (Khator et al. [6]); 6. Cluster Identification Method (Kusiak et al. [7]); and 7. Hamiltonian Path Heuristic (Askin et al., [8]). The SLC method (McAuley, [9]; Carrie, [10]; Waghodekar et al., [11]) merges clusters based on the maximum similarity of their members. Chandrasekharan et al. [12] analyzed the performance of the grouping efficiency in evaluating the solution qualities of a set of well-structured and ill-structured problems. The deficiency of the grouping efficiency has been investigated by Kumar et al. [13]. Chu et al. [14] compared three array-based machine-part grouping methods: ROC, DCA and BEA. Murugan and Selladurai (15) compared three array-based cell formation methods on a real time manufacturing data. Miltenburg and Zhang [16] compared nine cell formation methods including similarity measure method, non-hierarchical clustering and rank order methods. Cheng C.H. et al. [17] carried out comparative examination of selected cellular manufacturing clustering algorithms. Dimopoulos et al. [18] used the grouping efficacy performance measure in evaluating and comparing a genetic programming based SLC method to five other procedures. The following neural network models have been used to solve the machine and/or part grouping problems: back propagation network (Kaparthi et al. [19]), self-organizing network (Lee et al. [20]). Adaptive Resonance Theory (ART) (Dagli et al. [21], Kusiak et al. [22]. There are several variations of an ART network, namely, ART1 (Carpenter et al. [23, 24]), ART2 (Carpenter et al. [25]). The ART1 can handle binary input patterns, while others can process both binary and analogue. Kusiak. A, et al. [26] addressed on neural networks to form machine cells to map the concept of machine cell formation onto the network.

Akturk et al. [27] proposed an integrated algorithm that solves the machine/product-grouping problem by simultaneously considering the within-cell layout problem. Charles C. Willow [28] proposed a feed forward multi-layer neural network for machine cell formation in computer integrated manufacturing. Hark Hwang et al. [29] proposed another measure to enhance the performance of the model using p-median model. [30] Baroni et al. proposed on Similarity on binary data. Yong Yin et al. [31] compared the performance of 20 well-known similarity coefficients. Yong Yin et al. [32] developed a comprehensive overview and discussion for similarity coefficients. Prabahakaran et al. [33] addressed on an application of the maximal Spanning Tree approach for machine cell formation. Chang-Chun Tsai et al. [34] proposed a multi-functional MP model. Alhourani Farouq et al. [35] proposed a new ordinal production data similarity coefficient based on the sequence of operations and the batch size of the parts. Logendran et al. [36] proposed a nonlinear programming model, comprised of binary and general integer variables. Mingyuan, et al. [37] proposed an integrated model for production planning in cellular manufacturing (CM) systems. Zahir Albadawi et al. [38] proposed a new mathematical approach for forming manufacturing cells.

Mahdavi et al. [39] proposed a heuristic method based on iterative set partitioning for incremental cell formation where part of the operations can be processed on alternative machines. Mahdavi et al. [40] proposed on minimizing of the Exceptional Elements (EE) and number of voids in cells to achieve the higher performance of cell utilization. Bin Hu et al. [41] developed an integrated method to solve a multi objective cell formation problem that consists of an integer programming model and a heuristic algorithm for generating alternative cell formations. Steudel et al. [42] developed a similarity measure known as the Cell Bond Strength (CBS) which depends on part routing and production requirements. Harhialakis et al [43] proposed a two-stage heuristic algorithm to solve the cell formation problem. Sule [44] developed a procedure to determine the number of machines. Okogba et al [45] developed an algorithm to solve the part-machine cell formation problem. Heragu et al. [46] presented a heuristic method for forming part families and machine groups. Lin et al [47] proposed a two stage integer-programming model for forming part-machine cells.

Hassan M. Selim et al. [48] compared a modified single linkage clustering heuristic (MOD-SLC) against the three well-established machine cell formation methods. Adenso-Díaz, et al. [49] proceeded on part-machine grouping using weighted similarity coefficients. Foulds et al [50] proposed an approach to solve manufacturing cell creation with machine modification costs and the objective is to minimize the sum of the machine modification cost. Peker et al. [51] proceeded on parameter setting of the Fuzzy ART neural network to part-machine cell formation problem. Gajendra K. Adil et al. [52] proposed an enhanced diversity/similarity model to form part families. Venkumar et al. [53] addressed on Fractional cell formation in group technology using modified ART1 neural networks. Venkumar et al. [54] proposed the cell formation and fractional cell formation using Kohonen Self-Organizing Map (KSOM) neural networks.

While conducting the detailed literature survey, it has been found at many cell formation methods have been used to reduce the percentage of exceptional elements (PE) and to increase the grouping efficiency (GE). The results of the literature survey indicated the absence of an analysis on cell formation methods using the real time data to predict the performance. The findings of the literature survey highlighted that there is a wide scope for solving the cell formation problem towards achieving the optimal performance. A suitable new integrated approach is proposed and applied for analysing the performance measures by incorporating the ART1 neural network with modified single clustering algorithm (ART-MOD-SLC).

The remainder of this paper is organized as follows. Section 3 discusses the statement of the problem and Section 4 discusses about the existing clustering algorithms with examples and section 5 introduces a new integrated ART- MOD-SLC approach with numerical examples are presented to compare with other approaches in the literature. Finally, the conclusions are given in Section 6.

3. Problem Definition

Batch manufacturing is a dominant manufacturing activity in the world, generating great deal of industrial output. It accounts for 60 to 80 percent of all manufacturing activities. The major difficulties in batch manufacturing are due to high level of product variety and small manufacturing lot sizes. The product variations present design engineers with the problem of designing many different parts. The impact of these product variations in manufacturing is high investment in equipment, high tooling costs, complex scheduling and loading, lengthy setup time and costs, excessive scrap, and high quality control costs. For this purpose, some innovative methods are needed to reduce product cost and lead time and profitability. It needs a higher level of integration of the design and manufacturing activities in a company. Group technology (GT) provides such a link between design and manufacturing.

4. Methodology

4.1. Rank order clustering 2 (ROC2):

ROC is a well-known clustering technique that attempts to create a block diagonal form by repeatedly reallocating the columns and rows of a machine/part matrix according to binary values. ROC-2 was developed by King and Nakornchai (1982) to overcome the limitations of ROC. This algorithm is a faster and more efficient method compared with ROC. The main feature of ROC-2 is that it can identify block diagonal structure (of a machine part incident matrix) very quickly that makes it practicable to use in an interactive manner even for large matrices. The step-by-step procedure is shown in the Figure 1.

4.1.1. Algorithm:

Step 1: Start from the last column, move the rows with positive entries to the top of the matrix.
Step 2: Repeat step1 for all the columns.
Step 3: Start from the last row, move the columns with positive entries to the left of the matrix.
Step 4: Repeat step 3 for all rows.
Step 5: Compare the matrix with the previous result. If the matrices are different go to step otherwise go to step 6.
Step 6: Print the final machine-component incidence matrix.

Flow Chart.

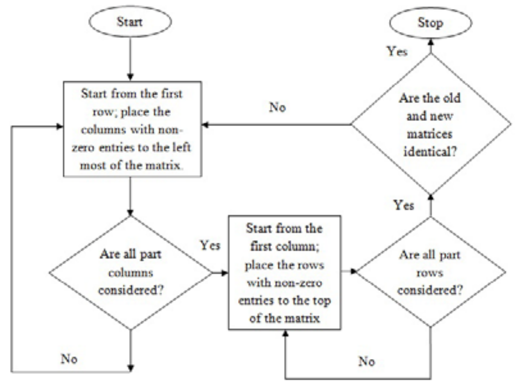

Figure 1: Flow Chart of Rank Order Clustering -2 (ROC-2).

4.1.2. Rank order clustering-2 (ROC-2) example:

Table 1: Initial Machine-Part Matrix of ROC-2.

a. Initial Metrix.

M/C	**Parts**							
	1	**2**	**3**	**4**	**5**	**6**	**7**	**8**
1	1		1					
2	1	1			1	1	1	1
3			1		1		1	1
4				1		1		
5	1		1		1	1		1
6			1			1		
7	1	1			1	1	1	1

b. Row Ordering.

Columns	**Row order**						
8	**1**	**2**	**3**	**4**	**5**	**6**	**7**
7	2	3	5	7	1	4	6
6	2	7	1	4	6	3	5
5	2	7	3	5	1	4	6
4	5	2	7	3	1	4	6
3	1	4	6	5	2	7	3
2	5	3	1	4	6	2	7
1	1	2	7	5	3	4	6
Final	2	5	7	1	3	4	6

c. Column Ordering

Rows	Column order							
6	**1**	**2**	**3**	**4**	**5**	**6**	**7**	**8**
4	4	7	1	2	3	5	6	8
3	4	7	1	2	3	5	6	8
1	3	6	8	4	7	1	2	5
7	4	7	2	3	6	8	1	5
5	7	6	8	1	4	2	3	5
2	6	8	1	3	5	7	4	2
Final	6	8	1	2	3	5	7	4

Table 2: Final Matrix of ROC-2.

M/C	Parts							
	6	**8**	**1**	**7**	**2**	**3**	**5**	**4**
2	1	1	1	1	1			
7	1	1	1	1	1			
5	1	1	1			1	1	
3	1	1				1		
1				1	1			1
4				1				1
6				1				1

4.2. Direct clustering analysis (DCA):

In the DCA algorithm, the initial matrix is rearranged according to the row and column assignments. After the rearrangement the rows and columns are rearranged to form the clustered machine component incidence matrix.

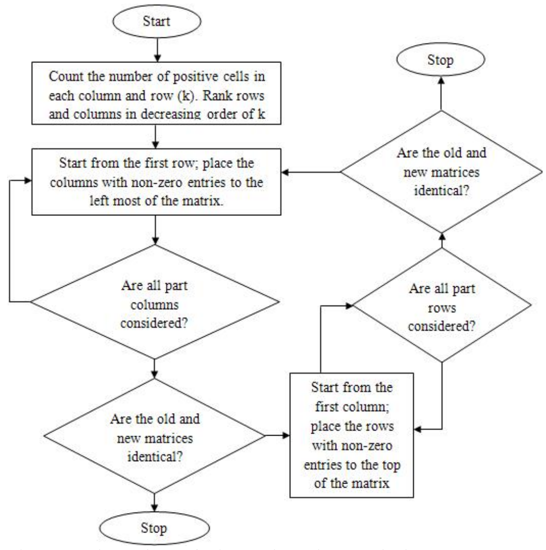

Figure 2: Flow Chart of Direct Clustering Analysis.

4.2.1. Algorithm

Step 0: Input Machine component incidence matrix (MCIM) formed from the operation sequence of each part.
Step 1: The row and column ranks are found by adding their corresponding positive entries.
Step 2: The matrix is rearranged according to the ranks.
Step 3: Start from the first row, move the columns with positive entries to the left of the matrix
Step 4: Repeat the step 3 for all the rows.
Step 5: Start from the first column, move the rows with positive entries to the top.
Step 6: Repeat the step 5 for all the columns.
Step 7: Compare the matrix with the previous result. If the matrices are different go to step 3 otherwise go to step 8.
Step 8: Print the final machine component incidence matrix.

4.2.2. Direct clustering analysis (DCA) example:

M/C	Parts							
	1	**2**	**3**	**4**	**5**	**6**	**7**	
1		1		1			1	3
2			1		1			2
3	1	1		1			1	4
4	1		1			1		3
5			1	1	1	1		4
	2	2	3	3	2	2	2	

Counting the positive cells.

M/C	Parts						
	6	**5**	**4**	**3**	**7**	**2**	**1**
5	1	1	1	1			
3			1		1	1	1
4	1			1			1
1			1		1	1	
2		1		1			

Conducting column interchanges based on First row.

M/C	Parts							
	7	**6**	**5**	**2**	**1**	**4**	**3**	
5		1	1			1	1	4
3	1			1	1	1		4
4		1			1		1	3
1	1			1		1		3
2			1				1	2
	2	2	2	2	2	3	3	

Ranking rows in descending order and columns in ascending order.

Freeze previous changes; continue the column interchanges based on the remaining until no further changes.

M/C	Parts						
	6	**5**	**4**	**3**	**7**	**2**	**1**
5	1	1	1	1			
4			1		1	1	1
3	1			1			1
1			1		1	1	
2		1		1			

Conducting row interchanges based on First column.

4.3. Single linkage clustering:

It is a hierarchical machine grouping method known as Single-Linkage Clustering using similarity coefficients between machines. The similarity coefficient between two machines is defined as the ratio of the number of parts visiting both machines and the number of parts visiting one of the two machines:

$$S_{ij} = \frac{\sum_{k=1}^{N} X_{ijk}}{\sum_{k=1}^{N} (Y_{ik} + Z_{jk} - X_{ijk})} \tag{1}$$

Where

Xijk = operation on part k performed both on machine i and j,
Yik = operation on part k performed on machine i,
Zjk = operation on part k performed on machine j.

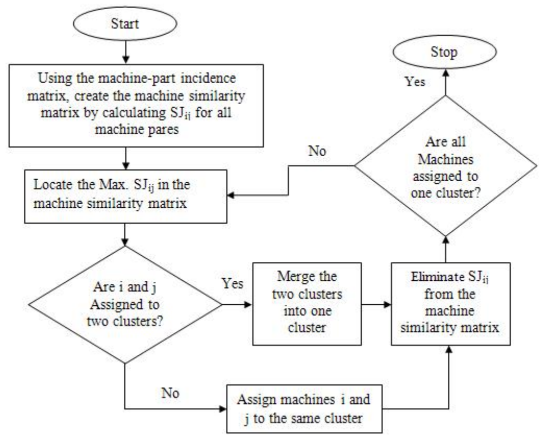

Figure 3: Flow Chart of Single Linkage clustering.

4.3.1. Single linkage clustering (SLC) Example:

Table 3: Initial Matrix of SLC.

M/C	Parts							
	1	**2**	**3**	**4**	**5**	**6**	**7**	**8**
1		1		1				
2	1	1				1	1	1
3			1			1		1
4				1			1	
5	1		1		1	1		1
6				1			1	
7	1	1				1	1	1

Table 4: Similarity Matrix of SLC.

Machine	Machine						
	1	**2**	**3**	**4**	**5**	**6**	**7**
1		0.33		0.67		0.67	0.33
2			0.33	0.17	0.43	0.17	1.00
3					0.60		0.33
4						1.00	0.17
5							0.43
6							0.17
7							

Table 5: Final Matrix of SLC.

M/C	Parts							
	4	**7**	**1**	**2**	**3**	**5**	**6**	**8**
4	1	1						
6	1	1						
1	1	1		1				
2		1	1	1			1	1
7		1	1	1			1	1
3					1		1	1
5			1		1	1	1	1

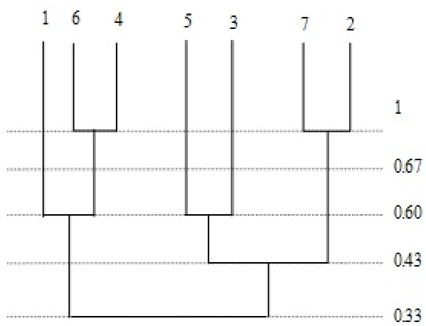

Figure 4: SLC Dendogram.

4.4. Modified single linkage clustering:

Similarity coefficients are either Jaccardian or non-Jaccardian, with respect to the similarity coefficient. The Jaccardian similarity coefficients are expressed as a measure of level of matches, in which the number of matches (Xij) is divided by a normalized quantity usually represented by the expected number of matches. Non-Jaccardian similarity coefficients have an additional term, the number of misses (Yij), appears in the numerator and then divided by the normalizing term. The status of the number of misses (Yij) in similarity coefficients applied to the CM problem is ambiguous. It refers to the number of parts not processed by either machine or the number of machines not needed by either part type. The researchers who adopted Jaccardian similarity coefficients assume that the similarity coefficients measure the degree of commonality between the two machines in terms of parts processed. Therefore, the number of misses does not contribute to the machine pair similarity coefficient. On the other hand, a significant part of the literature shows that Jaccardian similarity coefficients are unable to reflect the true values of similarity, as the Jaccardian measures do not consider the number of misses (Yij).

Baroni-Urban and Buser (1976) defined a set of properties of similarity coefficients and applied these properties to the several similarity coefficients. There does not exist any similarity coefficient which follows all the properties defined by Baroni-Urban and Buser (1976). Islam and Sarker (2000) modified the properties proposed by Baroni- Urban and Buser (1976) and stated them as follows (Sij is the machine i and machine j similarity coefficient):

- No mismatch, Sij→ 1 for Xi = Xj = 0.
- Minimum matches, Sij→ 0 for Xij, Yij→ 0.
- No match, Sij→ 0 for Xij, = 0.
- Complete match, Sij = 1 for Xij = number of parts.
- Maximum matches, Sij→ 1 for Xij + Yij→ number of parts.

The similarity measure developed by Baroni- Urban and Buser (1976) - BUB measure has conformed to the five properties. This similarity coefficient has superior properties of distribution compared to other coefficients because the distribution of its values is more normal and continuous and the BUB similarity coefficient is defined as follows:

$$SB_{ij} = \frac{X_{ij} + \sqrt{X_{ij}Y_{ij}}}{X_i + X_j + X_{ij} + \sqrt{X_{ij}Y_{ij}}} \quad (2)$$

Where SBij = BUB similarity between machine i and machine j, 0 ≤ SBij ≤ 1. In order to justify the application of non- Jaccardian similarity coefficients to the MCF problem, Islam and Sarker (2000) used properties 2 and 5 to conclude that both matches (Xij) and misses (Yij) must be included in the numerator of the defining similarity coefficient. To satisfy properties 2, 3, 4, and 5, the product Xij Yij is considered in addition to Xij in the numerator. The square root is used to maintain the order consistency (Baroni-Urban and Buser, 1976). When there are no misses (Yij = 0), BUB measure is reduced to Jaccard's measure which is the ratio of the number of parts processed by both machines to the total number of parts processed by both or one of the machines.

If (Yij) the BUB coefficient value increases to reflect the real similarity of machine/part pairs. Islam and Sarker (2000) modified BUB measure by adding the number of misses (Yij) to the denominator and called it 'relative matching measure'. The Jaccard measure has conformed to only three out of the same five properties namely, properties 1, 3 and 4.

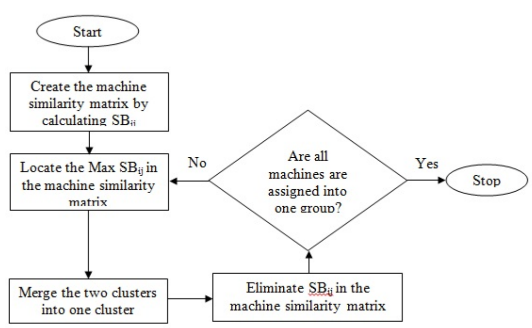

Figure 5: Flow chart of MOD-SLC.

4.4.1. MOD-SLC Example:

Table 6: Initial machine component incidence matrix.

M/C	Parts							
	1	2	3	4	5	6	7	8
1	0	1	0	1	0	0	0	0
2	1	1	0	0	0	1	1	1
3	0	0	1	0	0	1	0	1
4	0	0	0	1	0	0	1	0
5	1	0	1	0	1	1	0	1
6	0	0	0	1	0	0	1	0
7	1	1	0	0	0	1	1	1

Table 7: Similarity Co-efficient Matrix of MOD-SLC.

M/C	1	2	3	4	5	6	7
1	0	0.33	0	0.62	0	0.62	0.33
2			0.5	0.5	0.54	0.5	1
3				0	0.75	0	0.5
4					0	1	0.33
5						0	0.54
6							0.33
7							0

$$SB_{12} = \frac{X_{ij} + \sqrt{X_{ij} Y_{ij}}}{X_i + X_j + X_{ij} + \sqrt{X_{ij} Y_{ij}}} = 0.33$$

Xij = 1 ; Yij = 2; Xi = 1; Xj = 4

Table 8: Final Matrix of MOD-SLC.

M/C	7	4	5	6	3	8	2	1
4	1	1	0	0	0	0	0	0
6	1	1	0	0	0	0	0	0
1	0	1	0	0	0	0	1	0
3	0	0	0	1	1	1	0	0
5	0	0	1	1	1	1	0	1
2	1	0	0	1	0	1	1	1
7	1	0	0	1	0	1	1	1

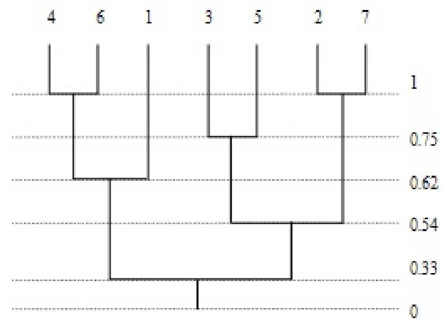

Figure 6: MOD-SLC Dendogram.

5. Proposed ART-MOD-SLC Approach

A cell formation problem can be viewed as a clustering problem that parts with similar machine operation can be grouped into same cluster. There are several neural networks that can be used to solve the clustering problem. In this research work, the application of ART for the machine cell/ part family clustering has been demonstrated. The ART1 network accepts an input vector X = {xi, i = 1, 2,…….N} directly from a binary machine part incidence matrix and assigns it to a cluster whose classified parts match with the input vector. Then, a vigilance test is carried out to determine whether the input vector meets the expectation or not. If input vector passes the test it is accepted as a member of cluster and the set of weights associated with the cluster are changed.

The problem of cluster formation methods uses a different strategy for cluster formation; their relative performance has often been compared in terms of the number of inter-cell moves they generate. The MCF problem cluster analysis-based solution approaches consist of two phases. The first step is to develop an ART network for clustering the raw data (Machine Part Incident Matrix) and the second phase is to apply a solution methodology to solve the MCF problem.

5.1. Architecture of ART-MOD-SLC:

The figure below shows the architecture of ART-MOD-SLC:

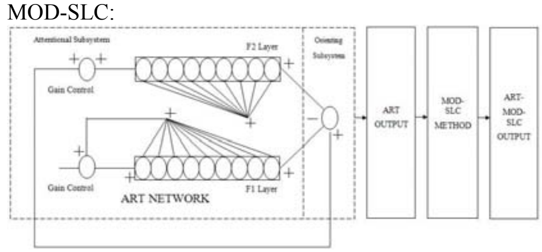

Figure 7: Architecture of ART-MOD-SLC.

5.2. ART-MOD-SLC algorithm:

The ART-MOD-SLC algorithm is explained in detail as below and also shown in the flow chart -Figure 8

Step 0: Define the number of neurons in input layer Nin and the number of neurons in the output layer Nout and select the value of vigilance parameter ρ between 0 and 1.

  - Volume 5, Number 3 (ISSN 1995-6665)

Nin = the number of columns of machine part incidence matrix.
Nout = the maximum expected number of machine cells.

Step 1: Enable all output units and initialize top down weights Wt and bottom up weights Wb.

$$W^t = 1 \tag{3}$$

$$W^b = \frac{1}{(1+N_{in})} \tag{4}$$

Wt = Top down weights from neuron j in output layer to neuron i in input layer.
Wb = Bottom up weight from neuron 'i' in the input layer to neuron 'j' in output layer.
Where, Netj is the output of neuron j in output layer.
Step 2: Present a machine vector X to input layer, X consists of zero/one elements.
Step 3: Compute-matching scores for all the enabled output nodes.

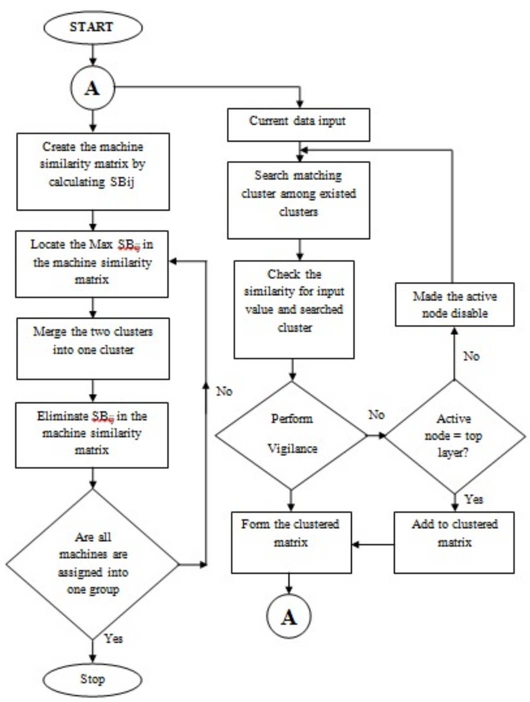

Figure 8: Flow chart of ART – MOD – SLC.

Step 4: Select the node with the largest value of matching scores as best matching exemplar, let this node be j. in the event of tie, the unit on left side is selected.

$$Net = \Sigma Wbji + xi \tag{5}$$

Step 5: Perform vigilance test to verify that input pattern X belongs to cluster (cell).

$$Netj = \max \{Netj\} \tag{6}$$

Step 6: Disable the best matching exemplar. Since the vector x does not belong to cluster j the output of node j selected in step 3 is temporarily disabled and removed from future competitions; Go to step 2.

Step 7: Adapt the best matching exemplar.

$$Wtij = Wtij * xi \tag{7}$$

$$W_{ij}^t = \frac{W_{ij}^t * X_i}{0.5 + \sum W_{ij}^t * X} \tag{8}$$

Step 8: Using the best matching exemplar obtained from the step 7, create the machine similarity matrix by calculating SBij for all machine pair.
Step 9: Locate the Max SBij in machine similarity matrix, are i and j are assigned to two clusters.
Step 10: By eliminating SBij in machine similarity matrix, merge the two clusters into one cluster.
Step 11: Check all the machines are assigned to one cluster then print the final machine component incidence matrix if not go to step 9.

5.2.1. ART-MOD-SLC Examples:

Example 1:

Table 9: Initial Matrix of ART-MOD-SLC (Final Matrix of ART1).

M/C	Parts								
	1	2	3	4	5	6	7	8	class
1	0	1	0	1	0	0	0	0	0
2	1	1	0	0	0	1	1	1	1
3	1	1	0	0	0	1	1	1	1
4	0	0	1	0	0	1	0	1	2
5	0	0	0	1	0	0	1	0	3
6	0	0	0	1	0	0	1	0	3
7	1	0	1	0	1	1	0	1	4

Table 10: Similarity Co-efficient Matrix of ART-MOD-SLC.

M/C	1	2	3	4	5	6	7
1		0.33	0.33	0	0.62	0.62	0
2			1	0.5	0.33	0.33	0.54
3				0.5	0.33	0.33	0.54
4					0.75	0	0.75
5						1	0
6							0
7							

Example Calculation:

$$SB_{12} = \frac{X_{ij} + \sqrt{X_{ij} Y_{ij}}}{X_i + X_j + X_{ij} + \sqrt{X_{ij} Y_{ij}}} = 0.33$$

Xij = 1; Yij = 2; Xi = 1; Xj = 4

Table 11: Final Matrix of ART-MOD-SLC.

M/C	Parts							
	6	**3**	**8**	**5**	**1**	**7**	**4**	**2**
2	1	0	1	0	1	1	0	1
3	1	1	1	0	0	0	0	0
4	0	0	0	0	0	1	1	0
7	1	0	1	1	1	1	0	1
5	1	1	1	0	1	0	0	0
6	0	0	0	0	0	1	1	0
1	0	0	0	0	0	0	1	1

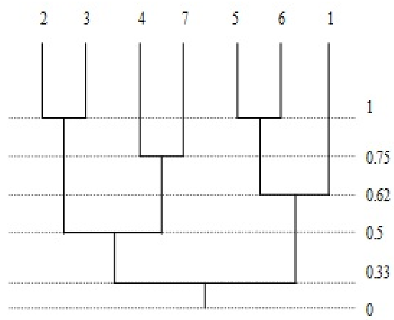

Figure 9: ART-MOD-SLC Dendogram.

Example 2:

Table 12 : Initial machine component incidence matrix

M/C	Parts									
	1	**2**	**3**	**4**	**5**	**6**	**7**	**8**	**9**	**10**
1	1	0	0	1	0	1	0	0	0	0
2	0	0	0	0	0	0	0	0	1	1
3	0	1	0	0	0	0	1	0	1	1
4	0	0	0	0	0	0	0	0	1	1
5	0	0	1	0	0	0	0	0	0	0
6	0	0	1	0	0	0	0	1	0	0
7	0	0	0	0	1	1	0	0	0	0
8	0	1	0	0	0	0	1	0	1	0
9	0	0	0	0	0	0	0	1	0	0
10	1	0	0	0	1	1	0	0	0	0

Table 13: Final Matrix of ART MOD-SLC.

M/C	Parts									
	2	**7**	**9**	**10**	**1**	**5**	**6**	**3**	**8**	**4**
4	1	1	1	1	0	0	0	0	0	0
3	1	0	1	1	0	0	0	0	0	0
9	1	1	1	0	0	0	0	0	0	0
10	0	0	0	0	1	1	1	0	0	0
8	0	0	0	0	0	1	1	0	0	0
1	0	0	0	0	1	0	1	0	0	1
6	0	0	0	0	0	0	0	1	1	0
5	0	0	0	0	0	0	0	1	0	0
7	0	0	0	0	0	0	0	0	1	0
2	0	0	1	1	0	0	0	0	0	0

5.3. Performance measures:

The performance of cluster formation methods can be evaluated either according to computational efficiency or according to clustering effectiveness (Chu and Tsai 1989). Clustering efficiency is normally measured in terms of program execution time, the amount of memory needed, and the complexity of the algorithm. In this research work, four measures have been selected because of their wide usage in the literature.

5.3.1. Number of exceptional elements (PE):

The number of off-diagonal positive entries (exceptional elements) in the final machine part incidence matrix can measure the quality of the cluster formation method. PE can be computed as

$$PE = e_0 \tag{9}$$

Where e_0, is the number of exceptional elements or the off-diagonal positive entries.

5.3.2. Machine utilization (MU):

MU indicates the percentage of times the machines within clusters (cells) are used in production. MU can be computed as (Chandrasekharan and Rajagopalan, 1986a)

$$MU = \frac{e_d}{\sum_{i=1}^{C} m_k n_k} \tag{10}$$

Where ed is the number of positive entries in the diagonal blocks,
mk is the number of machines in the kth cell,
nk is the number of parts in the kth cell, and
C is the number of cells.
The higher the value of MU, the better the machines is being utilized.

5.3.3. Grouping Efficiency (GE):

GE is an aggregate measure that takes both the number of exceptional elements and the machine utilization into consideration. A convex combination of both terms is considered to reveal the relative importance of each term. GE can be defined as

$$GE = \alpha MU + (1-\alpha)\frac{e_0}{M.N - \sum_{k=1}^{c} m_k n_k} \tag{11}$$

Where α is a weight; 0 ≤α ≤1, M is the total number of machines, N is the total number of parts, as a general rule, the higher the grouping efficiency, the better the clustering results.

5.3.4. Grouping Efficacy (GC):

GC overcomes the problems of selecting and the limiting range of GE. GC has the requisite properties like non-negativity, zero to one range and is not affected by the size of the machine-part matrix. GC, defined by Kumar and Chandrasekharan (1990) and Sandbothe (1998) is given as in equation

$$GC = \frac{e - e_0}{e_\gamma} \tag{12}$$

Where eγ is the number of zeros in the diagonal blocks.

5.4. Problem data source:

The 36 data sets have been classified into three groups based on the number of machines (M), three groups based on the number of parts (N), and three groups based on the density level (D). Table 14 shows the value ranges of M, N and D for each group. The selected density range values are based on the selected data sets and specific implementation in the literature. Densities between 0.10 and 0.30 represent the different scenarios adequately.

Table 14: Value Ranges of Machines and Parts.

No.	**Problem Source**	M	N	D
1	Kumar *et al.* (1986)	30	41	0.104
2	Chandrasekharan and Rajagopalan	24	40	0.136
3	Chandrasekharan and Rajagopalan	24	40	0.135
4	Chandrasekharan and Rajagopalan	24	40	0.136
5	Chandrasekharan and Rajagopalan	24	40	0.136
6	Chandrasekharan and Rajagopalan	20	35	0.193
7	Randomly generated	20	35	0.200
8	Randomly generated	20	35	0.204
9	Randomly generated	20	35	0.215
10	Randomly generated	20	35	0.211
11	Harhalakis *et al.* (1990)	20	20	0.197
12	Shafer and Rogers (1993b)	20	20	0.147
13	Randomly generated	20	20	0.210
14	**Murugan and Selladurai (2007)**	**16**	**15**	**0.217**
15	Chan and Milner (1982)	15	10	0.306
16	Chan and Milner (1982)	15	10	0.330
17	Balasubramanian and Panneerselvam	15	10	0.280
18	Randomly generated	15	10	0.193
19	Askin *et al.* (1991)	14	24	0.181
20	McAuley (1972)	12	10	0.316
21	Srinivasan *et al.* (1990)	10	20	0.245
22	Randomly generated	10	20	0.195
23	Askin *et al.* (1991)	10	15	0.326
24	Mukhopadhyay and Golpalakrishnan	10	10	0.240
25	Randomly generated	10	10	0.190
26	Arvindh and Irani (1994)	10	8	0.325
27	Srinivasan and Narendran (1991)	8	20	0.381
28	Kusiak *et al.* (1993)	8	9	0.236
29	Randomly generated	8	9	0.194
30	Mukhopadhyay *et al.* (1994)	7	11	0.270
31	Randomly generated	7	11	0.194
32	Mukhopadhyay *et al.* (1994)	7	9	0.412
33	Kusiak and Cho (1984)	6	8	0.458
34	Seifoddini (1989c)	5	18	0.470
35	Mukhopadhyay *et al.* (1994)	5	18	0.511
36	King and Nakornchai (1982)	5	7	0.400

Table 15 shows the data set groups and factor ranges for the above problem sets and grouped into nine groups with three factors based on the number of machines.

Table 15: Data set groups and factor ranges.

Factor	Group label	Value Range	Data Problems
M	M1	M≤8	3
	M2	8<M≤16	5
	M3	M>16	28
N	N1	N≤10	11
	N2	10<N≤25	18
	N3	N>25	7
D	D1	D≤0.2	15
	D2	0.2<D≤0.3	9
	D3	D>0.3	12

5.5. Comparative studies with other approaches:

The proposed ART-MOD-SLC cluster formation method has been designed and tested against MCF solution methods using the well-known cluster formation approaches on the selected data sets along with the real time manufacturing data. The ART-MOD-SLC is compared with four well-known cluster formation methods selected from the literature, namely ROC2, DCA, SLC and MOD-SLC. The comparison and evaluation are based on four different performance measures selected from the literature, namely Percentage of Exceptional Parts (PE), Machine Utilization (MU), Grouping Efficiency (GE) and Grouping Efficacy (GC).

The four performance measures, PE, MU, GE, and GC are computed for each data set in each group of the nine groups. Table 16 summarizes the computational results of average PE values for each data group. Table 17 summarizes the computational results of MU average values for each data group. Table 18 summarizes the computational results of average GE values and is an aggregate measure that takes both the number of exceptional elements and the machine utilization into consideration. Table 19 summarizes the computational results of average GC values for each data group.

From the results, the proposed ART-MOD-SLC approach has achieved the highest value of PE, MU, GE and GC and yields the best result towards the optimal performance for the entire GT problem and the results are highlighted and also presented graphically in figures 10 to 15.

Table 16: PE values for CF problems.

Group	ROC2	DCA	SLC	MOD-SLC	ART-MOD-SLC
M1	8.8197	7.0179	9.8054	7.6404	6.0652
M2	5.7583	4.9013	2.6786	3.6402	2.3461
M3	15.5804	14.348	6.0133	6.0508	5.9895
N1	6.0653	6.7029	3.3804	4.1899	3.1348
N2	11.0154	6.9867	8.3567	7.2227	6.5823
N3	14.8807	14.4546	5.5058	5.5103	5.2631
D1	8.2717	6.5401	3.6776	3.5758	3.3257
D2	12.1430	12.1979	4.3256	4.9919	4.1263
D3	11.1461	9.2712	10.0365	9.4346	8.9842
OVER	10.2812	9.0150	5.8155	5.6444	**5.0908**

Table 17: MU values for CF problems.

Group	ROC	DCA	SLC	MOD-SLC	ART-MOD-SLC
M1	0.7154	0.6625	0.7310	0.7439	0.7623
M2	0.7545	0.7173	0.6876	0.7281	0.5824
M3	0.4551	0.4514	0.6269	0.5824	0.6589
N1	0.7208	0.6927	0.6591	0.6910	0.7381
N2	0.6895	0.6427	0.7208	0.7390	0.7452
N3	0.4480	0.4384	0.6142	0.5877	0.6245
D1	0.5428	0.5176	0.6124	0.5847	0.6317
D2	0.5635	0.5566	0.6274	0.6537	0.6675
D3	0.8085	0.7536	0.8047	0.8332	0.8456
OVER	0.6321	0.6029	0.6759	0.6748	**0.6952**

Table 18: GE values for CF problems.

Group	ROC2	DCA	SLC	MOD-SLC	ART-MOD-SLC
M1	0.8250	0.8000	0.8387	0.8420	0.8526
M2	0.8642	0.8467	0.8373	0.8554	0.8732
M3	0.7033	0.7022	0.7927	0.7887	0.8127
N1	0.8432	0.8257	0.8212	0.8322	0.8543
N2	0.8160	0.7471	0.8396	0.8482	0.8512
N3	0.7011	0.6952	0.7983	0.7875	0.8010
D1	0.7614	0.7498	0.7904	0.7887	0.7998
D2	0.7580	0.7546	0.8110	0.8180	0.8243
D3	0.8658	0.8405	0.8707	0.8227	0.8957
OVER	0.7933	0.7797	0.8207	0.8265	***0.8405***

Table 19: GC values for CF problems.

Group	ROC2	DCA	SLC	MOD-SLC	ART-MOD-SLC
M1	0.6580	0.5541	0.6517	0.6869	0.6954
M2	0.7210	0.6916	0.6695	0.7036	0.7316
M3	0.4279	0.4250	0.6011	0.5710	0.6571
N1	0.6864	0.6576	0.6606	0.6643	0.6946
N2	0.6361	0.6164	0.6592	0.6910	0.7132
N3	0.4239	0.4135	0.6165	0.5736	0.6256
D1	0.5273	0.5083	0.5958	0.5723	0.6028
D2	0.5357	0.5257	0.6101	0.6332	0.6498
D3	0.7323	0.7010	0.7225	0.7628	0.7721
OVER	0.5941	0.5738	0.6388	0.6489	***0.6825***

5.6. Results and discussion:

The Figures below show the number of exceptional elements (PE).

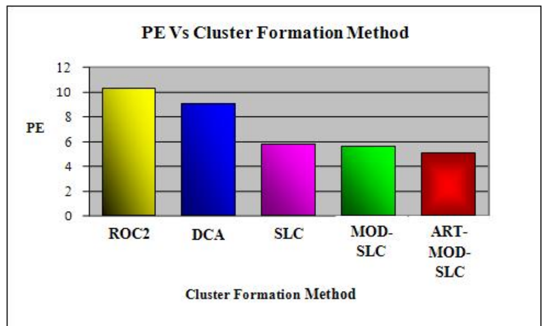

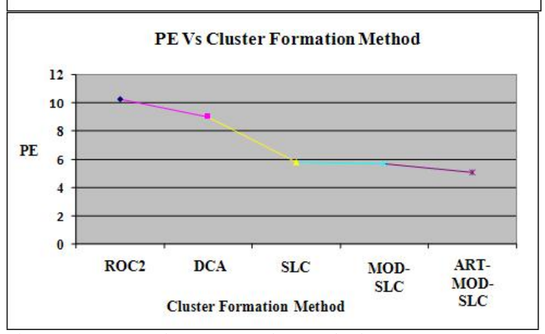

Figure 10: PE Vs Cluster Formation Method.

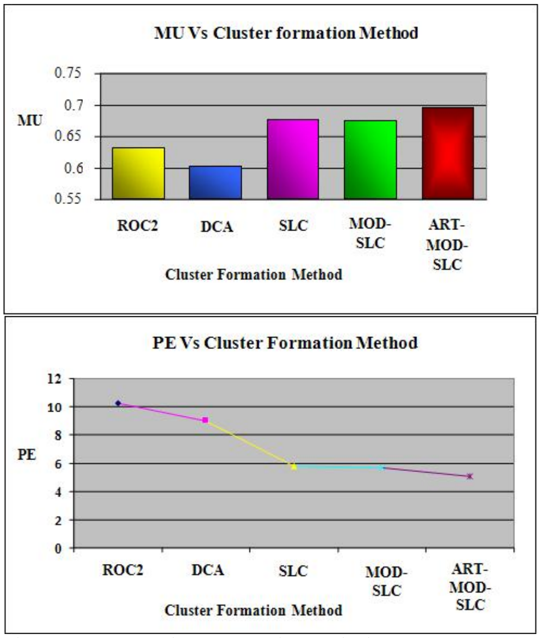

Figure 11: MU Vs Cluster Formation Method.

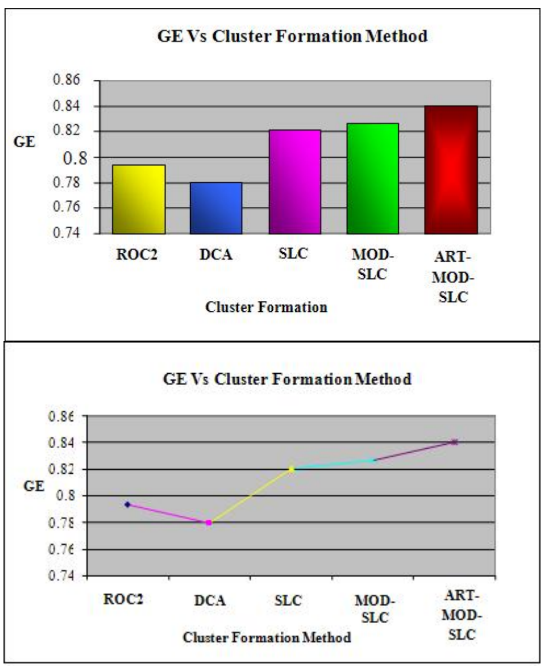

Figure 12: GE Vs Cluster Formation Method.

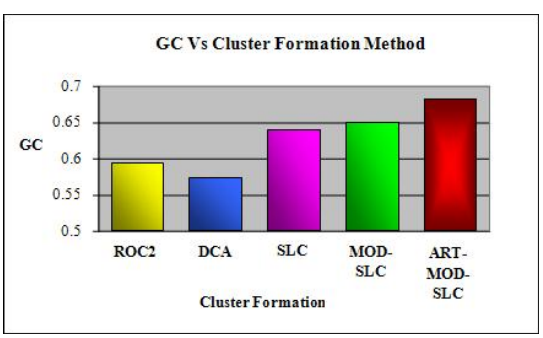

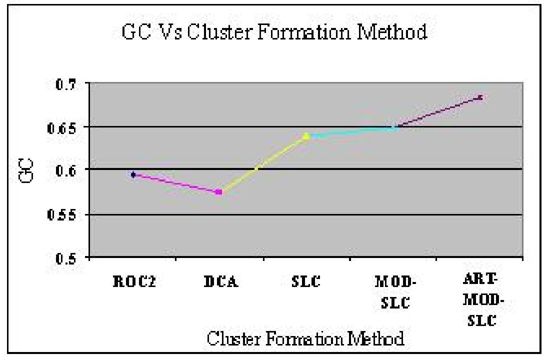

Figure 13: GC Vs Cluster Formation Method.

The following figures show the comparison of cluster formation methods.

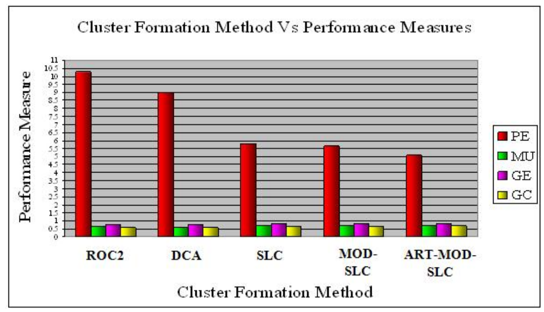

Figure 14: Cluster Formation Method Vs Performance Measures.

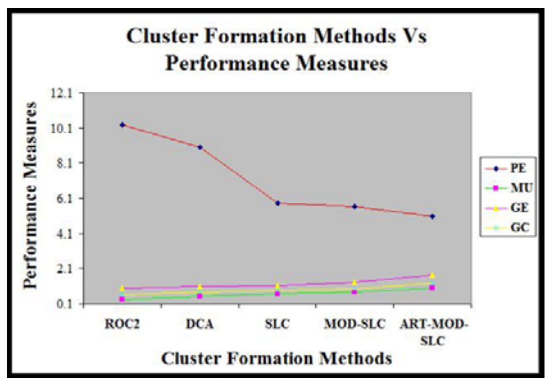

Figure 15: Cluster Formation Method Vs Performance Measures.

6. Conclusion

In this research work, an ART1 neural network has been integrated with MOD-SLC approach and successfully implemented for the cell formation problems collected from the literature, including the real time manufacturing data.

- Application of ART1 to machine-part matrix has been successfully demonstrated to form the clusters of a machine cell and part families. Thereafter machine and parts are arranged by Modified Single Linkage Clustering method (MOD-SLC).
- It is observed that the quality of grouping solution is influenced by the sequence of machines or parts in initial machine part incidence matrix. The numbers of clusters are used to calculate the group efficiency.

- Cluster validation is made after calculation of GE, PE, MU, and GC. Processing time does not increased significantly for large problems or complex conditions. ART-MOD-SLC achieved the higher value of grouping efficiency that yields better clustering results.
- The results are compared with popular existing algorithms and found that the modified ART-MOD-SLC solution is superior to others. The ART-MOD-SLC gives parts and machine clusters and the number of exceptional elements.
- The computational effort is very low in the ART-MOD-SLC compared with all other algorithms and is suitable for large size of machine-part incidence matrix.
- ART-MOD-SLC method has been tested against four MCF solution methods using the cluster formation approaches, namely ROC2, DCA, SLC, and MOD-SLC and also demonstrated an evaluative and comparative analysis using four different performance measures namely percentage of exceptional elements, within cell machine utilization, grouping efficiency, and grouping efficacy.
- The ART- MOD-SLC approach improves the average values of the four performance measures, PE, MU, GE and GC and the results are presented graphically.
- The performance of the four cluster formation methods considered (ROC2, DCA, SLC, and MOD-SLC) are poorer than the proposed ART-MOD-SLC approach.
- From the graphical results, the Percentage of Exceptional Elements (PE) reduced by 10%, Machine Utilization (MU) has been increased by 3%, Grouping Efficiency (GE) has been increased by 2% and Grouping Efficacy (GC) increased by 5% than the earlier approaches considered.

References

[1] McCormick W.T., Schweitzer, P.J. and White, T.W., ‘Problem decomposition and data reorganization by a cluster technique’, Operations Research, Vol. 20, No.5, 1972, pp.993-1009.

[2] King, J.R., ‘Machine-component grouping in production flow analysis: an approach using rank order clustering algorithm’, International Journal of Production Research, Vol. 18 No. 2, 1980, pp. 213-32.

[3] King J.R. and Nakornchai V., ‘Machine-component group formation in group technology: review and extension’, International Journal of Production Research, Vol.20, 1982, pp.117-133.

[4] Chandrasekharan M.P. and Rajagopalan R., ‘An ideal seed non-hierarchical clustering algorithm for cellular manufacturing’, International Journal of Production Research, 24, 2, 1986a, 451-464.

[5] Chan H.M. and Milner D.A.,‘Direct clustering algorithm for group formation in cellular manufacturing’, Journal of Manufacturing Systems, Vol. 1 No. 1, 1982, pp. 65-74.

[6] Khator, S.K. and Irani, S.A., ‘Cell formation in group technology: a new approach’, International Journal of Computers and Industrial Engineering, Vol. 12 No. 2, 1987, pp. 131-42.

[7] Kusiak A., Boe W.J. and Cheng C.H., ‘Designing cellular manufacturing systems: branch and bound and AI approaches’, IIE Transactions, Vol. 25 No. 4, 1993, pp. 46-56.

[8] Askin R.G., Creswell J.B., Goldberg J.B. and Vakharia A.J., ‘A Hamiltonian path approach to reordering the machine-part matrix for cellular manufacturing’, International Journal of Production Research, Vol. 29, No.6, 1991, pp.1081-1100.

[9] McAuley J., ‘Machine grouping for efficient production’, The Production Engineer, Vol. 51, No.2, 1972, pp.53-7.

[10] Carrie, A.S., ‘Numerical taxonomy applied to group technology and plant layout’, International Journal of Production Research, Vol. 11 No. 4, 1973, pp. 399-416.

[11] Waghodekar P.H. and Sahu S., 'Machine component cell formation in group technology. MACE’, International Journal of Production Research, Vol. 22 No. 6, 1984, pp. 937-48.

[12] Chandrasekharan M.P. and Rajagopalan R., ‘GROUPABILITY: an analysis of the properties of binary data matrices for group technology’, International Journal of Production Research, 27, 6, 1989, pp.1035-1052.

[13] Kumar C.S. and Chandrasekharan M.P., ‘Grouping efficacy: a quantitative criterion for goodness of block diagonal forms of binary matrices in group technology’, International Journal of Production Research, Vol.28, No.2, 1990, pp.233-243.

[14] Chu, C.H. and Tsai, M.,‘A comparison of three array-based clustering techniques for manufacturing cell formation’, International Journal of Production Research, Vol. 28 No. 8, 1990, pp. 1417-33.

[15] Murugan M. and Selladurai V., ‘Optimization and implementation of cellular manufacturing system in a pump industry using three cell formation algorithms’. International Journal of Advanced Manufacturing Technology. Vol.35, 2007, pp.135 -149.

[16] Miltenburg J. and Zhang W.J., ‘A comparative evaluation of nine well-known algorithms for solving the cell formation problem in group technology’, Journal of Operations Management, Vol.10, No.1, 1991, pp.44-73.

[17] Cheng, C.H., Kumar, A. and Motwani, J.,‘A comparative examination of selected cellular manufacturing clustering algorithms’, International Journal of Operations & Production Management, Vol. 15 No. 12, 1995, pp. 86-97.

[18] Dimopoulos C. and Mort N., ‘A hierarchical clustering methodology based on genetic programming for the solution of simple cell-formation problems’, International Journal of Production Research, 39, 1,2001, pp. 1-19.

[19] Kaparthi, S., Suresh, N.C. and Cerveny, R.P., ‘An improved neural network leader algorithm for part-machine grouping in group technology’, European Journal of Operational Research, Vol.69, 1993, pp.342-356.

[20] Lee H. and Garcia-Diaz A., ‘Network flow procedures for the analysis of cellular manufacturing systems’, IIE Transactions, Vol.28, No.4, 1996, pp.333-345.

[21] Dagli and Huggahalli, ‘Neural Network Approach to Group technology’.1993,pp.1-55.

[22] Kusiak A. and Chow W.S., ‘Efficient solving of the group technology problem’, Journal of Manufacturing Systems, Vol. 6 No. 2, 1987, pp. 117-24.

[23] Carpenter and Grossberg S, ‘Neural Dynamics of Category learning And Recognition’Vol.42, 1987, pp.238-286.

[24] Carpenter and Grossberg S, ‘The ART of Adaptive Pattern Recognition by a Self Organizing Neural Network’.Vol.21, No.3, 1988, pp.77-88.

[25] Carpenter G.A. and Grossberg S.,‘ART2: self-organisation of stable category recognition codes for analog input patterns’, Appl. Opt., Vol.26, No.23, 1987, pp.4919-4930.

[26] Kusiak A, Chung Y, ‘GT/ART: Using Neural Networks to Form Machine Cells’, Decision support systems, Vol.26, No.23,1991, pp.279-295.

[27] Akturk M.S., and Turkcan A., ‘Cellular manufacturing system design using a holonistic approach’, International Journal of Production Research, Vol.38, No.10, 2000, pp. 2327- 2347.

[28] Charles C. Willow, ‘A feed forward multi-layer neural network for machine cell formation in computer integrated manufacturing’, Vol 13, No.2,2002, pp. 75-87.

[29] Hark Hwang and Yong Hui Oh, 'Another similarity coefficient for the p-median modeling group technology', International Journal of Manufacturing Technology and Management', Vol.5, No. ½, 2003, pp. 38-45.

[30] Baroni-Urban C. and Buser M.W.,'Similarity of binary data', Systematic Zoology, Vol.25, 1976, pp.251-259.

[31] Yin Y. and Yasuda K., 'Similarity coefficient methods applied to the cell formation problem: A comparative investigation', Computers and Industrial Engineering, Vol.48, No. 3, 2005, pp.471-489.

[32] Yin Y. and Yasuda K.,'Similarity coefficient methods applied to the cell formation problem: A taxonomy and review', International Journal of Production Economics, Vol.101, No.2, 2006, pp.329-352.

[33] Prabbahakaran G., Sachithanandam M. and Venkiah N., 'Application of the Maximal Spanning Tree Approach for Machine Cell Formation', The International Journal of Advanced Manufacturing Technology, Vol. 20, No. 7, 2002, pp. 503-514.

[34] Chang-Chun Tsai and Chung-Ying Lee., 'Optimization of manufacturing cell formation with a multi-functional mathematical programming model', The International Journal of Advanced Manufacturing Technology, Vol.30, No. 3-4, 2006, pp. 309-318.

[35] Alhourani Farouq and Seifoddini Hamid., 'Machine cell formation for production management in cellular manufacturing systems', International Journal of Production Research, Vol. 45, No.4, 2007, pp. 913-934.

[36] Logendran R. and Karim Y.,'Design of manufacturing cells in the presence of alternative cell locations and material transporters', Journal of the Operational Research Society, Vol. 54, No.10, 2003, pp.1059-1075.

[37] Mingyuan Chen and Dong Cao., 'Coordinating production planning in cellular manufacturing environment using Tabu search', Computers and Industrial Engineering, Vol.46, No.3, 2004.

[38] Zahir Albadawi, Hamdi A. Bashir and Mingyuan Chen., 'A mathematical approach for the formation of manufacturing cells', Computers and Industrial Engineering, Vol.48, No.1, 2005, pp.3-21.

[39] Mahdavi I., Rezaeian J., Shanker K. and Amiri Z. Raftani, 'A set partitioning based heuristic procedure for incremental cell formation with routing flexibility', International Journal of Production Research. Vol.44, No.24, 15, 2006, pp. 5343-5361.

[40] Mahdavi I., Babak Javadi, Kaveh Fallah-Alipour and Jannes Slomp., 'Designing a new mathematical model for cellular manufacturing system based on cell utilization', Applied Mathematics and Computation, Vol. 190, No. 1, 2007, pp.662-670.

[41] Bin Hu, Mingyuan Chen and Defersha F.M., 'An integrated method for multiobjectives cell formation in cellular manufacturing systems', International Journal of Manufacturing Technology and Management, Vol.11, No. ¾, 2007,355-372.

[42] Steudel H.J. and Ballakur A.,'A dynamic programming based heuristic for machine grouping in manufacturing cell formation', Computers and Industrial Engineering, Vol.12, No.3, 1987, pp.215-222.

[43] Harhalakis G., Nagi R. and Proth J.M., 'An efficient heuristic in manufacturing cell formation for group technology applications', International Journal of Production Research,Vol.28,No.1, 1990, pp.185-198.

[44] Sule D.R., 'Machine capacity planning in group technology', International Journal of Production Research, Vol.29, 1991, pp.1909-1922.

[45] Okogba O.G., Chen, Changchit M.T. and Shell R.L., 'Manufacturing cell formation and evaluation using a new intercell flow reduction heuristic', International Journal of Production Research, Vol.30, 1992 pp.1101-1118.

[46] Heragu S.S. and Gupta Y.P., 'A heuristic for designing cellular manufacturing facilities', International Journal of Production Research, Vol.32, 1994, pp.125-140.

[47] Lin T.L., Dessouky M.M., Kumar K.R. and Ng S.M., 'A heuristic-based procedure for the weighted production-cell formation problem', IIE Transactions, Vol.28, No.7,1996, pp.579-589.

[48] Hassan M.Selim, Reda M.S.Abdel Aal and Araby I.Mahdi,, 'Formation of machine groups and part families: a modified SLC method and comparative study', Integrated Manufacturing systems, Vol.14, No.2, 2003, pp.123-137.

[49] Adenso-Díaz B, Lozano S, Eguía I, 'Part-machine grouping using weighted similarity coefficients', Pergamon Press Inc. Tarrytown, NY, USA, 2005.

[50] Foulds L. R., Foulds L. R., and Wilson J. M., 'The sustainable cell formation problem: manufacturing cell creation with machine modification costs Source', 2006.

[51] Peker Y. Kara, 'Parameter setting of the Fuzzy ART neural network to part-machine cell formation problem', International Journal of Production Research, 2004.

[52] Gajendra K. Adil and Jay B. Ghosh., 'Maximum diversity/similarity models with extension to part grouping'. International Transactions in Operational Research. Vol: 12 No.3, 2005, pp. 3-11.

[53] Venkumar P, Noorul Haq A., 'Fractional cell formation in group technology using modified ART1 neural networks', The International Journal of Advanced Manufacturing Technology, Vol.28,No.7-8,2006, pp.761-765.

[54] Venkumar P. and Noorul Haq A., 'Complete and fractional cell formation using Kohonen self-organizing map networks in a cellular manufacturing system', International Journal of Production Research. Vol. 44, No. 20, 2006, pp. 4257-4271.

JJMIE
Volume 5, Number 3, June 2011
ISSN 1995-6665
Pages 213 - 219
Jordan Journal of Mechanical and Industrial Engineering

Energy Conservation Using a Double-effect Absorption Cycle Driven by Solar Energy and Fossil Fuel

A. Ababneh*

Department of Mechanical Engineering,The Hashemite University, Zarqa, 13115, Jordan

Abstract

Energy conservation is a main theme nowadays in research mainly due to the recent sudden rise and wide fluctuations in energy prices. This uncertainty is viewed as an indication of reaching the depletion point of fossil fuel and consequently, energy conservation has been tackled from all various aspects. Herein, an assessment is made to evaluate the effectiveness of the cooling that result from a double-effect reversed-flow lithium bromide absorption cycle driven by a combination of solar energy and a fuel-fired boiler. The assessment is to show the cycle performance under various proportions of solar contribution to drive the cycle. The analysis was aided with a computer code that was developed specifically to evaluate the instantaneous daily total solar irradiation. The results have indicated impressive effective COP that may be obtained when varying the solar contribution whereby a potential of energy saving at least 45% when only 15% of the roof area is allocated to solar panels. The eventual goals of the study are for potential application in Jordan and in countries with similar environments with the aim to lessen the dependence on fossil fuel.

Keywords: Solar cooling; Energy conservation; Double effect absorption cycle; Use of renewable energy

Abbreviations

C	Sky diffusive factor
COP	Coefficient of Performance
D	Distance from earth to sun
D_o	Mean distance from earth to sun
GJ	Giga Joules
GH	high-temperature generator
GL	Low-temperature generator
H	Hour angle
H-HX	high-temperature heat exchanger
I	Extraterrestrial direct solar beam intensity (W/m^2) at distance D
I_b	Total solar irradiation on a plate tilted at an angle β
I_{bd}	Direct solar beam intensity (W/m^2)
I_o	Extraterrestrial direct solar beam intensity (W/m^2) at mean distance D_o
kW	kilo Watt
l	Latitude angle
L-HX	Low-temperature heat exchanger
SFDeAC	Solar-Fuel driven Double-effect Absorption Cycle

Greek Symbols

α	Altitude angle
β	Tilt angle from horizontal plane of the solar panels
δ	Solar declination angle
ϕ	Azimuth angle
θ	Angle between the direct sun beam and the normal to the panels
θ_z	Zenith angle
ρ	Optical reflectivity of the surrounding
τ	Optical depth attenuation of the solar beam

1. Introduction

Perhaps a reasonable strategy to lessen the degree of dependence on fossil-fuel is not to have a single comprehensive scheme, but rather to consider a multitude of hybrid schemes that seek to optimize the use of energy at the end application. A comprehensive scheme would be as in generating electricity from nuclear power plants since the later is much abundant than fossil fuel in terms of energy content [1].

Furthermore, for Jordan, as the rest of the world, has seen an upward shift in the living standards which lead to an increase demand for energy. In a specific area, a significant increase has been seen in the use of air-conditioning systems that runs on electricity which is normally generated in fossil-fuel power plants. Unfortunately, in addition to being a national burden since for Jordan nearly all natural gas and oil are imported, but it also means that probably more of the fossil fuel will be consumed at faster rates. Therefore, alternative systems that are energy efficient and rely on renewable energies

* Corresponding author. e-mail: ababneh_hu@hu.edu.jo

may serve to lessen the degree of increase in demand for fossil energy.

Fortunately for Jordan, although it lacks significant resources for natural gas and oil, however, it is one of those countries that have considerable solar irradiation. In a simple calculation, as predicted by the computer code developed herein, the average solar irradiation for Jordan on its 91971 square km is 2.62 x 10^{11} GJ for the months June through September, with the assumption that the entire area treated as a flat plate. This amount of energy is equal to about 1190 times more than the annual need of the country from fossil energy whereby the usage for the year 2007 is about 100,000 oil barrels per day [2] with each barrel contains about 6.1 GJ.

In the current study, energy saving is demonstrated through the utilization of solar energy which is coupled with a fuel-fired boiler to drive an efficient absorption cycle to obtain comfort cooling. Absorption cycles have received considerable attention in an attempt to improve their efficiency [3, 4, 5, and 6]. A successful implementation of solar cooling, however, would consequently imply drastic improvement in performance. The advantages of including the fuel-fired boiler is to make the system more dependable and to extend the operational hours as compared to previous work where the system was considered to be solely driven by solar energy [7]. Specifically, with such a combined system it can be tailored to be driven by a source of free energy at different proportions. Other advantages to the system is that absorption cycles may use water vapor as refrigerant, which is in complete harmony with the environment unlike R12, R22, R134a, etc. Also, it is of less harm to the environment since they lead to an eventual decrease of emission in green gases at power plants. Realistically, however, these systems are relatively large and require substantial initial capital cost, therefore, an initial potential application of these systems would be in large facilities like educational institutions and shopping malls where savings in running cost may offset the initial cost in a reasonable payback period.

The working principle of the basic absorption cycle is that a liquid pump replaces a compressor whereby the power requirement for pumping is far less than in the case of vapor compression. The working fluid in the absorption cycle; i.e., water, once it leaves the evaporator it gets absorbed by a liquid; i.e., lithium bromide solution, whereby the solution is pumped to the pressure of the condenser. In the high-pressure state heat is used to vaporize the refrigerant from the solution with the vapor continuing its typical refrigeration cycle while the high-concentration solution is repeated for absorption at the low evaporator pressure. The compatibility of these systems with solar energy is that the required thermal energy for their operation is required at moderate temperature, which may be provided by solar collectors; i.e., evacuated tubes.The absorption cycles are known for their low coefficient of performance (COP), e.g. about 65%. However, with two generators the cycle may be significantly enhanced, where in this configuration it is referred to as double-effect absorption cycle. There are options on how the generators are connected; namely, 1) in series; where the absorber connects to the high-temperature generator followed by the low-temperature, 2) in parallel; where both generators are connected to the absorber, or 3) reversed flow; where the low-temperature generator is connected to the absorber first followed by the high-temperature generator. The reversed flow arrangement is known to be more efficient yielding a theoretical COP of higher than unity. The overall improved efficiency is consistent with the second law of thermodynamics since the heat is supplied at higher temperature in the case of the double-effect.

The current interest in the absorption cycle driven by renewable energy resources has arisen during the recent intent of establishing a scientific incubator at the Hashemite University with one of the primary projects is in the area of solar cooling for desert climates. The main motive for the high interest in this project was the significant anticipated savings in electrical energy that is used for driving standard air-conditioning units for comfort cooling during operational hours.

Interest in the solar driven absorption cycle is not new. Assilzadeh et al. [8] have investigated the performance of a lithium bromide absorption cycle with application in Malaysia using a basic absorption cycle. Ghaddar et al. [9] have conducted modeling and simulation of a solar absorption system for Beirut. Hammad and Zurigat [10] tested a solar driven cooling system and they reported a COP of 0.55. Qu et al. [11] reported a successful installation at Carnegie Mellon University of a double-effect lithium bromide absorption system driven by natural gas heating source and solar energy collected by an array of parabolic trough solar collectors. They have demonstrated that the solar contribution was 39% during cooling and 20% during heating mode. Duff et al. [12] demonstrated in a building in Sacramento, California the use of the double-effect absorption cycle driven by integrated compound parabolic concentrator evacuated solar collectors, with the original gas-fired generator in the absorption system removed. They have obtained a maximum COP of 1.1.

In this article, the effectiveness of hybrid cooling system; i.e., a double-effect reversed-flow absorption cycle driven by solar energy combined with fossil fuel-fired boiler is assessed in terms of viability for application in Jordan; specifically in Az-zarqa city. The thermal energy required for operating the cycle primarily comes from the solar energy which is collected via evacuated tubes and any insufficiency in thermal energy is augmented by a fuel-fired boiler. A computer code was developed to compute solar irradiation. The system performance is measured using the coefficient of performance (COP) which is specifically defined herein as the net system's cooling divided by the net energy supplied by the boiler. Thus, when the system is solely dependent on solar energy its COP tends to infinity indicating no significant operational costs. The performance and energy savings are cast in terms of the percent of roof areas allocated to solar panels, which permit easiness for preliminary design purposes. The advantage of having the boiler, in addition to extending the time range of operation when solar irradiation drops below the design limit, is to make the overall cycle more reliable in supplying sudden rises in cooling demand as well as when solar irradiation drops due to fluctuation in weather conditions. Additionally, it provides design flexibility of limiting the surface area of the evacuated tubes that to be installed.

2. System Description

The double-effect reversed-flow absorption cycle using lithium-bromide solution is depicted in Figure 1. The shaded items are the components that are necessary for the absorption cycle. Also, shown in the figure the schematic arrangement of the hardware that is required for capturing the solar energy augmented by the fuel-fired boiler. Starting at the condenser the liquid refrigerant; i.e., water, is passed through the expansion valve to lower its pressure to that of the evaporator where absorbed heat completely vaporizes the saturated refrigerant (water). The water vapor is then absorbed by the bromide solution due to the strong affinity between the two, hence diluting the solution concentration. The diluted solution is pumped to a higher pressure corresponding to that of the low-temperature generator (GL), however, passing through a low-temperature heat exchanger (L-HX) whereby gaining heat from the returning high concentration solution coming back from the generators. In the double-effect absorption cycle part of the solution leaving the GL generator is directed to the high-temperature generator (GH), however, passing through a high-temperature heat exchanger (H-HX) whereby it gets heated from the returning high-concentration solution returning from the GH generator.

The required heat for the current system is provided via the solar panels, which consist of evacuated tubes, and augmented by a fuel-fired boiler to meet the demand over specified time range. The evacuated tube solar panels are chosen because they have higher efficiency at a moderately elevated temperature as well as they have moderate cost in comparison with other types of solar collectors. The efficiency of solar panels decreases with the difference between the operational temperature and the ambient. In estimating the solar panels efficiency at the desired temperature, an efficiency of 53% was obtained based on a formula that appears in [8]. However, the value that was used in the analysis is more conservative 39% [13].

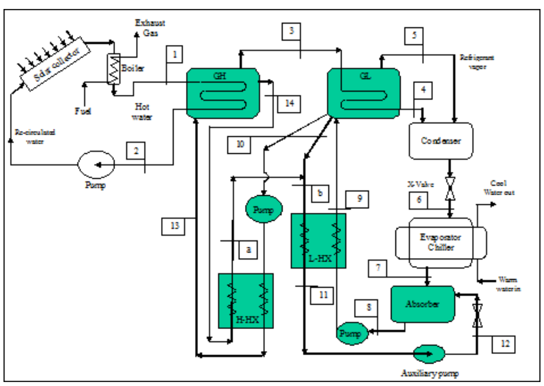

Figure 1: Reversed-flow double-effect lithium-bromide absorption cycle driven by solar energy and fuel-fired boiler.

3. Cycle Performance Assessment

The key parameter in evaluating the overall performance of the cycle is to obtain the Coefficient of Performance (COP), which is a measure of the cooling effects to the amount of the required input power needed to drive the system. The input power is mainly the thermal energy and little of electrical power required to drive the pumps where the later is of insignificant magnitude and hence it was neglected from the analysis.

The state conditions for this cycle are depicted in Table 1, which shows the temperature and the concentration level of the bromide solution along with the water refrigerant conditions at the state points that appear in Figure 1. In arriving at the states shown in the table it was assumed that the L-HX and H-HX have an effectiveness of 75% and 65%, respectively, while the boiler has an efficiency of 85%. Performing standard thermodynamic analysis [14 and 15] with these state conditions leads to 29.2 kW of thermal energy required at the high-generator so that the cycle may deliver 10 tons of cooling. Based on the analysis, the refrigerant (water) released from the GL and GH generators were found to be 0.00573 kg/s and 0.00927 kg/s, respectively, while the corresponding mass flow rates of the solutions leaving the two generators were 0.204 kg/s and 0.0962 kg/s, respectively. Therefore, the resulting COP of the cycle becomes 1.21. In other words, for every 1 kW of cooling the absorption cycle requires 0.83 kW of thermal energy. In the current configuration the solar collectors are intended to supply their maximum collected thermal energy while any deficient thermal energy required for meeting the load demand is offset by the fuel-fired boiler.

Table 1: Thermodynamic state conditions of the lithium-bromide absorption cycle.

State point	Temperature °C	Pressure kPa, absolute	Concentration %	Enthalpy kJ/kg
3	152	52	*Ref. sup vapor	2782.4
4	88	6.682	Ref. sat liquid	368.5
5	82	6.682	Ref. vapor	2653.2
6	38	6.682	Ref. sat liquid	159.2
7	Saturated	0.91	Ref. sat vapor	2511.2
8	40	0.8	58.5	108.2
9	66	6.682	58.5	160.0
10	82	6.682	60.2	200.0
11	49	6.682	63	151.2
12	49	6.682	63	151.2
13	127	52	60.2	285.6
14	152	52	66	348.9

*Note: Ref., sup and sat are abbreviations for refrigerant, superheated and saturated, respectively.

The thermodynamic cycle is depicted in Figure 2 showing the state points for the solution on the equilibrium chart of the aqueous lithium-bromide solution.

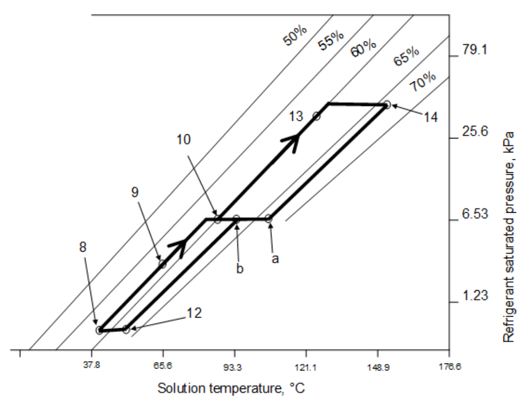

Figure 2: The cycle of the lithium bromide solution shown on the equilibrium chart.

4. Solar Irradiation

The incident solar radiation on a unit area with an arbitrary orientation was determined utilizing a developed computer code using Microsoft Excel-Visual Basic utility. The basic equations [16] that are used in the computer code to calculate the solar intensity begins with the extraterrestrial at the mean earth-sun distance D_o called the solar constant I_o which was established through measurements and found to be 1377 W/m^2. The extraterrestrial solar radiation at the actual distance D from the sun is given as an implied function of time through the following,

$$I = I_o\left(D/D_o\right)^2 \quad (1)$$

Because of the regular motion of the earth around the sun the distance ratio D/D_o can be expressed as a function of the day number N with January 1 is 1. The solar declination angle δ is given as

$$\delta = 23.45^o \sin\left[360\left(284+N\right)/365\right] \quad (2)$$

The altitude angle α and azimuth angle ϕ can be found from the following equations,

$$\sin(\alpha) = \cos(l)\cos(\delta)\cos(H) + \sin(l)\sin(\delta) \quad (3)$$

and

$$\sin(\phi) = \cos(\delta)\sin(H)/\cos(\alpha) \quad (4)$$

where l is the latitude angle and H is the hour angle which is found by dividing the number of minutes from solar noon by 4.

The direct solar beam I_{bd} that reaches the earth surface is computed as

$$I_{bd} = I\exp\left[(-\tau\sec(\theta_z)\right] \quad (5)$$

where τ is the optical depth attenuation of the solar beam as it passes through the atmosphere and θ_z is the zenith angle; i.e., between the solar beam and the vertical.

Through the declination angle, the local solar time which is correlated with the local standard time along with the altitude and the azimuth angles, the incident angle θ between the sun beam and the normal to the panels is determined through the following equation,

$$\cos(\theta) = \cos(\alpha)\cos(\gamma)\sin(\beta) + \sin(\alpha)\cos(\beta) \quad (6)$$

where β is the tilt angle of the panels and γ is the angle between the projections on a horizontal plane of the sun beam and the normal to the panels.

The total solar radiation I_b incident on a tilted plate at β can now be determined using the following equation,

$$I_b = I_{bd}\cos(\theta) + I_{diffuse} + I_{reflected} \quad (7)$$

where

$$I_{diffuse} = CI_{db}\left(1+\cos(\beta)\right)/2 \quad (8)$$

and

$$I_{reflected} = \rho I_{db}(C+\sin(\alpha))\left(1-\cos(\beta)\right)/2 \quad (9)$$

where ρ is the reflectivity of the surrounding and C is a sky diffuse factor.

5. Model Validation

The versatility of the computer code makes it a resourceful tool for predicting solar irradiation on any plate with arbitrary orientation located, not only in Jordan, but in any part of the world at different times throughout the year. However, prior to proceeding with the various design options for supplying the adequate thermal energy to drive the absorption cycle it was prudent to validate the output of the computer code. The output of the code was verified against published data in ASHREA [17] for the extraterrestrial solar radiation intensity throughout the year and against the direct normal at north latitudes 24°, 32°, and 40°. The results of the comparison are depicted in Tables 2 and 3. For the extraterrestrial solar radiation, the code is seen to predict the value with a maximum error of 0.9%. In the case of the direct normal the maximum error was 5.5% occurring at latitude 40° in the early hour of the day. Therefore, the code is considered to yield satisfactory prediction for the solar data.

Table 2: Comparison of extraterrestrial solar intensity from code versus published data

Month	I_o[1] (W/m^2)	I_o[2] (W/m^2)	Error Percent
January	1415.8	1424.3	0.6
February	1401.3	1412.2	0.8
March	1380.8	1392.7	0.9
April	1356.2	1367.7	0.8
May	1336.3	1346.6	0.8
June	1325.6	1333.4	0.6
July	1325.9	1331.7	0.4
August	1337.9	1341.6	0.3
September	1358.7	1361.3	0.4
October	1379.6	1385.2	0.4
November	1404.8	1408.2	0.2
December	1416.8	1422.5	0.4

[1]: Data taken from ASHREA. [2]: predicted values from the computer code

Table 3: Comparison of incident direct beam obtained from code versus published data for the month of July at different latitudes.

Solar time	24°, [1]	24°, [2]	%Error	32°, [1]	32°, [2]	%Error	40°, [1]	40°, [2]	%Error
700	615	647	5.1	640	674	5.2	656	692	5.5
800	754	790	4.7	760	797	4.8	760	798	5
900	823	859	4.3	823	860	4.4	817	856	4.7
1000	858	896	4.4	855	894	4.6	849	888	4.7
1100	877	915	4.3	874	912	4.3	868	905	4.3
1200	883	920	4.2	880	917	4.2	871	910	4.5

[1]: Data taken from ASHREA. [2]: predicted values from the computer code

6. Results

To assess the effectiveness of the Solar-Fuel driven Double effect Absorption Cycle (SFDeAC) in terms of energy conservation, the analysis started by finding the solar panel configuration that yields optimal output. The amount of solar irradiation incident on a plate is dependent on the tilt angle. To determine the optimal tilt angle for Az-Zarqa/Jordan the total solar irradiation on one square meter was computed for various orientations. This was carried out using the computer code for latitude and longitude equal to 32.08° and 36.1°, respectively, which correspond to the location of Az-Zarqa city. The calculations were conducted for the fifteenth day for the months June, July, August and September. The results are presented in Table 4 which shows the total solar irradiation summed up between the hours 8:00 am to 4:00 pm solar time for a plate oriented south and at tilt angles ranging from 40° from the horizontal plane down to 0° degrees decremented by 5 degrees. The results indicate that the maximum solar energy received varies with the tilt angle and at the same time the optimal tilt angle varies with the month whereby it is seen that it ranges from 5° to 30° for the months shown. For the current study the solar collectors tilt angle is set at 20° as an approximate optimal value for the entire hot weather season.

Table 4: Daily total incident solar radiation (kW-hr) on a tilted surface facing south*

Tilt angle deg (β)	June	July	August	September
40	5.91	5.94	6.19	6.47
35	6.21	6.23	6.40	6.56
30	6.47	6.48	6.58	6.60
25	6.69	6.68	6.70	6.60
20	6.86	6.83	6.78	6.55
15	6.98	6.94	6.80	6.45
10	7.05	6.99	6.78	6.30
5	7.07	7.00	6.71	6.11
0	7.04	6.96	6.60	5.87

* The total is for the hours between 8:00 am to 4:00 pm.

For evaluation of any solar cooling systems, the instantaneous solar irradiation for the particular site must be known. In the present work the total solar radiation rate incident on a plate tilted 20° from the horizon was computed utilizing the computer code and the results are depicted in Figure 3. Since solar irradiation varies from day to day the results seen in Figure 3 are for the 15th day which was considered to be typical for the entire indicated months. The figure reveals that the instantaneous total solar irradiation is vividly lower for the month of September than the months June, July and August; a difference of ~100 to ~150 Watts. For this reason the following assessment will exclude the month of September since mainly cooling load drops with lower solar irradiation and normally design parameters are set for maximum conditions. Furthermore, maintaining a 20° tilt angle when excluding September will result in conservative estimates of the solar panels areas, as will be seen later.

The success of solar cooling systems relies on the determination of the minimum surface area of solar panels to meet the cooling demand. However, as mentioned previously rather than depending solely on solar energy the fuel-fired boiler supplies the deficient heat to drive the cycle. The assessment then is to determine the amount of energy contributions from both solar and boiler for different percentages of the roof area that are occupied by solar panels and their effects on the end performance of the system as a whole. Clearly, with higher percent of the roof area given to solar panels will definitely imply less need for the boiler, however, the capital and maintenance costs will rise as well. To carry out the rest of the analysis, the cooling load demand was assumed that it may be approximated as 110 W per each square meter of the roof area; this load is typical for relatively populated buildings.

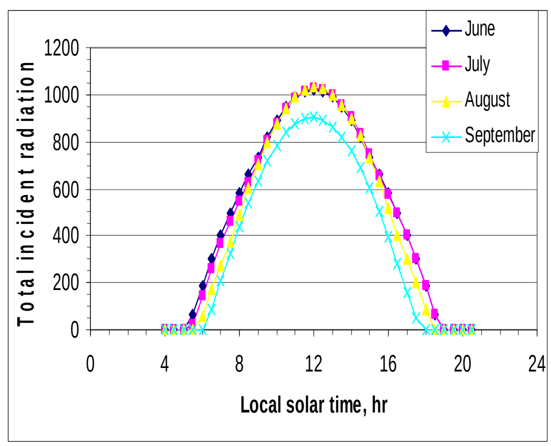

Figure 3: Total solar flux (W) computed on the 15th day for the indicated months.

To evaluate the conserved energy using the SFDeAC system the COP was computed over the entire day for different percent roof areas which to be occupied by solar panels. The COP was defined as the supplied cooling load, which was kept fixed for the entire day and as determined by the roof area size, relative to the net energy inputted by the boiler where the later was assumed to have 85% efficiency. To distinguish this method of computing the COP, it will be referred to herein as the effective COP. Thus, when the system is using all the heat from the solar radiation, the COP will tend to infinity; e.g., with the assumption that power for pumps, electronics, etc is negligible. Figure 4 shows the effective COP over the entire day for different percents of the roof area that are given to solar panels. Clearly it is revealed that for the

  - Volume 5, Number 3 (ISSN 1995-6665)

cases of 15% and 20% the boiler would be turned on for the entire day, however, with the later case the COP is seen to reach up to 9 at solar noon indicating less energy received from the boiler. For larger percentages of the roof area allocated to solar panels; i.e., 25%, 30% and 40%, there are time periods that the thermal energy given to the cycle is entirely supplied by the solar panels thus yielding an infinite effective COP; i.e., the boiler is turned off.

For the purpose of comparison and further analysis the daily COP which was computed as the energy in the form of supplied cooling over a specific time period divided by the amount of energy supplied by the boiler for the same period. The results are given in Table 5 whereby the daily COP is seen to increase either by increasing the solar panel areas (percent of roof area) or by shortening the time period where the later is due to the fact that solar irradiation is higher (Figure 3). Observe that impressive COPs are obtained for percentages of 25% and higher and approaching infinity for 40% during the period 9 am to 3 pm which, for the later case, is an indication that the boiler is remaining basically turned off for the entire period.

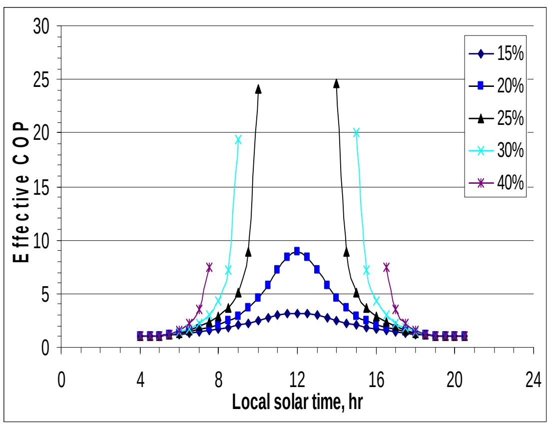

Figure 4: Instantaneous effective COP with varying roofing-area percent allocated to solar panels.

Table 5: System daily COP variation with different daily time periods

	Percent of roofing area used for solar panels				
Time period	15%	20%	25%	30%	40%
7 am to 5 pm	2.16	3.25	5.76	9.41	28.06
8 am to 4 pm	2.39	4.04	9.68	23.36	525.03
9 am to 3 pm	2.66	5.22	23.70	227.51	∞

The results presented in Table 5 was taken further to assess the energy savings when compared with a typical electrical-base air-conditioning unit that runs at a COP of 3.5 with the electrical power received from typical fossil-fuel power plant that has a conversion efficiency of 35% [18]. This means that each one kW of electricity generated 2.86 kW of fossil fuel power is consumed which in turn can be utilized to obtain 3.5 kW of cooling, or equivalently for every 1 kW of cooling 0.82 kW of fossil fuel power is consumed. This information was used as a basis for computing energy saving when using the SFDeAC. Table 6 depicts the percent of energy saving that may result when using the SFDeAC absorption system. The table vividly reveals significant amount of savings on fossil fuel can be obtained even when only 15% of the roof area is allocated to solar panels; assuming that power plants are mainly driven by fossil fuel as the case in Jordan. The apparent savings in energy is that the system's requirement for thermal energy is partially supplied by solar energy, which is a free source of energy.

However, for any scheme that is proposed for energy conservation for it to be adopted it must bring with it financial saving to the end consumer. Considering the current cost of energy in Jordan whereby for electricity it is 0.067 JD per kW-hr; e.g., depending on the usage amount, and for diesel 0.45 JD/L, then for each one kW-hr of cooling the running cost of an electrical-base system that has COP equal to 3.5 is 0.0191 JD while for the SFDeAC with 20% roof area the cost are 0.0127 JD and 0.0103 JD during the daily periods 7 am to 5 pm and 8 am to 4 pm, respectively. Included in these estimates the assumptions that the calorific value and specific gravity for fossil fuel are 46000 kJ/kg and 0.85, respectively. Thus the corresponding percent of savings on running cost is 33.5% and 46.1%, respectively. These impressive savings are a result of using a renewable source of energy; i.e., solar energy. For the 15% roof area during the period 7 am to 5 pm, the running cost is 0.0192 JD which is slightly above than the running cost associated with the electrical-base system. Financial savings on running cost of less than 20% perhaps would not be as attractive simply because of longer payback periods that are associated with relatively high initial capital cost. Nonetheless, given up 20% of the roof area to solar panels may be a plausible solution in many cases; e.g., in public and commercial buildings. Furthermore, the cooling load was based on relatively high cooling demand; however, for smaller buildings and individual homes the cooling load may be less than 80 W/m^2 which means less percent of the roofing area may be allocated to solar panels and still exceed the saving indicated for the case 20% of the roof given up to solar panels.

Table 6: Percent of energy saving using the solar-fossil fuel driven absorption cycle

	Percent of roofing area used for solar panels				
Time period	15%	20%	25%	30%	40%
7 am to 5 pm	45	63	80	87	95
8 am to 4 pm	49	70	88	95	100
9 am to 3 pm	54	77	95	99	100

Potentially therefore these results indicate that this kind of hybrid cooling system driven by solar energy and coupled with fuel-fired boiler for running the absorption system has feasible application in Jordan and in areas that have similar solar irradiation intensity. For example, in the Hashemite University campus, the summer working hours start from 8:00 am to 3:00 pm which coincides with the daily period of higher effective COP. Additionally, most of the buildings have vast roofing areas that can easily afford 25% to solar panels. Similar situations may be found in companies with office buildings that are typically occupied during the day time. Also, the scheme may be implemented to shopping malls during the daylight where appropriate. In multistory buildings, solar panels are now being placed on side walls to offset the limited roof area. Evidently, such a scheme collectively along with other efficient schemes, significant headways may be achieved in energy conservation.

7. Conclusion

A reversed-flow double effect lithium-bromide absorption cycle driven by solar energy and a fuel-fired boiler was considered for the potential of comfort cooling application in local areas with the intent of conserving energy and lowering running cost. A computer code, using Microsoft Visual Basic utility, was developed to compute the solar irradiation in any part of the world and in particular for the Az-Zarqa city/Jordan to aid in evaluating the contribution of the solar energy to the operation of the absorption cycle. The code was verified against published data and found to agree reasonably well yielding an error of ~5% for the incident irradiation as demonstrated. For optimal efficiency the solar panels are positioned such that they are facing south and tilted at an angle of 20 degrees from the horizontal plane. The overall system performance was evaluated based on the effective COP which excludes the contribution of the solar energy. The solar energy contribution was measured in terms of the percent of the roof area that is allocated to solar panels. Results were obtained for various contributions of the solar energy and with the rest of the system's thermal requirement being supplied by the boiler. Energy savings were seen up to 45% on fossil fuel with as low as 15% of the roof area given up to solar panels. However, a 20% of the roof area allocated to solar panels would be necessary for obtaining savings on running cost. The data presented can also be used as guidance for preliminary design for determining the solar contribution based on the percent of the roof area that is to be allocated to solar panels. It was concluded that the SFDeAC is a feasible system for application in Jordan with the intent of saving fossil fuel energy and lowering running cost.

References

[1] El-Wakil, M.M. Powerplant Technology. McGrow-Hill; 1984.

[2] Jordan ministry of energy and minerals, "Energy statistics", www.memr.gov.jo

[3] J.A. Nanrique, "Thermal performance of ammonia-water refrigeration systems". International Communications in Heat and Mass Transfer, Vol. 19, No. 6, 1991, 779-789.

[4] G.D. Mathur, "Solar-operated absorption coolers". Heating/Piping/Air Conditioning, Vol. 61, No. 11, 1989, 103-108.

[5] A.M. Siddiqui, "Optimum generator temperatures in four absorption cycles using different sources of energy". Energy Conversion and Management, Vol. 34, No. 4, 1993, 251-266.

[6] M. Thorbbloom, B. Nimmo, "Modification of the absorption cycle for low generator firing temperatures". In Proceedings of the Joint Solar Energy Engineering Conference ASME, New York, USA, 1994.

[7] A.K. Ababneh, "Energy saving in cooling systems using solar-driven absorption cycles". ICEGES Conference, Amman, Jordan, 2009.

[8] F. Assilzadeh, S.A. Kalogirou, Y. Ali, K. Sopian, "Simulation and optimization of a LiBr solar absorption cooling system with evacuated tube collectors". Renewable Energy, Vol. 30, No. 8, 2005, 1143-1159.

[9] N.K. Ghaddar, M. Shihab, F. Bdeir, "Modeling and simulation of solar absorption system performance in Beirut". Renewable Energy, Vol. 10, No. 4, 1997, 539-558.

[10] M. Hammad, Y. Zurigat, "Performance of a second generation solar cooling unit". Solar Energy, Vol. 62, No. 2, 1998, 79-84.

[11] M. Qu, H. Yin, D.H. Archer, "A solar thermal cooling and heating system for a building: Experimental and model based performance analysis and design". Solar Energy Vol. 84, 2009, 166-182.

[12] W.S. Duff, R. Winston, J.O. Gallagher, "Performance of the Sacramento demonstration ICPC collector and double effect chiller". Solar Energy Vol 76, August 2003, 175-180.

[13] A.Badran, "Electrical and thermal applications for solar energy". Jordan Contractors Association symposium, Amman, Jordan, 2008.

[14] Cengel, Y.A. and Turner, R.H. Fundamentals of Thermal-Fluid Sciences. 2nd ed, Mc-Graw Hill; 2005.

[15] Howell, J.R. and Buckius, R.O. Fundamentals of Engineering Thermodynamics, Mc-Graw Hill; 1987.

[16] Goswami, D. Y., Kreith, F. Energy Conversion. Taylor and Francis Group; 2007.

[17] Fundamentals, ASHRAE (American Society of Heating, Refrigeration and Air-Conditioning Engineers). Atlanta, GA, 1993.

[18] Eastop, T.D. and Croft, D.R. Energy Efficiency for Engineers and Technologists. UK: Longman Group; 1995.

JJMIE

Volume 5, Number 3, June 2011
ISSN 1995-6665
Pages 221 - 225

Jordan Journal of Mechanical and Industrial Engineering

Characteristics of Transient Behavior of Gas Flow in Microchannels

M. Ashhab*,[a] A. Muhtaseb[b]

[a]Department of Mechanical Engineering, The Hashemite University, Zarqa, 13115, Jordan

[b]Mechanical Engineering Department, University of Jordan, Amman, 11942, Jordan

Abstract

In this paper, a three-dimensional numerical model of transient incompressible gaseous flow in microchannels was established. The influence of changing the inlet velocity on the transient fluid flow is analyzed – using finite volume software (Fluent 6.3). The study showed that the transient period is decreased when the inlet velocity is increased, the maximum velocity is almost twice the entrance velocity, and the pressure has a small variation in the entrance of the channel and after that it becomes constant. It was concluded that despite of the fact that the transient behavior in micro systems is usually neglected due to its quick response, the transient terms of the Navier Stokes equations should be taken into consideration when dealing with flow behaviors that may occur in micro or nano seconds.

Keywords: Microchannels; Gas Flow; Navier Stokes; Transient Response

Nomenclature

Dh	hydraulic diameter (lm)
h	channel height (lm)
T	temperature (K)
t	Time (Second)
a	tangential momentum accommodation coefficient
l	dynamic viscosity (N/m2 s)
Re	Reynolds number
c	specific heat ratio (J/(kg K))
Kn	Knudsen number
leff	modified dynamic viscosity (N/m2 s)
c	specific heat ratio
P	pressure (Pa)
f	Dancy friction factor
u v w	x y z-axes velocity (m/s)
U	averaged velocity (m/s)
q	density (kg/m3)
Uc	centerline velocity (m/s)
Us	slip velocity (m/s)
Uw	wall velocity (m/s)
k	mean free path (lm)

Subscripts

w	wall
in	inlet
out	outlet

1. Introduction

Microchannels are considered the very elementary structure of all micro and/or nano systems that include the process of fluid flow. Several researchers studied the microchannels and found out that the both flow and heat characteristics differ from that in the classical systems; these different characteristics are detailed in the paper of Mohamed GH in 1999 [1].

Rarefaction, viscosity heating, surface roughness and compressibility significantly affect the flow and heat characteristics in the gaseous flow; either of these issues are considered separately or simultaneously [2]. In reference to Knudsen number Kn, Beskok and Karniadakis [3] classified the gas flow in microchannels into four flow regimes: continuum flow regime ($Kn < 0.001$) at which the compressibility plays a key role, slip flow regime ($0.001 < Kn < 0.1$), transition flow regime ($0.1 < Kn < 10$) and free molecular flow regime ($Kn > 10$).

The effect of microchannels in continuum region was studied by Asako et al [4,5] without handling the effect of rarefaction where it is found that both friction factor and Reynolds number in quasi-fully developed region are functions of Mach number; and they set these correlations there. Numerical analysis of fully developed laminar slip flow and heat transfer in trapezoidal microchannels had

* Corresponding author. e-mail: sami@hu.edu.jo

been studied by Bin et al. [6] with uniform wall heat flux boundary conditions. In their investigation, the compressibility effect was neglected. The influences of velocity slip and temperature jump on friction coefficient and Nusselt number were investigated in detail. Orhan and Mete [7] analyzed laminar forced convective heat transfer of a Newtonian fluid in a micropipe where they took into account the viscous dissipation effect, the velocity slip and the temperature jump at the wall.

Wei et al. [8] investigated the steady-state convective heat transfer for laminar, two-dimensional, incompressible rarefied gas flow by the finite-volume finite difference scheme with slip flow and temperature jump conditions. Several boundary conditions were considered, and flow and heat transfer characteristics were studied systemically. Nishanth et al. [9] provided solution of the Navier-Stokes equations for gaseous slip flow in long microchannels with a second-order accurate slip boundary condition at the walls.

The compressibility effect had been taken into account in their analysis, which is usually neglected. They pointed out that the compressibility effect can not be neglected in rarefaction flow. Recently, T.T. Zhang [2] performed a study of compressibility effect combined with rarefaction effect on local friction factor in slip region.

It was noted that there is no study made previously on the transient fluid behavior in microchannels, due to the fact that most of the used applications occur in a relatively large time scale. But what if we are dealing with a very rabid system that deals with nanoseconds for example! Towards this end work had handled here showing some of the air behaviors in microchannels and analyzing the fluid flow in the transient region.

2. Model Setup

The work in this research intends to investigate the transient hydrodynamics behavior of fluid flow in microchannels by adopting the continuum approach but with no-slip flow boundary conditions. In order to verify the validity of the continuum approach with no-slip flow boundary conditions we refer to the Knudsen number which is defined as the mean free path for the particle dynamics divided by the hydraulic diameter of the microchannel. The Knudsen number must have a value less than 0.001 for our approach to be valid. The mean free path for the particle dynamics in the atmosphere, and assuming standard temperature and pressure, i.e. 25 °C and 1 atm, is $\lambda \approx 8 \times 10^{-10}$ m, or approximately 2.6×10^{-9} ft. The hydraulic diameter of the channel used is 20×10^{-6} m. Therefore, the knudsen number is equal to 4×10^{-5} which is less than 0.001 and consequently Navier stokes equation with no-slip conditions shall be used.

In this paper, a square-cross sectional microchannel is analyzed, as shown in Fig. 1. The length of channel is L and the hydraulic diameter is $D_h = \dfrac{4 \times cross - \sec tionalarea}{perimeter}$. In our case, D_h equals the height of the square.

The simulations are performed based on the following assumptions:

- The governing equations based on Navier-Stokes equations with no-slip boundary can be used to describe the physical processes.
- The flow is laminar (very small Re number, in our case the maximum Re = 137.5).
- Incompressible fluid (Ma ≤ 0.3)
- The body forces and the effect of viscosity heating are neglected.
- The heat transfer is not considered in the calculation.

The resulting governing equations are

Continuity equation:

$$\frac{\partial \rho}{\partial t} + \frac{\partial \rho u}{\partial x} + \frac{\partial \rho v}{\partial y} + \frac{\partial \rho w}{\partial z} = 0$$

Momentum equations:

$$\rho\frac{Du}{Dt} = \left(\frac{-\partial(p)}{\partial x}\right) + \mu_{eff}\left(\frac{\partial^2 u}{\partial x^2} + \frac{\partial^2 u}{\partial y^2} + \frac{\partial^2 u}{\partial z^2}\right) + \frac{\mu_{eff}}{3}\frac{\partial}{\partial x}\left(\frac{\partial u}{\partial x} + \frac{\partial v}{\partial y} + \frac{\partial w}{\partial z}\right)$$

$$\rho\frac{Dv}{Dt} = \left(\frac{-\partial(p)}{\partial y}\right) + \mu_{eff}\left(\frac{\partial^2 v}{\partial x^2} + \frac{\partial^2 v}{\partial y^2} + \frac{\partial^2 v}{\partial z^2}\right) + \frac{\mu_{eff}}{3}\frac{\partial}{\partial x}\left(\frac{\partial u}{\partial x} + \frac{\partial v}{\partial y} + \frac{\partial w}{\partial z}\right)$$

$$\rho\frac{Dw}{Dt} = \left(\frac{-\partial(p)}{\partial z}\right) + \mu_{eff}\left(\frac{\partial^2 w}{\partial x^2} + \frac{\partial^2 w}{\partial y^2} + \frac{\partial^2 w}{\partial z^2}\right) + \frac{\mu_{eff}}{3}\frac{\partial}{\partial x}\left(\frac{\partial u}{\partial x} + \frac{\partial v}{\partial y} + \frac{\partial w}{\partial z}\right)$$

Ideal gas law:

$$P = \rho RT$$

Variation in diffusion coefficient μ_{eff} is given by:

$$\mu_{eff} = \frac{\mu}{(1 + Kn)}$$

The boundary conditions of the above described problem are expressed as follows

On the wall: $y = \pm 0.5h \rightarrow U_w = 0.0$.

At the inlet: $x = 0.0 \rightarrow U =$ Constant (different three inlet velocities are considered).

At the outlet: $x = L$, $P = P_{out}$.

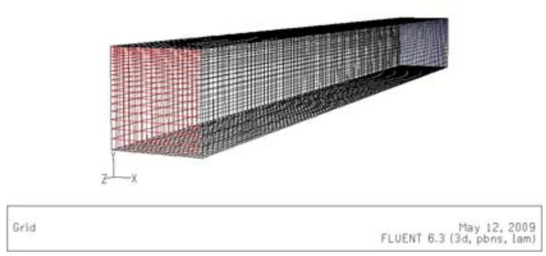

Figure 1: Meshed 3-dimensional microchannel used for analysis.

3. Numerical Method

The governing equations with boundary conditions as described in the previous section were solved by the CFD code, CFX-ACE. The equations were discretized by means of a fully implicit second-order finite-volume approach with second-order upwind advection scheme. In this work, the grid points used in the x, y, and z directions were selected to be 20, 20 and 200 respectively as this channel size achieves the best performance [2].

Fluent (finite volume method based software) is used to get the results. The numerical solution is obtained by an explicit iteration procedure and the solution converges when the maximum residuals of continuity equation was less than 10^{10}.

4. Results and Discussion

4.1. Velocity distribution with time:

The center line velocity distribution versus the time are presented in Figs 2, 3, 4 and 5 for the case of Dh = 20 μm, inlet velocities of 0.1, 1.0 and 10 m/s respectively and for incompressible flow. Note that the center line velocities increase with time. The time needed for the transient period shrinks as the inlet velocity increases.

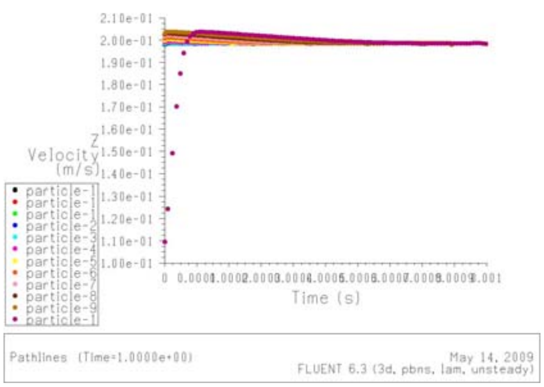

Figure 2: Velocity magnitude versus time at the centerline of the microhannel when the inlet velocity is 0.1m/sec.

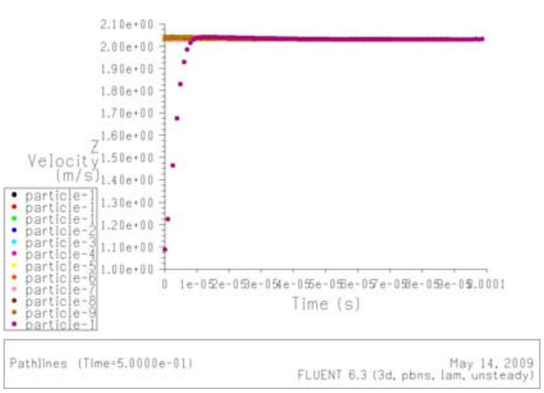

Figure 3: Velocity magnitude versus time at the centerline of the microchannel when the inlet velocity is 1.0m/sec.

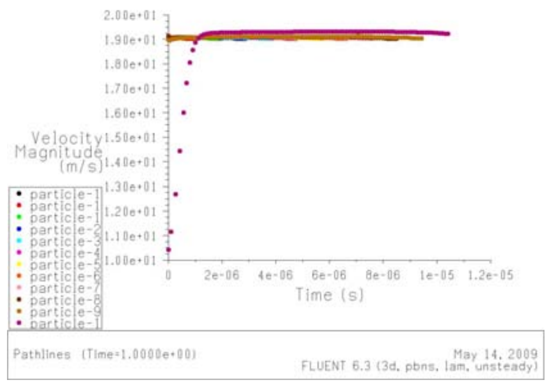

Figure 4: Velocity magnitude versus time at the centerline of the microchannel when the inlet velocity is 10 m/sec.

4.2. Velocity distribution along the Microchannel:

The variation of the velocity along the channel for the three above mentioned velocities is shown in Figs 5, 6 and 7 respectively at which the velocity vectors are displayed.

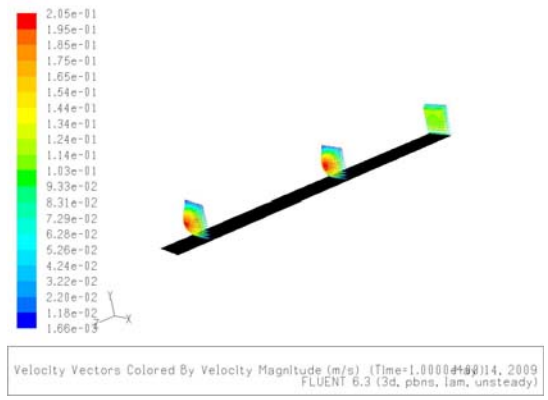

Figure 5: Velocity vectors along the microchannel when the inlet velocity is 0.1 m/sec.

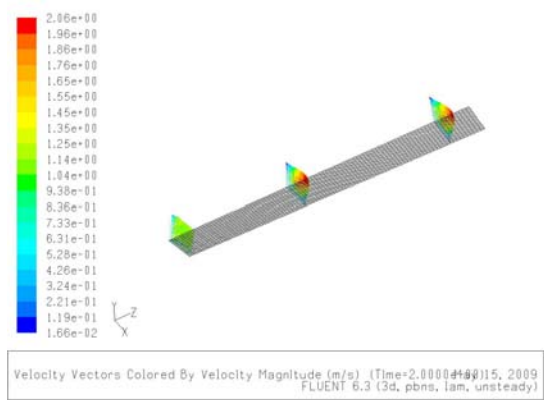

Figure 6: Velocity vector along the microchannel when the inlet velocity is 1.0 m/sec.

  - Volume 5, Number 3 (ISSN 1995-6665)

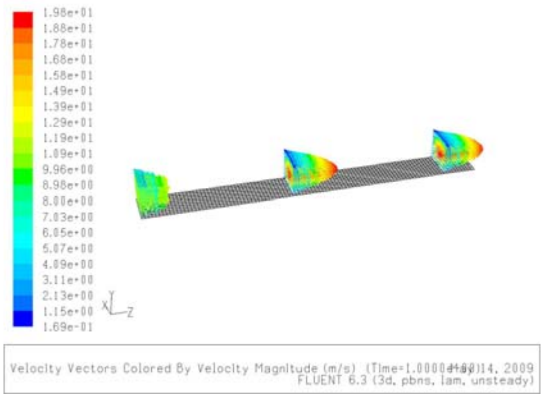

Figure 7: Velocity vector along the microchannel when the inlet velocity is 10m/sec.

From all of the above figures it is clear that all the percentage of the maximum velocity over the inlet velocity is almost constant with an average factor of 2.03, that is $U_{\max} = 2.03 \times U_{in}$. This implies that the maximum velocity is twice the entrance velocity in the transient region.

4.3. Pressure distribution along the Microchannel:

From the pressure contours shown in Figs 8, 9 and 10, it is clear that the upstream pressure can have small variation from one point to another at the same cross-section. Going a small distance to the downstream direction, it is clear that the pressure becomes constant across the same cross section.

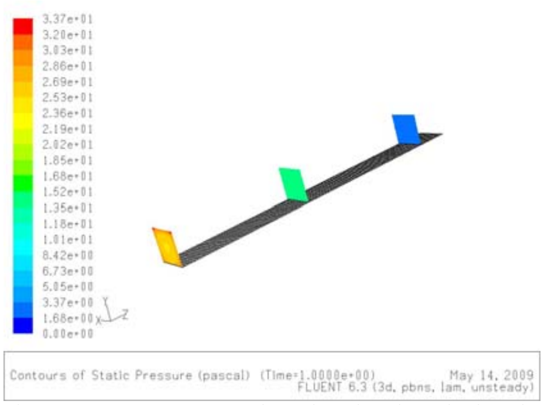

Figure 8: Pressure contours along the microchannel when the inlet velocity is 0.1m/sec.

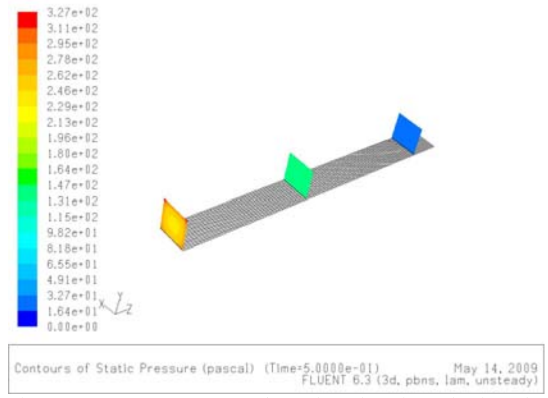

Figure 9: Pressure contours along the microchannel when the inlet velocity is 1.0m/sec.

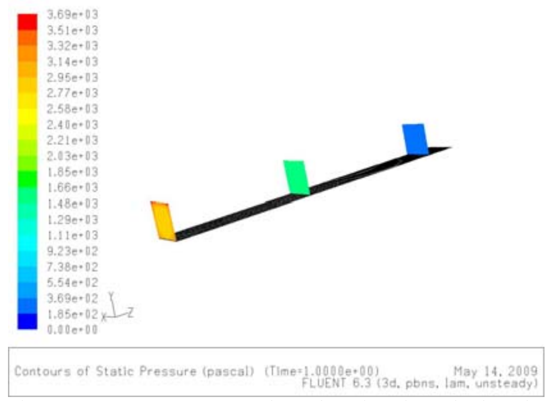

Figure 10: pressure contours along the microchannel when the inlet velocity is 10m/sec.

It can be clearly noted from Figs 7,8 and 9 that the maximum pressure occurs at the walls of the channel at the inlet, where also and the maximum inlet velocity and the maximum wall pressure occur. The relationship of the maximum pressure with the inlet velocity is linear while fixing the cross-sectional area and is found as

$$P_{\max} = 373.7 U_{in} - 46.7$$

The maximum pressure in the microchannel is important since the fluid particles could be pressure sensitive and may be destroyed if exposed to high values of pressure.

5. Conclusion

Although the transient behavior of fluids in microchannels was not a spot of concern to many researchers before, the transient behavior and transient terms of Nevier-Stokes equations shall be taken in consideration when dealing with applications that occur in a micro and/or nanoseconds. Both of the maximum channel velocity and the maximum channel pressure have linear relationships with the inlet velocity which was proven and derived in this work based on numerical solution and computer simulation.

References

[1] GH. Mohamed "The fluid mechanics of microdevices". J Fluid Eng, , Vol. 121, 1999, 5-33.

[2] T.T. Zhang, L. Jai, Z.C. Wang, C.W. Li. "Slip flow charactestics of compressible gaseous in microchannels", Energy Conversion and Management 2009.doi:10.1016/j. enconman. 2009.03.032.

[3] A. Beskok , GE. Karniadakis "Simulation of heat and momentum transfer in complex micro-geometries". J Thermophys Heat Transfer Vol. 8, 1994, 355-70.

[4] Y. Asako, K Nakayama, T. Shinozuka "Effect of compressibility on gaseous flows in a micro-tube". Int J Heat Mass Transfer Vol. 48, 2005, 4985-94.

[5] Y. Asako, T Pi, ET Stephen, FY Mohammad. "Effect of compressibility on gaseous flows in micro-channels". Int J Heat Mass Transfer Vol. 46, 2003, 3041-50.

[6] C. Bin, W.C. Guang, Y. Quan, "Fully developed laminar flow and heat transfer in smooth trapezoidal microchannel". Int Commun Heat Mass Vol. 32, 2005, 1211-20.

[7] Orhan A, Mete A. "Heat and fluid flow characteristics of gases in micropipes". Int. J Heat Mass Transfer Vol. 49, 2006,1723-30.

[8] S. Wei , K. Sadik , G. Yazicioglu Almila "A numerical study of single-phase convective heat transfer in microtubes for slip flow". Int J Therm Sci Vol. 46, 2007, 1084-94.

[9] D . Nishanth, A . Abhishek, A . Amit. "Analytical solution of gaseous slip flow in long microchannels". Int J Heat Mass Transfer Vol. 50, 2007, 3411-21.

JJMIE

Volume 5, Number 3, June 2011
ISSN 1995-6665
Pages 227 - 234

Jordan Journal of Mechanical and Industrial Engineering

Computer–Aided Maintenance Planning System for Industrial Companies

A. Mukattash[a], R. H. Fouad*[,a], H. Kitan[b], and M. Samhouri[a]

[a]Industrial Engineering Department, Hashemite University, Zarqa, Jordan
[b]Production Engineering Department, University of Technology, Baghdad, Iraq

Abstract

Significant advances in computer hardware and software development have affected most areas of business and industry, and the area of maintenance planning and management is no exception. The use of computerized maintenance management systems, which are commonly referred to as CMMS, is no longer a luxury or frivolous business overhead; in many cases, it is requirement. Enterprises that want to attain ISO, QS certification will discover that application of CMMS is a fundamental requirement to successfully obtain and maintain such certifications.
A variety of software packages are available, and many have been around for a number of years. Today, CMMS are used for all aspects of maintenance planning, management and control. CMMS must be flexible and adaptable, because every firm is considered unique. A general guide has been developed, which can easily be applied to specific situations to assist in justifying the computer for Maintenance System Evaluation (MSE). MSE has always required the manipulation of large amounts of data and development of more cost-effective processing storage and database systems has brought the use of computers to the fore in this area. Since, the relationships are complex between factors affecting maintenance activities and their interactions; a computer-aided model is developed with main purpose of determining the evaluation factors and their pointers. This model will approximate the complex relations for practical purposes. A model with eight various factors and there pointers for MSE were proposed in this paper. The MSE approach uses the input data as well as the factors that reflect unique operating conditions and specific objectives of the firm. The model would help in measuring the effectiveness of maintenance activities in order to determine the deviations from the planned work. It will also perform instant corrective actions required according to the degree of deviation and its effect on the production continuation and with the minimum shutdowns possible.

Keywords: Computerized Maintenance Management Systems (CMMS); Computer- Aided Maintenance; Maintenance System Evaluation (MSE); Maintenance Activity Factors; Effectiveness of Maintenance Activities; and Maintenance Planning

1. Introduction

In today's global economy with fierce competition to attain and maintain the competitive edge in productivity and quality, a key factor often is neglected. The planning and management of productive maintenance activities in industrial manufacturing organizations rarely are given the attention they deserve Stephens [22]. Many solutions are being exposed, such as future automated factory, zero inventories and integrated manufacturing system. These solutions cannot be successful without highly reliable machines and equipments.

Two issues regarding computer-aided maintenance are addressed: The first is fundamental knowledge, including both theories and methodologies required for practitioners to perform maintenance activities effectively. The revolutionary advances in information telecommunication, and computing technologies at modern factories forced the need for new approaches in process design, materials management, technologies, and human resources. The second and equally pressing issue is to understand how to implement the right maintenance tools and techniques, based on the introduced theories and methodologies, to solve problems in a very short time in order to guarantee success Lee and Wang, [13]. Today, leading firms understand the necessity of linking production planning with resource supply using dependent demand techniques like Enterprise Resource Planning (ERP) in order to provide the increasing business needs in more effective and efficient ways Spathis and Constantinides [21].

The knowledge that has been gained in linking production with maintenance planning is essential to compressing the computer- aided evaluating system for maintenance activities. Applying this knowledge will help reduce waste and greater productivity. It became apparent that maintenance was not just about keeping machinery in a good working order but it involved learning by sharing communal experiences, and feeding the result back into design, operation and maintenance itself [4].Maintenance has always been in the business of dealing with large amounts of data. The advent of the microcomputer in the late 1970s began a revolution in maintenance systems.

* Corresponding author. e-mail: rhfouad@hu.edu.jo

Only now, in the mid-1980s, are we beginning to saw a mature system which addresses the following maintenance tasks Carter [4] and Retterer and Kowallski [19]. System Fault Reporting / Repair Control, Labor Control and Reporting, Equipment / Spare Parts Inventory Control, Maintenance Data Recording Analysis.

This research aims in developing a computerized program for evaluating maintenance system's activities so that the maintenance performance level can be evaluated as well. In the age of minimal inventories and highly automated complex machinery, automated maintenance systems are required to truly accomplish the goals of a Computer-Aided Manufacturing (CAM) and Computer-Integrated Manufacturing an automated and maintenance planning and diagnostics system can provide a rapid planning and scheduling response to changing system conditions (CIM) Lin and Chen [14].

Lee and Wang [13] and Candy [3] both suggested that the overall goal of the maintenance function is to make capacity available to production in a reliable and stable manner. This should enable organizational objectives such as the following to be met; 1) Responsive customer service, 2) Consistent product quality, 3) Reliable product output, 4) Cost efficient operations, maintenance and supported departments, and 5) High utilization of equipment and other resources.

In the past two decades, changes in the production environment have made the task of making decisions about allocating maintenance resources and scheduling maintenance work more difficult. An information-processing model is applied by Laura Swanson [11] to study how the maintenance function applies different strategies to cope with the environmental complexity. Computer-Aided Reliability-Centered Maintenance (RCM) a based plant maintenance management system has been studied and investigated by Hossam A. et. al. [8], and Jesu´s Carreteroa et.al.[10]. A survey of models and algorithms for winter road maintenance system design for snow disposal was developed by Nathalie Perriera et.al [17].Implementation and benefits of introducing a CMMS into a textile manufacturing company is investigated in C.D. O'Donoghue, and J.G. Prendergast [18]. Recently; Celso et.al. [5] presented a model for preventive maintenance planning by genetic algorithms based in cost and reliability. Similarly genetic algorithms for integrated preventive maintenance planning and production scheduling for a single is presented by N. Sortrakul, H.L. Nachtmann, and C.R. Cassady [23]. (Farhad Kianfar [7] proposed a numerical method to approximate optimal production and maintenance plan in a flexible manufacturing system. Hsu-Hua Lee [9] presents a cost/benefit model for investments in inventory and preventive maintenance in an imperfect production system. This paper is an extension of the initial research on the English system used in batteries industry at General Company for liquid Battery Industries was carried out by Mukattash and Kitan [1].

In today's global economy with fierce competition to attain and maintain the competitive edge in productivity and quality, a key factor often is neglected. The planning and management of productive maintenance activities in industrial manufacturing organizations rarely are given the attention they deserve Stephens [22]. Many solutions are being exposed, such as future automated factory, zero inventories and integrated manufacturing system. These solutions cannot be successful without highly reliable machines and equipments.

Two issues regarding computer-aided maintenance are addressed: The first is fundamental knowledge, including both theories and methodologies required for practitioners to perform maintenance activities effectively. The revolutionary advances in information telecommunication, and computing technologies at modern factories forced the need for new approaches in process design, materials management, technologies, and human resources. The second and equally pressing issue is to understand how to implement the right maintenance tools and techniques, based on the introduced theories and methodologies, to solve problems in a very short time in order to guarantee success Lee and Wang, [13]. Today, leading firms understand the necessity of linking production planning with resource supply using dependent demand techniques like Enterprise Resource Planning (ERP) in order to provide the increasing business needs in more effective and efficient ways Spathis and Constantinides [21].

The knowledge that has been gained in linking production with maintenance planning is essential to compressing the computer- aided evaluating system for maintenance activities. Applying this knowledge will help reduce waste and greater productivity. It became apparent that maintenance was not just about keeping machinery in a good working order but it involved learning by sharing communal experiences, and feeding the result back into design, operation and maintenance itself [4].Maintenance has always been in the business of dealing with large amounts of data. The advent of the microcomputer in the late 1970s began a revolution in maintenance systems. Only now, in the mid-1980s, are we beginning to saw a mature system which addresses the following maintenance tasks Carter [4] and Retterer and Kowallski [19]. System Fault Reporting / Repair Control, Labor Control and Reporting, Equipment / Spare Parts Inventory Control, Maintenance Data Recording Analysis.

This research aims in developing a computerized program for evaluating maintenance system's activities so that the maintenance performance level can be evaluated as well. In the age of minimal inventories and highly automated complex machinery, automated maintenance systems are required to truly accomplish the goals of a Computer-Aided Manufacturing (CAM) and Computer-Integrated Manufacturing an automated and maintenance planning and diagnostics system can provide a rapid planning and scheduling response to changing system conditions (CIM) Lin and Chen [14].

Lee and Wang [13] and Candy [3] both suggested that the overall goal of the maintenance function is to make capacity available to production in a reliable and stable manner. This should enable organizational objectives such as the following to be met; 1) Responsive customer service, 2) Consistent product quality, 3) Reliable product output, 4) Cost efficient operations, maintenance and supported departments, and 5) High utilization of equipment and other resources.

In the past two decades, changes in the production environment have made the task of making decisions about allocating maintenance resources and scheduling maintenance work more difficult. An information-processing model is applied by Laura Swanson [11] to study how the maintenance function applies different strategies to cope with the environmental complexity. Computer-Aided Reliability-Centered Maintenance (RCM) a based plant maintenance management system has been studied and investigated by Hossam A. *et. al.* [8], and Jesu´s Carreteroa *et.al.*[10]. A survey of models and

algorithms for winter road maintenance system design for snow disposal was developed by Nathalie Perriera *et.al* [17].Implementation and benefits of introducing a CMMS into a textile manufacturing company is investigated in C.D. O'Donoghue, and J.G. Prendergast [18]. Recently; Celso *et.al.* [5] presented a model for preventive maintenance planning by genetic algorithms based in cost and reliability. Similarly genetic algorithms for integrated preventive maintenance planning and production scheduling for a single is presented by N. Sortrakul, H.L. Nachtmann, and C.R. Cassady [23]. (Farhad Kianfar [7] proposed a numerical method to approximate optimal production and maintenance plan in a flexible manufacturing system. Hsu-Hua Lee [9] presents a cost/benefit model for investments in inventory and preventive maintenance in an imperfect production system. This paper is an extension of the initial research on the English system used in batteries industry at General Company for liquid Battery Industries was carried out by Mukattash and Kitan [1].

2. Experimental Measurements

Traditionally, maintenance organizations have operated in a "fire-fight" mode. "Preventing fires" has often been given a minor or causal emphasis.

The fire-fighting mode (fix it when it breaks) is called Corrective Maintenance, while the latter (fix it before it breaks) is called Preventive Maintenance (PM) as shown in Fig.A1 appendix Lindbeck and Wygant, [12] and Burton et. al. [2]. A key distinction among these three perspectives relates to the time interval between the recognition of the need to perform a maintenance activity and the time the maintenance activity is performed.

3. Evaluating Factors Scoring for Maintenance Activities

The evaluation approach of maintenance activities usually categorizes a given maintenance system by scoring its activities more often on a scale of one to four. The higher the category scores for a factor, the greater the importance of the other categories. This is usually done with the objectives of:

- Labor usage efficiency improvement.
- Unexpected breakdowns reduction.
- Downtime reduction.
- Maintenance scheduling improvement.
- Preventive maintenance program improvement, Dhavale and Otterson, [6]:

The user has the choice to eliminate some of the factors entirely, adding new factors, changing, adding or deleting pointers in a given factor and changing their scores. The user should examine critically according his firm conditions.

4. Measuring System of Maintenance Activities

The main objective for measuring and evaluating maintenance activities in a firm is to determine the followings:

- Performance level of maintenance system.
- Deviations from maintenance plan.
- Required corrective actions.

Different evaluating systems to maintenance activities have been developed in industrial countries (Ettlcin and Jahing, 1986, Mann and Coates, [16] ,(Simith [20] and Malek and Kaitan, [15]. Any firm can use an evaluating system according to nature of their industrial function. Some of these systems used on the national levels such as, The English system used in automobile industries , The American system used in engineering industries , The Egyptian system used in chemical industries, The Soviet system used in metallurgical industries , The Yugoslavian system used in mechanical industries and The English system used in batteries industry. All of these systems for measuring and evaluating maintenance activities are used to annually evaluate the efficiency of maintenance plan execution according to certain determined goals.

5. Case Study

The English system used in battery industries has been applied in the one of the Middle East companies called General Company for Liquid Battery Industries. A computer program written in visual basic was built as an evaluation system for maintenance activities in this company and the results for each factor and their pointers are compared with the standard values at "Chloride" company. It was found necessary to modify it with regard to:

- Factors and pointers for planning efficiency.
- Factors and pointers for loading efficiency.
- Factors and pointers for costs.
- Factors and pointers for productivity.

The modified approach in applying "Chloride" system is based on identifying two pointers for each factor. This modifying method depends on four parameters, which reflect the own production environment of battery Industry Company as follows:

- Size of company and the type of functional organization to production department.
- Varieties and continuity of production type.
- Work nature, time and operating environment.
- Skills, number, stability of maintenance workforce.

The actual measured values for the major (4) factors (planning, loading, costs, and productivity) depend on the determined pointers for each factor. These eight pointers represent the basic for measuring the maintenance activities. A flow chart that illustrates the algorithm steps required for measuring the efficiency of maintenance activities in the chosen company is shown in Fig.1 below.

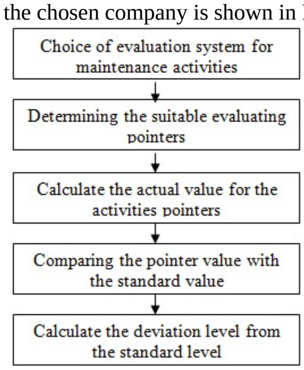

Figure 1: Flow chart of the steps of measuring maintenance activities efficiency

5.1. Planning Efficiency Factor Calculations:

5.1.1. Workforce effectiveness (LE) Pointer:

L.E = (Z-Q) / Z x R

Where:

Z= Total operation hours,

Q= Total absenteeism hours,

and

R = Workforce skillfulness average.

The calculation procedure for LE is shown in Fig. 2 below.

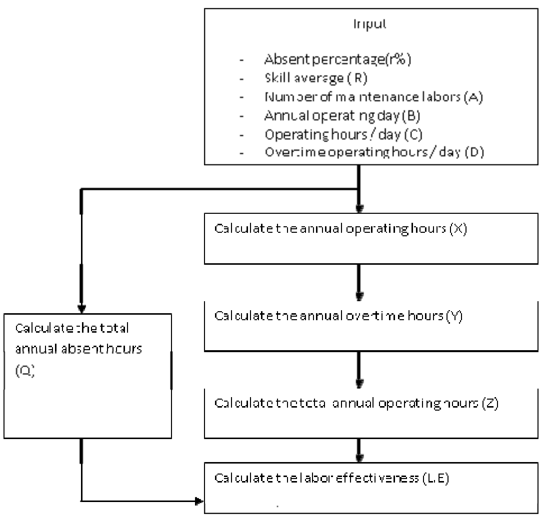

Figure 2: Calculation procedure for labor effectiveness.

5.1.2. Executed Maintenance Work/planning maintenance Work Pointer (KT):

KT = BT/AT × 100

Where:
BT = Number of actual maintenance hours,

AT = Number of planned maintenance hours.

The calculation procedure of KI for each department and KT for the overall company is shown in Fig. 3 below.

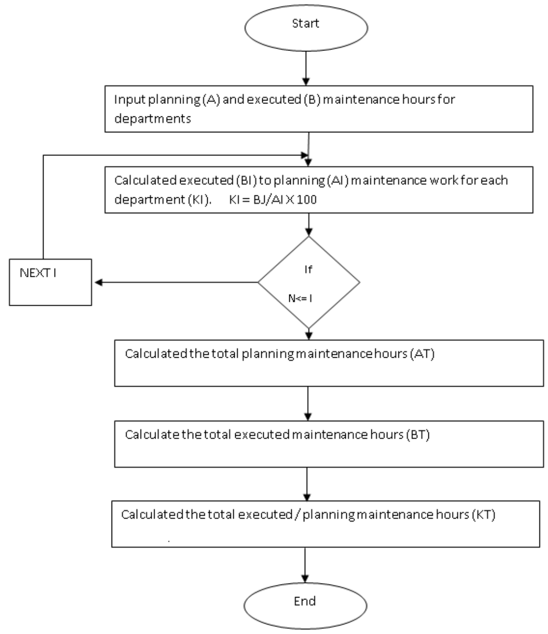

Figure 3: Calculation procedure for executed / planning maintenance hours.

5.2. Loading Efficiency Factor Calculations:

5.2.1. Total Preventive Maintenance Hours / Total Maintenance Hours Pointer (KP):

KP = PT / AT × 100

Where:

PT = Preventive maintenance hours,

AT = Total maintenance hours

5.2.2. Corrective Maintenance Hours / Total Maintenance Hours Pointer (KC):

KC = CT / AT × 100

The calculation procedure for preventive and corrective maintenance hours / total planning is shown in Fig. 4 below

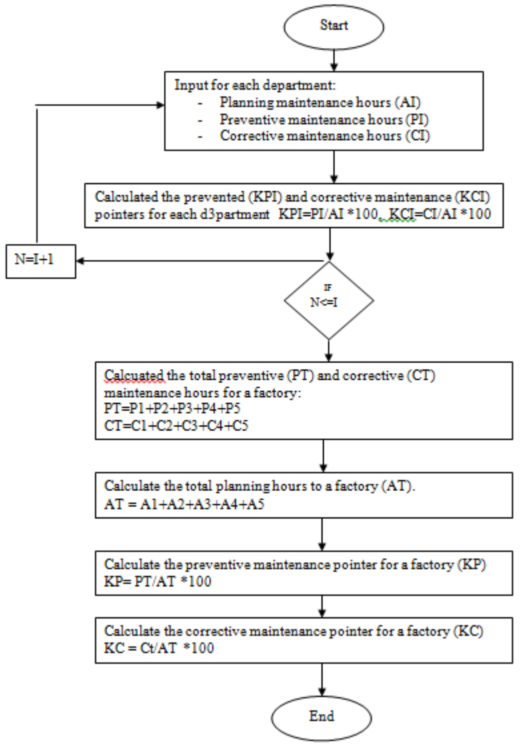

Figure 4: Calculation procedure for preventive and corrective maintenance hours / total planning maintenance hours

5.3. Costs Factor Calculations:

5.3.1. Maintenance Costs / Capital Investment pointer (KI):

KI = TCM / CI × 100

Where:

TCM = Total maintenance cost,

CI = Capital investment

5.3.2. Direct and General Maintenance Cost / Total Maintenance Costs pointer (K2):

K2 = (DMC + GMC) / TMC × 100

Where:

DMC = Direct Maintenance Costs,

GMC = General Maintenance Costs.

The calculation procedure of costs factor pointers is shown in Fig. 5.

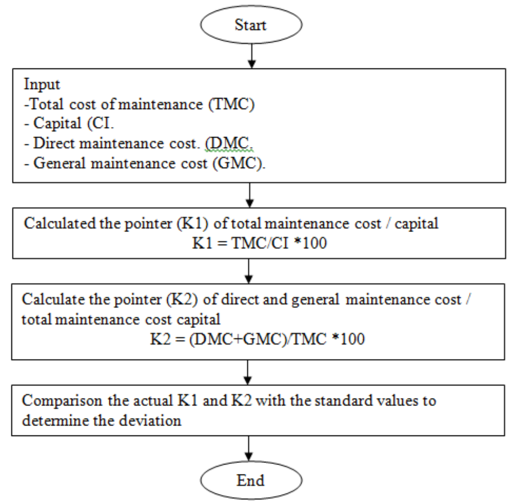

Figure 5: Calculation procedure of costs factor pointers.

5.4. Productivity Factor Calculations:

5.4.1. Labors Utility pointer (LU):

LU = AW / TW × 100

Where:

AW = Actual Work,

TW = Total Work.

The flow chart shown in Fig. 6 depicted the steps for calculation of KI for each department and KT for the overall company.

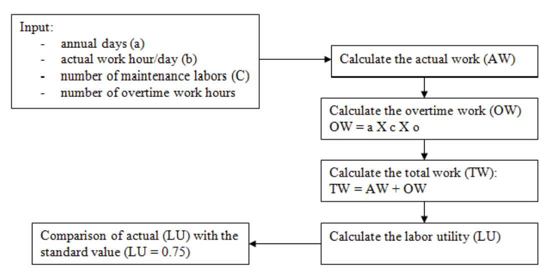

Figure 6: Calculation procedure of Labors utility (LU) pointer

5.4.2. Production Breakdown Time for Maintenance / Total Operating Time (machine-hr) Pointer (MB):

MB = TBhs / E

Where:

Bhs = Total breakdown hours,

E = total energy.

The calculation procedure of production breakdown for maintenance is shown in Fig.7 below.

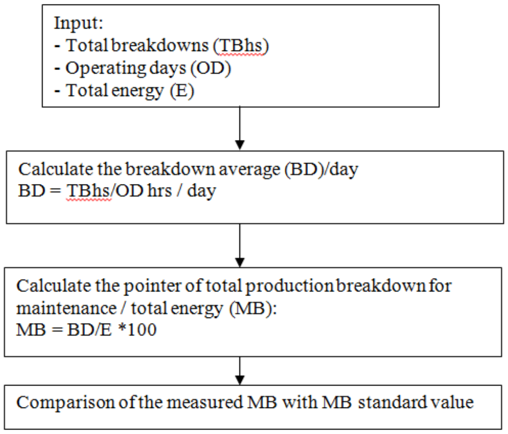

Figure 7: Calculation procedure of production breakdown for maintenance

An example of execution the algorithm steps sequencing for maintenance system evaluation (MSE) is illustrated through the different menus as shown in fig A2 appendix and figs. (8, 9, and 10) below

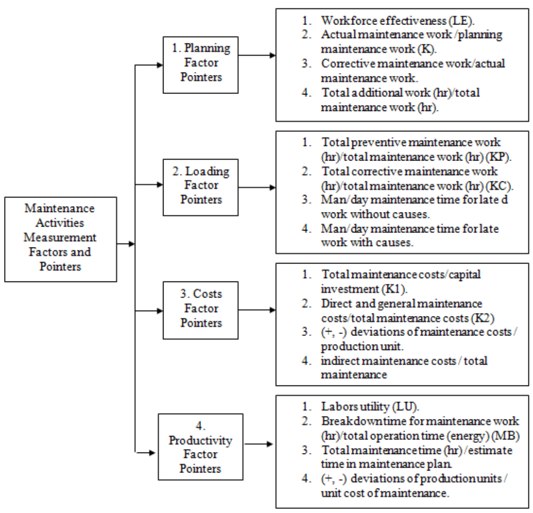

Figure 8: English system menu

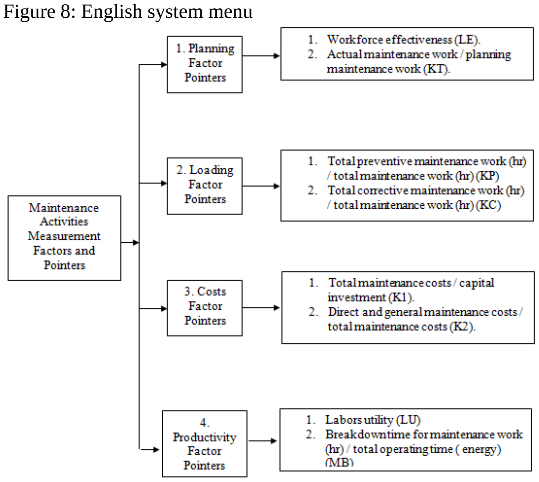

Figure 9: Selected pointers menus

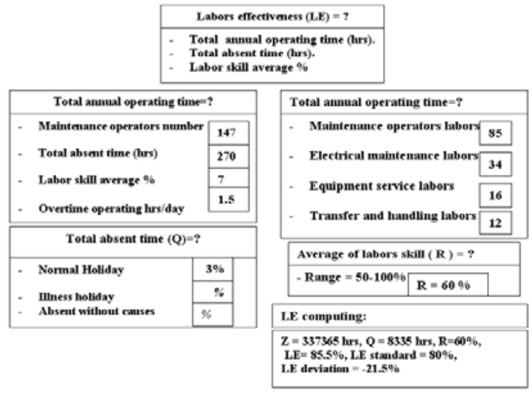

Figure 10: LE calculation menu

6. Results Analysis

The deviations of maintenance activities measurements from targeted levels resulted from comparing the actual results with standard values. These deviations for the selected factors and their pointers are illustrated in Table 1. The lack of labor effectiveness (LE) ranked as the first one as the actual value is (58.5%) while the standard value is (80%). Which means a deviation value around (58.5-80=-21.5%). The production breakdown pointer for maintenance has actual value of (7.8%) with a deviation value of (7.8-3 = 4.8%).

Table (1): Results of MES maintenance activities factors and pointers

Factors	Pointers	Pointers Values			Factors Values		
		Actual Value %	Standard Value %	Deviation	Actual Value %	Standard Value %	Deviation%
Planning	Workforce Effectiveness	58.5	80	-21.5	56	82.5	-26.5
	Actual Maintenance Work / Planned Work	53.5	85	-32			
Loading	Preventive Maintenance Hours / Total Maintenance Hours	18.5	25	-6.5	50	50	0
	Corrective Maintenance Hours/total Maintenance Hours	81.5	75	+6.5			
Costs	Total Maintenance Costs / Capital Investment	6.5	6	+6.5	38.25	45.5	-7.25
	Direct and General Maintenance Cost / Total Maintenance Costs	70	85	-15			
Productivity	Labors Utility	67	75	-8	37.4	39	-1.6
	Breakdown Time / Total Operating Time	7.8	3	+4.8			

7. Conclusion

Maintenance management may be a key strategic variable in the quest for waste that will lead eventually to strong competitive advantage. Leading companies understand the necessity for linking production planning with maintenance planning activities in order to reduce waste. Waste is inherently greater if production and maintenance plans are not linking, made poorly or not followed closely.

The knowledge that has been gained in linking production planning with maintenance planning is essential to for a proactive maintenance program. And it also essential to compressing the computer-aided evaluating system for maintenance activities. Applying the knowledge will help in reducing waste and greater productivity.

Throughout the inspection of all actual values of pointers for maintenance activities in the company, some of other conclusions are:

- Cannot give an indication of the costs, which are resulted from the production breakdown (interruptions) because of machines breakdowns on the direct cost of the product. Thus, the management doesn't take care for maintenance in relative to the size of loses because of the frequency of production breakdowns. This situation appears in deviation value (-21.5%).
- Do not reflect the machines breakdowns as a major reason to prevent execution production plan in quality and quantity. This lead the management reasoning to consider the preventive maintenance cost as additional financial and managerial load. Also it dose not give a precise assessment of and the required cost for preventive maintenance and take the corrective maintenance as an alternative. The preventive and corrective maintenance deviations reflect above management reasoning respectively (18.5-25 = -6.5%), (81.5-75 = +6.5%).
- According to the above conclusions, the necessity to consider computer – aided evaluation to maintenance activities is important. This computer system is simple in reasoning and application in short intervals (i.e. weekly, monthly) instead or beside the present systems that have long evaluating intervals (i.e. semester, annual). This short intervals computer system is active and flexible to take the corrective actions in proper position and time in relation to the degree of deviation for each evaluating pointer. It also reflects the positive state for production continuity in fewer breakdowns.

References

[1] A. Mukattash, and Kitan, H., "Computer–Aided Maintenance Activities Measurement System in Industrial Companies", First National Conference of Mechanical Engineering (IES2000), Najaf, Iraq, 2000.

[2] J.S. Burton, A. Banerjee, and C. Sylla, "A Simulation Study of Sequencing and Maintenance Decisions in A Dynamic Job Shop", Computers Ind. Engine, Vol.17, 1989, 1-4.

[3] W.L. Candy, "Maintenance Groups Make and Implement Own Suggestions for Improving Productivity", IE, 1982

[4] J. Carter, "Maintenance Management-Computerized Systems Come of the Age", Computer-Aided Engineering Journal, 1985.

[5] Celso Marcelo F. Lapaa, Cla´udio Ma´rcio N.A. Pereiraa, b, Marcio Paes de Barros. "A Model for Preventive Maintenance Planning by Genetic Algorithms Based in Cost and Reliability". Reliability Engineering and System Safety Vol. 91, 2006, 233–240.

[6] Dhavale, D. G. and Otterson, G. L. "Maintenance by Priority" IE 1980.

[7] Farhad, Kianfar, "A Numerical Method to Approximate Optimal Production and Maintenance Plan in Flexible Manufacturing System", Applied Mathematics and Computation Vol. 170, 2005, 924–940.

[8] Hossam A. Gabbar, Hiroyuki Yamashita, Kazuhiko Suzuki, Yukiyasu Shimada. "Computer-Aided RCM-Based Plant Maintenance Management System" Robotics and Computer Integrated Manufacturing, Vol. 19, 2003, 449–458.

[9] Hsu-Hua Lee, "A Cost/Benefit Model for Investments in Inventory and Preventive Maintenance in an Imperfect Production System", Computers & Industrial Engineering Vol. 48, 2005, 55–68.

[10] Jesu´s Carreteroa, Jose´ M. Pe´reza, Fe lix Garc´a-Carballeiraa, Alejandro Caldero´na, Javier Ferna´ndeza, Jose D. Garc´aa, Antonio Lozanob, Luis Cardonab, Norberto Cotainac, Pierre Pretec. "Applying RCM in large-scale systems: a case study with railway networks" Reliability Engineering and System Safety Vol.82, 2003, 257–273.

[11] Laura Swanson, "An information-processing model of maintenance management", Int. J. Production Economics Vol. 83, 2003, 45–64

[12] Lindbeck, J.R. and Wygant, R.M. "Product Design and Manufacture" Prentic-Hill, Inc. 1995

[13] J. Lee and B. Wang "Computer-Aided Maintenance Methodologies and Practices" Klvwer Academic 1999

[14] Z. Lin, and S. Chen, "Measuring Sequencing Planning With Dynamic Programming". INT. J. Computer Integrated Manufacturing, Vol. 8, No.4, 1995.

[15] A. A. Malek,, H. S. Kaitan, "A System for Measuring And Evaluating Maintenance Activities in Industrial Organizations" Al-Muhandis-112, 1992

[16] L. Mann and E. R. Coates "Evaluation Computer For Maintenance Management" IE FEB 1980.

[17] Nathalie Perriera, André Langevina, James F. Campbellb, "A survey of models and algorithms for winter road maintenance. Part II: system design for snow disposal". Computers & Operations Research Vol. 33, 2006, 239–262.

[18] O'Donoghue C.D., and Prendergast J.G., "Implementation and Benefits of a Computerized Maintenance Management System into a Textile Manufacturing Company, Journal of Materials Processing Technology 153–154 , 2004, 226–232

[19] B.L. Retterer, and R. A. Kowallski, "Maintainability: A historical Perspective" IEEE Transactions on Reliability, Vol. 33, No. 1, 1984.

[20] Simith, D. J., "Reliability and Maintainability in Perspective" 3rd edition Macmillan Education LTD, 1988

[21] C. Spathis, and S. Costantinides, "The usefulness of ERP systems for effective management", Industrial Management and Data Systems, Vol. 103, No. 9, 2003, 677-685

[22] M. P. Stephens, "Productivity and Reliability-Based Maintenance Management", Pearson Education, ISBN: 0-13-096657-6, 2004.

[23] N. Sortrakul, H.L. Nachtmann, and C.R. Cassady, "Genetic algorithms for integrated preventive maintenance planning and production scheduling for a single machine". Computers in Industry Vol. 56, 2005, 161–168.

Appendix

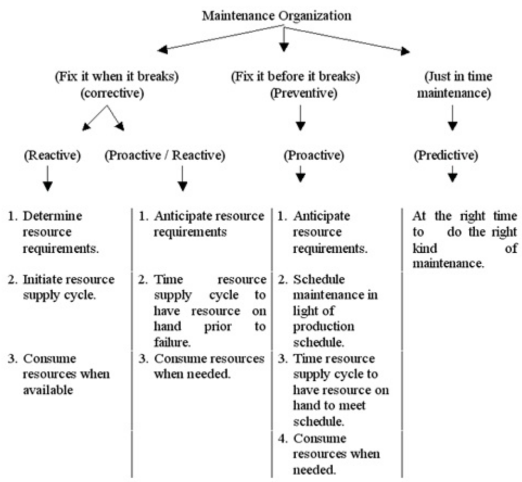

Figure A1: Maintenance Management Perspectives.

THE VARIOUS MAINTENANCE EVALUATION FYSTEMS

1. Battery English system used in automobile industries.
2. American system used in engineering industries.
3. Egyptian system used in chemical industries.
4. Soviet system used in metallurgical industries.
5. Yugoslavian system used in mechanical industries.
6. English system used in industries.

Figure A2: Main menu of the program.

JJMIE

Volume 5, Number 3, June 2011
ISSN 1995-6665
Pages 235 - 240

Jordan Journal of Mechanical and Industrial Engineering

Performance of Pre-heated Cottonseed Oil and Diesel Fuel Blends in a Compression Ignition Engine

M. Martin*,[a], D. Prithviraj[a]

[a] School of Mechanical Engineering, SRM University, Kattankulathur - 603203 (Tamil Nadu), India.

Abstract

Viscosity of vegetable oil is considered a constraint for its use as an alternate fuel for Internal Combustion(IC) engines. In this experimental investigation, the viscosity of cottonseed oil (CSO), which is considered a potential alternate fuel, is reduced by blending it in different proportions with diesel, and its viscosity at various temperatures was analyzed and used as a fuel in a compression ignition (CI) engine. Performance, combustion and emission parameters at various loads were calculated using a single cylinder CI engine and compared with neat diesel and cottonseed oil. A remarkable improvement in the performance of the engine is noticed as the viscosity of the oil is reduced. Brake thermal and volumetric efficiencies of the engine increased with a significant reduction in the exhaust gas temperature. Reductions in smoke, CO and HC emissions are also noticed. Results show that a blend containing 60% of cottonseed oil with diesel, which is heated to a temperature of 70°C, can be used as an alternate fuel without any engine modification.

Keywords: Cottonseed oil (CSO); Diesel; viscosity; Temperature; Blend

Abbreviations

IC	Internal Combustion
CSO	Cottonseed oil
CI	compression ignition
HC	Hydrocarbon
CO	Carbon Monoxide
TDC	Top Dead Center
cSt	Centi Stoke
PH	Preheated
BSU	Bosch Smoke Units
PPM	Parts per Million
bTDC	Before Top Dead Center
cc	Cubic Centimeter
Cp	Specific Heat at Constant Pressure
CR	Compression Ratio
SAE	Society of Automotive Engineers

Symbols

°C	Degree centigrade
°CA	Degree crank angle
hr	Hour
K	Kelvin
kJ	Kilo Joules
kW	Kilo Watt
kg	Kilogram
P	Pressure (bar)
rev/min	Revolutions per minute
rpm	Revolutions per minute
T	Temperature (K)
t	Time (s)

* Corresponding author. e-mail: hod.auto@ktr.srmuniv.ac.in

1. Introduction

The idea of using vegetable oil began in the year 1893 itself when diesel engines came into existence. In the year 1911, Rudolf Diesel operated his first engine using straight vegetable oil (peanut oil).

The physical and combustion properties of vegetable oils are closer to that of diesel and in this context; vegetable oils can stand as an immediate candidate to substitute for fossil fuels. The greatest advantages of vegetable oils are that they are obtained from seeds of various plants. In view of this, researchers have started showing renewed interest towards vegetable oils because of its advantages as a potential alternate fuel. Vegetable oils are renewable and eco-friendly in nature and at the same time, it can be easily produced in rural areas.

Sustainable development of a country depends on the extent that it is managing and generating its own resources. This also helps in conservation of depletion of non-renewable petro-products. However due to inherent high viscosity and low volatility, vegetable oils would pose problems such as fuel flow and poor atomization and constrain their direct use in engine without any modifications.

Vegetable oils are either edible or non-edible. Some of the edible oils are sunflower oil, palm oil, rice bran oil, and cottonseed oil. The non-edible oils are mahua oil, jatropha oil, rubber seed oil, etc. As rice bran and cottonseed oil (CSO) are not very much in use for cooking purpose, these can be used as substitute for diesel in CI engines. Cottonseed oil has several properties closer to that of diesel but certain properties such as high viscosity and low volatility pose problem when used as an alternate fuel for C.I engines.

The potential of using vegetable oil for diesel engines was studied by Recep Altin et al. [1], Yoshomoto .y et al. [2] and Kensuke Nishi et al.[3]. The engine performance was very much similar to that for diesel with little power loss and slight increase in the emission level. Karaosmanoglu.F et al [4] studied long-term utilization of vegetable oil and no significant increase or loss in power was noticed. Nwafor O.M.I et al. [5] carried out combustion studies on both diesel fuel and vegetable oil fuel with standard and advanced injection timings. Advanced injection timing compensates the effects of the longer delay period and slower burning rate that is exhibited by vegetable oils.

The problems related to low volatility and high viscosities are offset by subjecting the oil into the process of transesterification, and the high viscosity can be reduced. Methyl and ethyl esters of vegetable oil (called as bio-diesel) have the physical and chemical properties closer to that of diesel. The performance and emission characteristics of the diesel engine using methyl ester are comparable with that of diesel as per Dilip Kumar Bora et al. [6]. Babu A.k et al. [7] also has reported problems related to high viscosity.

Blending vegetable oil with diesel decreases the viscosity and improves the volatility. This improved properties results in better mixture formation and spray penetration. A number of investigators tried the vegetable oils in varying proportions with diesel. Results obtained from experiments shows that vegetable oil and diesel blends showed improvement in engine performance [8, 9]. Pre heating the vegetable oil reduces the viscosity and improves combustion characteristics (Pramanik. K [10]).

This paper examines the use of preheated cottonseed oil diesel blends on the performance of a single cylinder diesel engine. Preheating the vegetable oil decreases the viscosity and improves the atomization and mixing process, which results in better combustion.

2. Experimental Setup

A single cylinder, water cooled, four stroke direct injection compression ignition engine with a compression ratio of 17.5: 1 and developing 5.2 kW power at 1500 rpm was used for this work. Fuels used were diesel, cottonseed oil and blends of cottonseed oil-diesel pre heated to 70°C. The cylinder pressure and top dead centre (TDC) signals were acquired and stored using a high-speed computer based digital data acquisition system. The stored signals were processed with specially designed software to obtain the performance and combustion parameters. Viscosity of the fuel was measured with a Saybolt viscometer. A CRYPTON exhaust gas analyzer was used to measure carbon monoxide (CO) and hydrocarbon (HC) levels. The analyzer is a fully microprocessor controlled system employing nondestructive infrared techniques. Smoke level was measured using a standard BOSCH smoke measuring system.

3. Experimental Procedure

During all the tests, the rated power and speed of the engine (5.2 kW @ 1500 rpm) were maintained. Load was changed in 5 levels, 20%, 40%, 60%, 80% and 100%. Load, speed, air flow rate, fuel flow rate, exhaust gas temperature, exhaust emissions of HC, CO and smoke were stored in the computer at all load conditions. Cylinder pressure and TDC position signals were also recorded to obtain combustion parameters.

4. Results and Discussion

4.1. Effect of preheating cottonseed oil and blending with diesel:

Table.1 shows the variation of viscosity of diesel, CSO and the blends at 30°C. The high viscosity of CSO drastically falls with the increase in the quantity of diesel in the blend. Even with an addition of 20% diesel, the viscosity of the blend drops from 49.6 cSt to 22.3 cSt, which is 55.04% less than that for CSO. With further increase in the quantity of diesel in the blend the viscosity dropped. The viscosities of 40%, 60% and 80% diesel with CSO are 16.2, 11.6 and 7.2 cSt respectively. The corresponding percentage reduction in viscosity is 67.33%, 76.61% and 85.48%. Therefore, to bring the viscosity close to diesel, 60-80% of diesel has to be added to CSO.

Table 1: Viscosity of diesel, CSO and blends @ 30°C.

Fuel	Diesel	CSO	20% Diesel	40% Diesel	60% Diesel	80% Diesel
Viscosity (cSt)	4.59	49.6	22.3	16.2	11.6	7.2

In order to reduce the viscosity, the blends were heated from 20°C to 90°C in steps of 10°C. Table.2 shows the results obtained. Variation of viscosity of diesel, CSO and blends at various temperatures are shown in Figure.1. From Table.2 the viscosity of 20%, 40% and 60% diesel blends at 70°C are close to that for diesel. Therefore, blends containing 20%, 40% and 60% diesel were tried as a fuel for the CI engine and results for 20% and 40% are presented in this paper keeping in mind the maximum reduction of diesel usage.

Table 2: Viscosity of Diesel, CSO and blends at various temperatures.

Temperature (°C)	Kinematic Viscosity (cSt)					
	Diesel	CSO	20% Diesel	40% Diesel	60% Diesel	80% Diesel
30	4.59	49.6	22.3	16.2	11.6	7.2
40	3.4	32.7	16.2	13.1	10	6.2
50	3.1	23.3	11.7	10.3	8	5.1
60	2.7	16.8	8.3	6.6	5.2	4.2
70	2.2	9.3	6.4	5.3	4.6	3.6
80	2	6.2	5.4	4.9	3.8	2.8
90	1.9	5.3	4.9	4.1	3.4	2.6

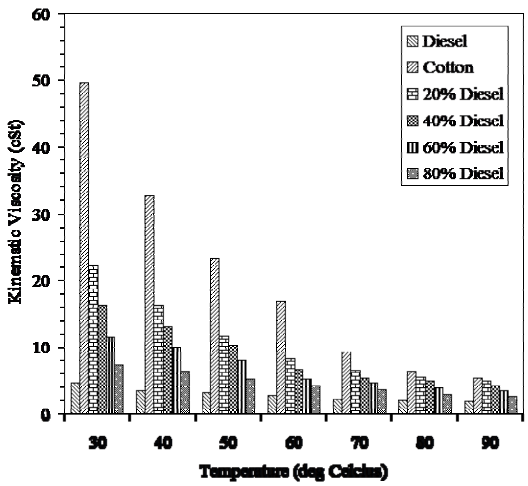

Figure 1: Variation of viscosity of diesel, cottonseed oil and blends with various temperatures.

4.2. Brake thermal efficiency:

The brake thermal efficiency plots in Figure.2 shows an increase of brake thermal efficiency with increase in the engine load, as the fuels are preheated. The brake thermal efficiency of CSO increased from 28% to 28.8%. The blend containing 20%and 40% diesel, preheated to 70°C shows an increase in brake thermal efficiency, which is very close to diesel. The values are 30% and 30.5% as against 32.3% for diesel at 100% load. This is due to the reduction in viscosity, density and improved atomization, fuel-air mixture formation and increase in the heating value as the proportion of diesel in the blend increases.

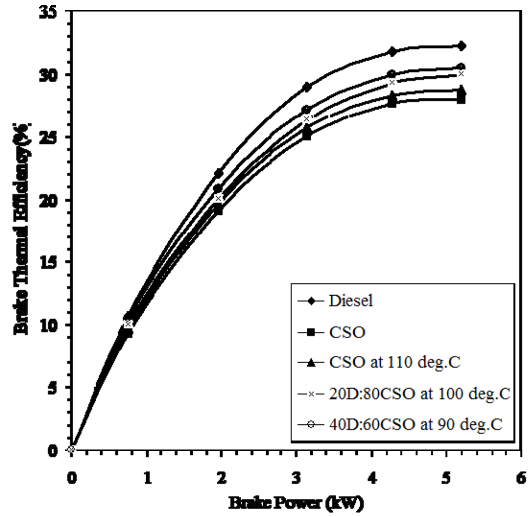

Figure 2: Variation of brake thermal efficiency with brake power.

4.3. Volumetric efficiency:

Figure.3 shows the variation of volumetric efficiency with brake power. There is an improvement of volumetric efficiency with preheat when compared to CSO at room temperature. The volumetric efficiency of preheated oil increased from 82.3% to 83% at the peak load. The trend is the same for the blends also. Volumetric efficiency is 84.6% for diesel and 84.12% for 40% preheated diesel blend. The low volumetric efficiency of neat CSO is due to its high exhaust gas temperature. High exhaust gas retained temperature will lead to heat the incoming fresh air and this will result with in reduction of volumetric efficiency. As seen in Figure. 4, the exhaust gas temperature decreases, when the fuel mixture is heated. Due to that, there is improvement in volumetric efficiency with preheated fuels, but it is still lower compared with diesel value of 84.6%.

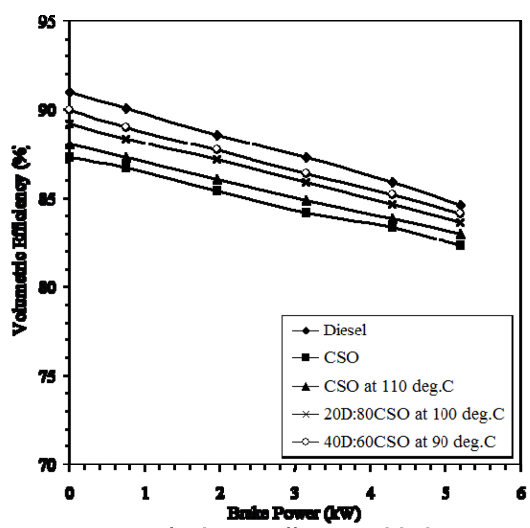

Figure 3: Variation of Volumetric efficiency with brake power.

4.4. Exhaust gas temperature:

The variation of exhaust gas temperature is shown in Figure.4. There is an increase in exhaust gas temperature with neat CSO. It is 445.1ºC for CSO and 407.3ºC for diesel at full load. This is mainly due to higher viscosity of CSO leads to late burning of fuel. There is a slight increase in exhaust gas temperature with preheated neat CSO. The exhaust gas temperature reduces as the proportion of diesel is raised due to the better vaporization of mixture. Exhaust gas temperatures is 423.5ºC for 20% and 416.1ºC for 40% preheated diesel blend at the peak load condition. The reduction in the exhaust gas temperature of the blends indicates that the premixed combustion of the preheated blend has improved. This is mainly due to the reduction in the viscosity of the fuel.

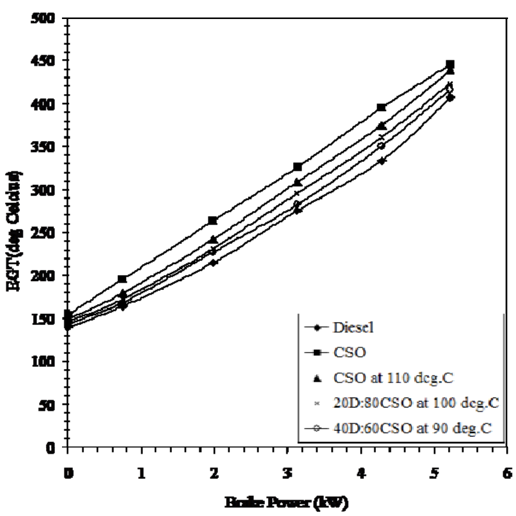

Figure 4: Variation of Exhaust gas temperature with brake power.

4.5. Smoke

Figure.5 shows the variation of Smoke emission with brake power for diesel, CSO and for the preheated blends. The results show that the smoke level increased with the power output of the engine for all the fuels. With preheated CSO, the smoke level is 3.6 BSU that is lower than unheated oil, which is 3.9 BSU. Preheated blends also showed the same trend. The smoke emission is 3.4 BSU with diesel and 3.5 BSU with the preheated 40% diesel blend. When compared to CSO, this value is low which indicates a better combustion. Still the trend at the full load is comparatively high for CSO and the blends.

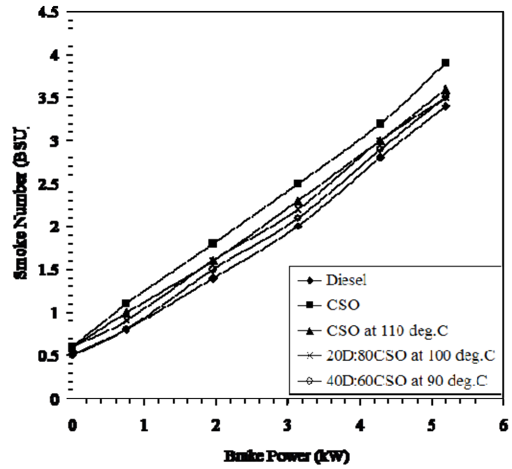

Figure 5: Variation of Smoke with brake power.

4.6. HC and CO emission:

Continuous exhaust gas sampling shows a significant reduction in the hydrocarbon and carbon monoxide emissions with the preheated CSO and the blends as compared to neat CSO. Nevertheless, through out the load range, the HC and CO emissions for CSO, preheated CSO and blends were higher than that for diesel. However, the HC and CO levels are less for preheated CSO when compared to neat CSO. This trend indicates that the combustion efficiency improve with preheat. The improved spray and fuel distribution inside the combustion chamber has resulted in better combustion rate and hence the reduction in the HC and CO emissions with preheat. The variation of HC and CO with brake power for the different fuels is shown Figure.6 and Figure.7. The HC and CO emissions reduce as the viscosity of the fuel decreases. These results indicate that the viscosity of the fuel influences the HC and CO emissions.

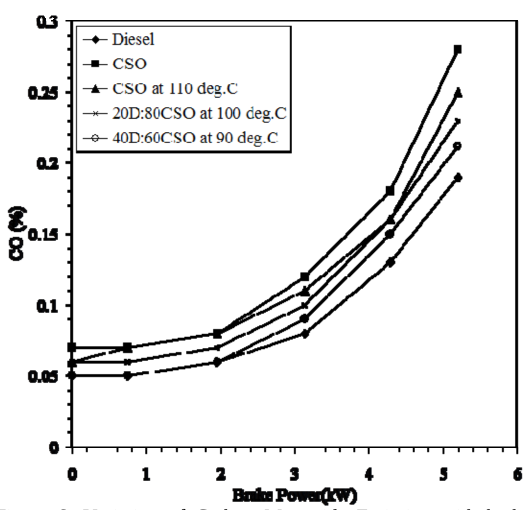

Figure 6: Variation of Carbon Monoxide Emission with brake power.

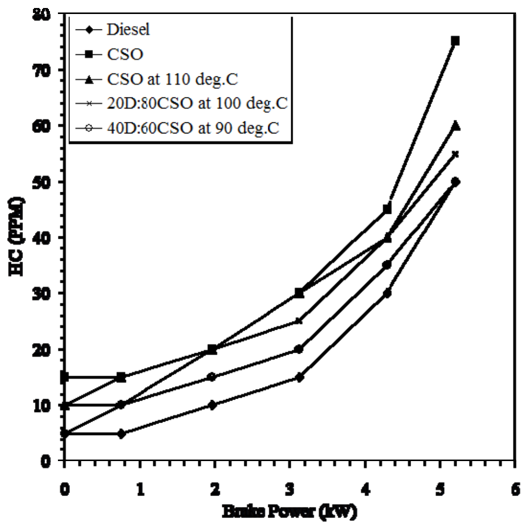

Figure 7: Variation of Hydrocarbon Emission with brake power.

4.7. Peak pressure and maximum rate of pressure rise:

Figure.8 and Figure.9 show the variation of peak pressure and max rate of pressure rise. The values with neat diesel is the highest followed by the preheated blends and cottonseed oil. The peak pressure with diesel is 73.21 bar followed by the 40% diesel blend whose value is 72.84 bar at the peak load. The increase in the pressure is due to the cracking of the double bond of the carbon chain, which might have produced light volatile compounds.

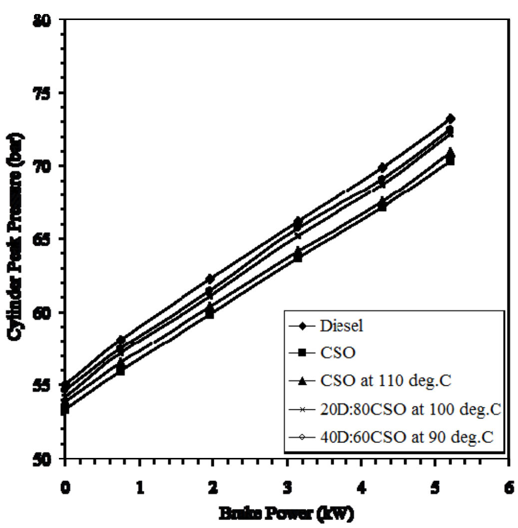

Figure 8: Variation of Cylinder Peak Pressure with brake power.

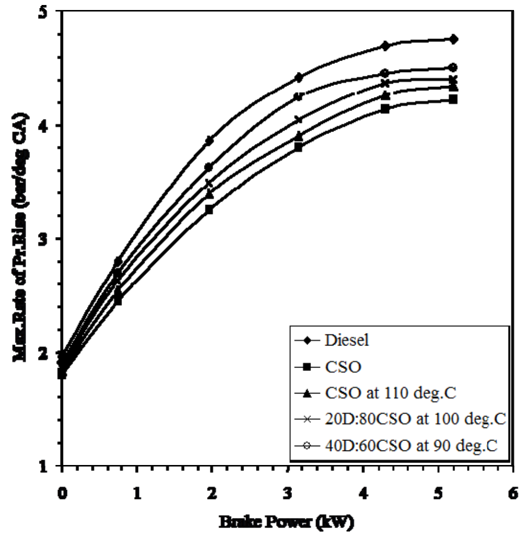

Figure 9: Variation of Maximum rate of pressure rise with brake power.

5. Conclusion

A single cylinder compression ignition engine was operated successfully on preheated and neat cottonseed oil. The following conclusions are drawn based on the experimental results at 5.2 kW load:

- Lower thermal efficiency (28%) is found in neat CSO compared to diesel (32.3%). However, preheating the mixture increases the thermal efficiency.
- The exhaust gas temperature is higher for CSO compared to diesel. This is due to the late burning of CSO. It is further reduced with preheated CSO and diesel mixture.
- Significant reduction in smoke level with preheated CSO and diesel mixture compared to neat CSO is observed. The improvement in volatility of preheated mixture is beneficial in improving the fuel evaporation resulting smoke reduction.
- NO emission for the CSO operation is 703 ppm and 756 ppm with diesel at full load. Marginal increase in NO emission with preheated mixture of CSO and diesel than neat CSO because of increased fuel temperature leads to high combustion temperature is observed.
- The concentration of premixed combustion phase is lower for CSO compared to diesel. However, the rate of heat being released improves with preheated CSO and diesel mixture.
- Combustion duration and ignition delay is longer with CSO as compared with diesel at all loads. There is a reduction in combustion duration and ignition delay with preheated mixture (40% diesel and 60% CSO) at 90°C.

It is concluded that the preheating the fuel mixture (40% diesel and 60% CSO) is the effective method to reduce emission and improving performance of a diesel engine.

References

[1] Recep Altin, Selim Cetinkaya and Huseyin Sardar Yucesu, "The potential of using vegetable oil fuels as fuel for diesel engines", International Journal of Energy conversion and management Vol. 42, 2001, 529-538.

[2] Y. Yoshimoto, M. Onodera and H. Tamaki, "Performance and emission characteristics of diesel engines fueled by vegetable oils", SAE Technical Paper Series , Paper No. 2001-01-1807/4227.

[3] Kensuke Nishi, Koji Korematsu and Junya Tanaka, "Potential of rape seed oil as a diesel engine fuel", SAE Technical Paper Series, Paper No.2004-01-1858.

[4] F. Karaosmanoglu, G. Kurt and T. Ozaktas, "Long term C.I engine test of sunflower oil", International journal of Renewable Energy, Vol. 19, 2000, 219-221.

[5] O. M. I. Nwafor and G. Rice, "Performance of rapessed oil methyl ester in diesel engine", International journal of Renewable Energy, 0960-1481 Vol. 95, 1995 00022-4.

[6] Dilip Kumar Bora, Milton Polly, Vikas Sandhuja and L. M. Das, "Performance evaluation and emission characteristics of a diesel engine using mahua oil methyl ester (MOME)", SAE Technical Paper Series, Paper No. 2004-28-0034.

[7] K. Babu and G. Devaradjane, "Vegetable oil and their derivatives of fuel for C.I engines: An Overview", SAE Technical Paper Series, Paper No. 2003-01-0767

[8] O. M. I. Nwafor and G. Rice, "Performance of rapeseed oil blends in a diesel engine", International Journal of Applied Energy, Vol.54, No.4, 1996, 345-354.

[9] P. K. Devan and N. V. Mahalakshmi, "Performance, emission and combustion characteristics of poon oil and its diesel blends in a DI diesel engine", Fuel, Vol. 88, 2009, 861-867.

[10] K. Pramanik, "Properties and use of jatropha curcas oil and diesel fuel blends in compression ignition engine", International Journal of Renewable Energy, Vol. 28, 2003, 239-248.

[11] Holman J P. "Experimental methods for engineers", New York: McGraw-Hill**.**

JJMIE
Volume 5, Number 3, June 2011
ISSN 1995-6665
Pages 241 - 245
Jordan Journal of Mechanical and Industrial Engineering

Reasons behind Energy Changes of the Jordanian Industrial Sector

Y. Abdallat [a], A. Al-Ghandoor*,[b], I. Al-Hinti [c]

[a] *Department of Industrial Engineering, Jordan University, Amman, Jordan*
[b] *Department of Industrial Engineering, The Hashemite University, Zarqa, Jordan*
[c] *Department of Mechatronics Engineering, German-Jordan University, Amman, Jordan*

Abstract

In order to identify main drivers behind changes in electricity and fuel consumptions in the industrial sector in Jordan; a Laspeyers decomposition technique was used to identify the factors affecting this demand during 1998-2005 years Changes have been disaggregated into production, structural, and efficiency effects. Results of the decomposition analysis prove that rapid increases in industrial production output had the most important implications on increasing energy demand in this sector which causes an annual energy increase of 10.9% yr^{-1}. However, these increases were countered mainly by efficiency gains and to a lesser extent by structural changes in the industrial sector. The analysis showed that the structural effect contributes to an annual energy decrease of around 2.28% yr^{-1} while the efficiency effect contributes to an annual energy decrease of 5.65% yr^{-1}.

Keywords: Decomposition; Laspeyers index; Jordan; Energy; Efficiency; Structural

1. Introduction

Jordan is considered among low-middle income countries, within the Middle East Region, with an average income per capita of about US$ 2,770, in 2007, and its population reached 5.723 million inhabitants [1, 2]. It suffers from a chronic lack of adequate supplies of natural resources including fresh water, crude oil and other commercial minerals. Thus, Jordan depends heavily on imports of crude oil, refined products and natural gas from neighboring Arab countries as main sources of energy. Its current imports of around 100,000 barrels of crude oil per day are placing the country under extreme economic pressures, especially with increasing unit price of oil in the international market. The annual energy bill has been rapidly increasing over the past few years due to high rates of population and economic growth combined with the consecutive increase in oil price. Consequently, there has been a growing concern about energy consumption and its adverse impact on the economy and environment, with special focus on the industrial sector, because its contribution accounted for about one third of final energy and electricity consumption.

In recent years, concerns about energy consumption in Jordan have been growing, especially in the industrial sector, which was probably affected the most by the economic and technological changes that the country has witnessed during the past two decades. Therefore, the provision of reliable information on industrial energy use is essential.

Decomposition techniques have been conducted extensively to better understand the historical variations in energy use, and three main factors have been identified in [3]: changes in the industrial activity (production effect), changes in the structure of production output over time (the structural effect), and changes in energy efficiencies of individual industries (the efficiency effect). This technique has been used to analyze energy changes in different countries [4-13]. Related literature can be found in [14-16]. This technique is based on economic index numbers; over one hundred of such indexes have been described by [17]. Comparisons and linkages between decomposition methods and economic index numbers can be found in literature [18-19]. An overview of several decomposition methods was outlined by [20-21].

In Jordan, there are several studies that analyzed current and future energy requirements for different sectors and industries [22-26]; however, few decomposition studies have been reported recently in Jordan. While the previous papers conducted by the authors [27-28] were concerned with the electricity consumption and did not take into consideration the fuel consumption in the Jordanian industrial sector, in this paper, the Laspeyers approach decomposition technique is applied to examine the role of production, structural, and efficiency effects that impact the Jordanian industrial energy demand (both fuel and electricity) during the period from 1998 to 2005. Between these years, there was rapid growth in the demand for energy in the Jordanian industries, led by strong growth in industrial activity and increasing penetrations of new facilities that are occupied with new technologies. This kind of research is useful for analysts and policy makers concerned with energy issues in Jordan, especially those interested in future directions of energy demand in Jordan.

* Corresponding author. e-mail: gandoor2002@yahoo.com

The paper is organized as follows: the next section presents the energy use in Jordan; section 3 describes the different data sources utilized in this study; section 4 presents a descriptive analysis of the industrial energy demand and production output growth; section 5 presents the decomposition analysis using Laspeyers decomposition technique; section 6 presents the results and discussions; and section 7 presents some concluding remarks.

2. Energy Use in Jordan

In 2005, Jordan's consumption of primary energy (crude oil and petroleum products, natural gas, renewable energy, imported electricity) amounted to 7.028×10^6 Ton Oil Equivalent (TOE) while the final energy consumption was 4.802×10^6 TOE. Final energy consumption in Jordan is mainly distributed between three major sectors: transportation, industrial, and residential. The distribution of final energy consumption among different sectors over the past five years is presented in Table 1[29]. It can be seen that the industrial sector is the second largest consuming sector of final energy The share of this sector has been nearly constant over the past few years at nearly 24% of final energy consumption.

Table 1: Sectoral distribution of the final energy consumption in Jordan during the period 2001-2005 (Thousand TOE)

Year	Sector				Total
	Transport	Industrial	Household	Other	
2001	1411 (38.2%)	826 (22.4%)	849 (23.0%)	606 (16.4%)	3692 (100%)
2002	1435 (37.7%)	846 (22.2%)	868 (22.8%)	662 (17.4%)	3811 (100%)
2003	1495 (37.0%)	878 (21.7%)	945 (23.4%)	722 (17.9%)	4040 (100%)
2004	1693 (37.4%)	1034 (22.8%)	1007 (22.2%)	792 (17.5%)	4526 (100%)
2005	1779 (37.0%)	1159 (24.1%)	1060 (22.1%)	804 (16.7%)	4802 (100%)

3. Description of Data Sources

This study examines and carefully distinguishes between the *site* and *embodied* energy content of electricity. The embodied energy value accounts for the generation and transmission energy losses associated with electricity production, while the site electricity value includes only the site heat value of electricity (3,600 *kJ/kWh*). Electricity used in the manufacturing sector mainly originates from two sources: purchased electricity and electricity produced onsite. In this paper, the heat rate of the electricity is defined as the ratio of the site energy content of electricity produced to the total energy content of fuel input used to produce it. The heat rate of the electricity depends on the generation technology mix used to provide the electricity to the manufacturing sector and has been estimated by as 34% [30]. In this study, the embodied energy has been used for the analyses between years 1998 and 2005. All data were retrieved from various years of Jordan's statistical yearbooks as published by different governmental agencies. The focus on this time frame largely reflects the availability of data as required for the purposes of this study.

Ideally, the fine level of disaggregation level is desirable in order to accurately disentangle the structural effect from efficiency effect [8]. However, the choice for a level of sector disaggregation is mainly dictated by the data availability. Due to data availability constraint, the Jordanian industrial sector was disaggregated into seven sub-sectors; namely, mining of chemical and fertilizer minerals, paper, plastics, petroleum, cement, iron and steel, and other industries[1].

The source of information for the annual energy consumption is the Jordanian National Electric Power Company [31] and the Jordanian department of statistics [32]. It is worthwhile mentioning here that all disaggregated physical energy quantities in a specific period for all Jordanian industries were calculated by converting the monetary values (which are the only available sources of energy data) of each energy source to its corresponding physical value by using the average fuel price in that period. The energy values used in this study are the summation of fuel energy and the embodied energy of electricity. Production output is based on the value added as reported by the Jordanian department of statistics [32]. Use of this value avoids the issue of 'double counting' when a product produced by one industry is an input for another industry. A change in the value added from one year to another includes an increase (or decrease) in price resulting from inflation (deflation); such changes do not reflect a change in output. Therefore, before using estimates of the added values as an output measure, they were adjusted for the effect of changes in price using the producer price index (1999 constant) obtained from the Department of Statistics [33].[2]

4. Historical Jordanian Industrial Production and Energy Demand

As shown in Figure 1, a constant rapid growth of the Jordanian industrial production with an annual average growth rate of 13.2% has been witnessed between years 1998 and 2005. The value added of the industrial sector has increased from 1,468 million dollars in 1998 to 2,822 million dollars in 2005 at constant 1999 prices.

As shown from this table, the overall production outputs of all industries have increased between 1998 and 2005 years (as indicated by positive annual growths); however, these increases are at different rates. As an example, the "Other industries" sub-sector (non intensive energy industries) has a dominant share within industrial sector and its importance has increased during this period: from a share of about 63.1% in 1998 to about 69.6% in 2005 with production output average annual growth of 16%; an average growth greater than the total industrial production annual growth. Chemicals manufacture, tobacco products, and food products were among the

[1] This disaggregation level is justified since the mining of chemical and fertilizer minerals, paper, plastics, petroleum, cement, and iron and steel sub-sectors are the main intensive industries in Jordan. In 2005, they contributed to about 70% of total energy demand. The "Other" industries include food, tobacco, textiles, wearing apparel, tanning and dressing of leather, wood, publishing and printing media, chemicals, fabricated metals, machinery, transportation, and furniture industries. These industries were grouped together since no individual data is available for each of them and such industries can be considered as electricity non-intensive industries.

[2] The data set can be obtained from the corresponding author upon request.

largest contributors to the non intensive industries. On the other hand, mining of chemicals and fertilizer minerals (ex., potash and phosphate) is the next important industrial activity (intensive energy industry) but its share has declined from 17.9% in 1998 to 14.1% in 2005 with average annual production output growth rate of 7.3% which is much lower than the total industrial production output growth rate. A similar situation can be observed for petroleum, cement, and plastics sub-sectors. These industries can also be considered as intensive energy industries. Although the average annual production output growth for iron and steel, and paper industries (intensive electricity industries) have increased during this period; their shares are small to have significant impacts on annual energy demand. From the above analyses, one can conclude that there was a shift in Jordanian industrial structure toward non intensive energy industries; and hence, a contribution due to the structural effect on energy demand change during the study period is expected

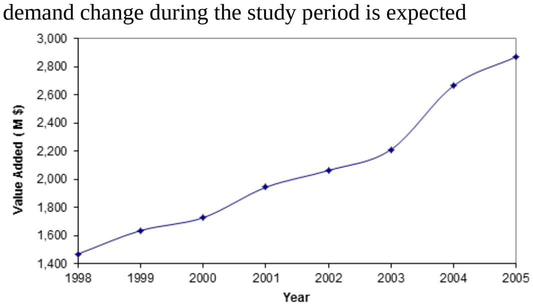

Figure 1: Growth in industrial value added in Jordanian industrial sector.

Table 2: Shares of value added and average annual growth rate of the manufacturing industries (%).

Industry	Year								Average Annual Growth (%)
	1998	1999	2000	2001	2002	2003	2004	2005	
Mining of chemicals and fertilizer minerals	17.9	16.1	15.1	13.6	12.7	12.2	12.5	14.1	7.3
Paper	1.6	2.2	2.1	2.5	2.6	2.4	2.5	2.4	27.1
Plastics	2.1	2.4	2.2	2.5	2.7	2.6	2.2	2.0	12.1
Petroleum	5.9	5.4	5.1	3.9	4.0	3.6	3.2	2.4	4.3
Cement	6.9	6.6	6.3	6.4	5.8	5.6	5.4	5.2	6.4
Iron and Steel	2.5	3.1	3.2	3.3	3.2	3.7	3.8	4.3	32.2
Others	63.1	64.2	66.0	67.8	69.0	69.9	70.4	69.6	16.0
Total	100.0	100.0	100.0	100.0	100.0	100.0	100.0	100.0	13.2

As shown in Figure 2, changes in energy demand in the Jordanian industrial sector had an approximately constant growth with an average annual growth rate of 3.4% which is much lower than the annual growth for production output. Table 3 summarizes the average annual growth rates and the shares of energy use for the seven disaggregated sub-sectors.

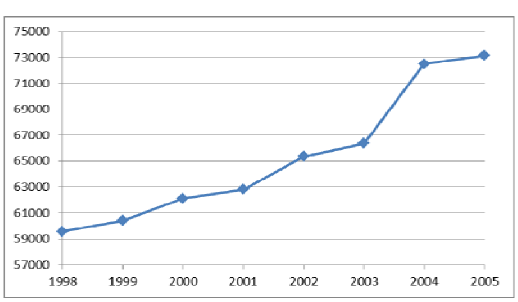

Figure 2: Growth in energy demand (TJ) in the Jordanian industrial sector.

Table 3: Shares of energy use and annual growth rate of the manufacturing industries (%).

Industry	Year								Average Annual Growth (%)
	1998	1999	2000	2001	2002	2003	2004	2005	
Mining of chemicals and fertilizer minerals	25.1	21.9	20.5	18.7	18.0	18.2	18.4	19.4	-0.6
Paper	2.0	2.1	2.8	3.1	3.0	2.9	2.8	2.8	9.9
Plastics	1.8	2.1	2.3	2.2	2	2	2	2	4.9
Petroleum	16.2	17.8	18.3	15.8	15.5	15.8	15.1	14.9	1.9
Cement	25.9	24.0	22.9	26.8	26.9	26.0	26.6	26.2	3.6
Iron and Steel	3.1	4.2	3.3	3.6	3.7	4.6	5.1	5.3	16.1
Others	25.9	27.9	30.0	29.7	30.8	30.5	30.0	29.5	5.8
Total	100.0	100.0	100.0	100.0	100.0	100.0	100.0	100.0	3.4

It is clearly shown from this table that all types of industries have annual growth of energy use smaller than the annual growth of production output shown in Table 2 which means that all industries gained improvement in energy efficiency over the study. A general conclusion that can be drawn here is that there was a significant energy efficiency improvement during the 1998-2005 period.

5. Methodology

The methodology adopted in this study has been used before in [27]. Three factors will be studied in this paper; namely, the production, structural, and efficiency factors. The production factor is a measure of changes in total industrial production output as measured by constant value added from one year to another. Structural factor is a measure of production shift from/to energy intensive to/from energy non intensive industries while the efficiency factor is an indication of the amount of energy used per unit of constant value added of individual industries. Decreases in energy intensities mean improvement in energy efficiency and vice versa. Improvement in energy efficiency is associated with the technical characteristics of the equipment being run, including fans, compressors, electric furnaces, boilers, ect.

The total change in industrial energy demand between t and 0 years can be expressed as follows:

$$(\Delta E_{TOT})_{0,t} = (\Delta E_{OUT})_{0,t} + (\Delta E_{STR})_{0,t} + (\Delta E_{EFF})_{0,t} \quad (1)$$

Where,

$(\Delta E_{TOT})_{0,t}$: Total change in industrial energy demand between *t* and 0 years (TJ).

$(\Delta E_{OUT})_{0,t}$: Change in industrial energy demand due to changes in activity between t and 0 years (TJ).

$(\Delta E_{STR})_{0,t}$: Change in industrial energy demand due to structural effect between t and 0 years (TJ).

$(\Delta E_{EFF})_{0,t}$: Change in industrial energy demand due to efficiency effect between *t* and 0 years (TJ).

According to the modified Laspeyers decomposition method proposed by [8], production, structural, and efficiency factors can be estimated as follows:

$$\Delta E_{OUT} = (Y_t - Y_0)\sum_i (y_{i,0} I_{i,0}) \tag{2}$$

$$\Delta E_{STR} = \sum_i (Y_t y_{i,t} I_{i,t} - Y_t y_{i,0} I_{i,t}) = Y_t \sum_i (y_{i,t} - y_{i,0}) I_{i,t} \tag{3}$$

$$\Delta E_{EFF} = \sum_i (Y_t y_{i,t} I_{i,t} - Y_t y_{i,t} I_{i,0}) = Y_t \sum_i (I_{i,t} - I_{i,0}) y_{i,t} \tag{4}$$

Where,

Y = total industrial production value added (Million $ in 1999 constant prices).
Y_i = production value added of industry i (Million $ in 1999 constant prices).
y_i = production share of industry i (= Y_i/Y).
I_i = energy intensity of industry i (= E_i/Y_i).
Y = total industrial production value added (Million $ in 1999 constant prices).
Y_i = production value added of industry i (Million $ in 1999 constant prices).
y_i = production share of industry i (= Y_i/Y).
I_i = energy intensity of industry i (= E_i/Y_i).

The summation is taken over all sub-sectors. A change in production factor is obtained by allowing production to change with time, while holding all others constant. Changes in structure are accounted for by differences between the amount of energy use that would be used if each sub-sectoral activity at year t was produced at the energy intensity of year 0 and if the aggregate production at year t was composed in the same way as at year 0. Changes in efficiency represent the difference between the observed energy use and what the energy use would be if each sub-sectoral activity at year t was produced at the energy intensity of year 0.

6. Results and Discussion

By implementing the methodology described earlier, the growth in energy demand between years 1998 and 2005 can be decomposed into production, structural, and efficiency factors. These factors as vary with time are shown in Figure 3. During this period, the production effect contributes largely to this increase, and cause 10.9% yr^{-1} increase in energy use during this period. On the other hand, improvements in energy efficiency accounts for 5.65% yr^{-1} decline in energy use. The structural effect had the least effect during this period and results in 2.28% yr^{-1} decline in energy use. The three affects together make the energy use to increase at annual rate of 3.4% yr^{-1}.

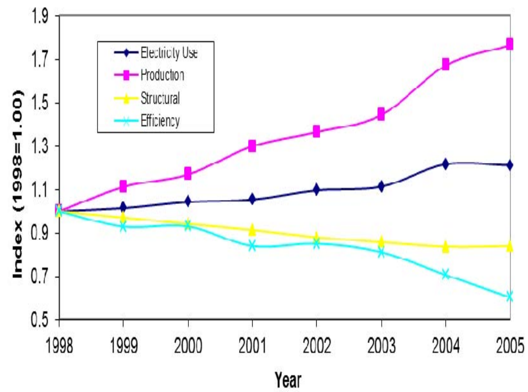

Figure 3: Time series decomposition for the Jordanian industrial energy demand.

In order to gain more insights for the energy demand changes between years 1998 and 2005; results of the analysis are compared between 1998 and 2005 and shown in Table 4. Again, it is obvious that the most important factor that has shaped industrial energy demand in Jordan was the production effect. However, decreases in the energy intensity countered this increase in demand. By 2005, industrial energy intensity was only 67% of 1998 value. As discussed before, there was a shift from energy-intensive industries in Jordan during the study period; however, this structural shift was not the most important factor. In comparison with an approximate 14,627 TJ decrease in demand between 1998 and 2005 attributed to structural effect, a decrease of 28,086 was attributed to the efficiency effect.

Table 4: Jordanian industrial sector energy demand decomposition results between 1998 and 2005 years.

	2005 compared to 1998
	Contribution (TJ)
Production effect	56,748
Structural effect	-14,627
Efficiency effect	-28,086
Total	14,035

7. Conclusion

This paper showed that the main driver behind the energy demand increase between years 1998 and 2005 was the rapid increase in industrial production output. However, significant improvements on efficiency effect, due to implying innovation, technical change, diffusion and adaptability to more efficient technologies and the structural changes in the industrial sector has countered this rapid increase.

These kind of studies give a depth understanding of the energy development in the past in order to give policy makers and analysts indication of how energy demand, and required capacity, may change into future. This paper can be considered as a milestone for improving and restructuring the Jordanian industrial sector in the near future for purposes of reducing its energy use.

References

[1] Department of Statistics, DoS. Statistical Yearbook 2005, Amman, Jordan; 2006.

[2] National Population Committee. National population strategy. General Secretariat of National Population Committee. Amman, Jordan; 2000.

[3] B.W. Ang, F.Q. Zhang, K.H. Choi, "Factorizing changes in energy and environmental indicators through decomposition". Energy, Vol. 23, No. 6, 1998, 489-495.

[4] G. Ostblom, "Energy use and structural changes: factors behind the fall in Sweden's energy output ratio". Energy Economic, Vol. 4, No. 1, 1982, 21-28.

[5] C. Jenna, R. Cattell, "Structural changes and energy efficiency in industry". Energy Economics, Vol. 5, No. 2, 1983, 114-123.

[6] W.R. Reitler, H. Schaefer, "Analysis of the factors influencing energy consumption in industry: a revised method". Energy Economics, Vol. 9, No. 3, 1987, 145-148.

[7] T. Gardner, M. Elkhafif, "Understanding industrial energy use: structural and energy intensity changes in Ontario industry". Energy Economics, Vol. 20, 1998, 29-41.

[8] Z. Zhang, "Why did energy intensity fall in China's industrial sector in the 1990s?. The relative importance of structural change and intensity change". Energy Economics Vol. 25, 2003, 625-638.

[9] P. Gonzalez, R. Suarez, "Decomposing the variation of aggregate electricity intensity in Spanish industry". Energy, Vol. 28, 2003, 171-184.

[10] S. Bhattacharyya, A. Ussanarassamee, "Changes in energy intensities of Thai industry between 1981 and 2000: a decomposition analysis". Energy Policy, Vol. 33, 2005, 995-1002.

[11] V. Ediger, O. Huvaz, "Examining the sectoral energy use in Turkish economy (1980-2000) with the help of decomposition analysis". Energy Conversion and Management, Vol. 47, 2006, 732-745.

[12] P. Steenhof, "Decomposition of electricity demand in China's industrial sector". Energy Economics, Vol. 28, 2006, 370-384.

[13] A. Al-Ghandoor, P.E. Phelan, R. Villalobos, B.E. Phelan, "U.S. manufacturing aggregate energy intensity decomposition: the application of multivariate regression analysis". International Journal of Energy Research, Vol. 32, 2008, 91-106.

[14] H.G. Huntington, "The impact of sectoral shifts in industry on U.S. energy demand". Energy, Vol. 14, No. 6, 1989, 363-372.

[15] B.W. Ang, "Decomposition methodology in industrial energy demand analysis". Energy, Vol. 20, No. 11, 1995, 1081-1095.

[16] B.W. Ang, F.Q. Zhang, "Survey of index decomposition analysis in energy and environment studies". Energy, Vol. 25, No. 12, 2000, 1149-1176.

[17] Fisher I. The making of index numbers. Houghton Mifflin: Boston; 1972.

[18] G. A. Boyd, D.A. Hanson, T. Sterner, "Decomposition of changes in energy intensity: a comparison of the Divisia Index and other methods". Energy Economics, Vol. 10, No. 4, 1998, 309-312.

[19] F.L. Liu, B.W. Ang, "Eight methods for decomposing the aggregate energy-intensity of industry". Applied Energy, Vol. 76, 2003, 15-23.

[20] C. Liu, "A study on decomposition on industry energy consumption". International Research Journal of Finance and economics, Issue 6, 2006, 73-77.

[21] Lu, S. Lin, C. Lewis, "Decomposition and decoupling effects of carbon dioxide emission from highway transportation in Taiwan, Germany, Japan, and South Korea. Energy Policy, Vol. 35, No. 6, 2007, 3226-3235.

[22] A. Tamimi, "Energy situation in Jordan". Energy Conversion and Management, Vol. 34, No. 6, 1993, 519-521.

[23] J.O. Jaber, M. Mohsen, S. Probert, M. Alees, "Future electricity-demands and greenhouse-gas emissions in Jordan". Applied Energy, Vol. 69, 2001, 1-18.

[24] J.O. Jaber, "Future energy consumption and greenhouse gas emissions in Jordanian industries". Applied Energy, Vol. 71, 2002, 15-30.

[25] B. Akash, M. Mohsen, "Current situation of energy consumption in the Jordanian industry". Energy Conversion and Management, Vol. 44, 2003, 1501-1510.

[26] A. Al-Ghandoor, I. Al-Hinti, J.O. Jaber, S.A. Sawalha, "Electricity consumption and associated GHG emissions of the Jordanian industrial sector: Empirical analysis and future projection". Energy Policy, Vol. 36, 2008 , 258-267.

[27] A. Al-Ghandoor, I. Al-Hinti, A. Mukattash, Y. Abdallat, "Decomposition analysis of electricity use in the Jordanian industrial sector". International Journal of Sustainable Energy, Vol. 29, 2010, 233-244.

[28] A. Al-Ghandoor, J.O. Jaber, M. Samhouri, I. Al-Hinti, Understanding aggregate electricity intensity change of the Jordanian industrial sector using decomposition technique". International Journal of Energy Research, Vol. 33, 2009, 255-266.

[29] Ministry of Energy and Mineral Resources. Annual Report 2005, Amman, Jordan; 2006.

[30] A. Al-Ghandoor, J.O. Jaber, I. Al-Hinti, "Assessment of energy and exergy utilizations in the Jordanian utility sector". Jordan Journal for Mechanical and Industrial Engineering, Vol. 3, No.1, 2009, 1-8.

[31] National Electric Power Company, NEPCO. Annual report 1998-2005. Amman, Jordan; 1999-2006.

[32] Department of Statistics, DoS. Statistical Yearbook 1998-2005. Amman, Jordan; 1999-2006.

[33] Department of Statistics, DoS. Price indices. Retrieved on Dec. 15, 2010 from http://www.dos.gov.jo/sdb_ec/sdb_ec_e/index.htm), Amman, Jordan.

JJMIE

Volume 5, Number 3, June 2011
ISSN 1995-6665
Pages 247 - 253

Jordan Journal of Mechanical and Industrial Engineering

Salt Fog Corrosion Behavior of Nanostructured TiAlN and AlCrN Hard Coatings on ASTM-SA213-T-22 Boiler Steel

V. Chawla*,[a], D. Puri[a], S. Prakash[a], B. Sidhu[b]

[a] Metallurgical & Materials Engineering Department, I.I.T. Roorkee, Roorkee-247667, India

[b] Mechanical Engineering Department, G.N.D.E.C., Ludhiana-142021,India

Abstract

In this work, TiAlN and AlCrN coatings were deposited on ASTM-SA213-T-22 boiler steel using Balzer's rapid coating system (RCS) machine under a reactive nitrogen atmosphere. The corrosion resistance of the substrate, TiAlN-coated and AlCrN-coated samples in a 5 wt% NaCl solution was evaluated and compared by salt fog (spray) test for 24 hrs, 48 hrs and 72 hrs. The weight loss per unit area increases with the duration of the test. The samples were monitored and analyzed by using Weight loss measurement, XRD and SEM/EDAX techniques. The weight loss per unit area in case of nanosructured thin TiAlN coating is less than as compared to the nanostructured AlCrN coating and uncoated boiler steel in all test conditions.

Keywords: Salt fog test; Physical vapor deposition; Corrosion; Nanostructured coatings; Pitting

1. Introduction

In a wide variety of applications, materials have to operate under severe conditions such as erosion, corrosion and oxidation at higher temperature in hostile chemical environments. Therefore, surface modification of these components is necessary to protect them against various types of degradation [1]. Many methods to modify the surface of a material have existed for a much longer time , but a formal definition of the discipline of surface engineering was given only a decade ago [2]. One only has to think about the fire hardening of wooden spears - the formation of a carbonized surface on the spear tip – a practice already known in the Stone Age. Surface modification technique i.e. coatings provide a way of extending the limits of the use of the materials at the upper end of their performance capabilities, by allowing the mechanical properties of the substrate materials to be maintained while protecting against wear, oxidation and corrosion [3]. Coating technology is one of the more rapidly growing technologies in the field of materials [4].

Deterioration of the materials due to marine salts in coastal regions has been, for many years, a significant and ongoing problem. Marine salts adversely affect the durability of the infrastructure and reduce its service life [5]. The sea spray, composed primarily of seawater along with particles naturally generated by the action of wind on the seawater surface, introduces ionic species into the atmosphere, principally chlorides and sulphates [5]. The air containing sea spray causes accumulative deposition of ions on the external surface of structures that penetrate the interior of the material through ionic diffusion causing its degeneration. Such environments are extremely dangerous to the materials as salts can penetrate and crystallize inside the material, causing deterioration of the physical infrastructure. As reported by Dobrzanski et al., [6]; the chloride-rich seawater is a harsh environment that can attack the materials by causing pitting and crevice corrosion. Every engineering metal or alloy is susceptible to pitting.

As reported by Bao et al., [7]; it seems no research works have been conducted on the corrosion behavior of high temperature corrosion resistant coatings in Cl-containing marine environment. Therefore, it is meaningful to investigate the ambient environmental corrosion behavior of substrate and coatings in accelerating mode, i.e., by salt spray (Fog) tests. Therefore, the present work has been focused to compare the corrosion behavior of nanostructured thin (by physical vapor deposition process) TiAlN and AlCrN coatings on ASTM-SA213-T-22 boiler steel, by salt spray tests in 5.0 wt% NaCl solution.

2. Experimental Details

2.1. Development of coatings:

TiAlN and AlCrN coatings; with a thickness around 4µm, were deposited on low-carbon steel ASTM-SA213-T-22, which has a wide range of applications in boilers, especially when the service conditions are stringent from the point of temperature and pressure. The actual chemical composition of the substrate steel analyzed with the help of Optical Emission Spectrometer of Thermo Jarrel Ash (TJA 181/81), USA make. The actual chemical composition of the T-22 has been analyzed with the help

* Corresponding author. e-mail: vikkydmt@gmail.com

of Optical Emission Spectrometer of Thermo Jarrel Ash (TJA181/81), U.S.A make. Normal and actual chemical composition is reported in Table 1. Specimens with dimensions of approximately 20mm x 15mm x 5mm were cut from the alloy sheet. Polished using emery papers of 220, 400, 600 grit sizes and subsequently on 1/0, 2/0, 3/0, and 4/0 grades, and then mirror polished using cloth polishing wheel machine with 1µm lavigated alumina powder suspension. The specimens were prepared manually and all care was taken to avoid any structural changes in the specimens. The nanostructured thin TiAlN and AlCrN coatings; with a thickness around 4µm, were deposited on the substrates at Oerlikon Balzers Coatings India Limited, Gurgaon, India. A front-loading Balzer's rapid coating system (RCS) machine (make Oerlikon Balzers, Swiss) was used for the deposition of the coatings. The grain size of the thin films was estimated by Scherrer formula from XRD diffractogram and by Atomic force microscopy (AFM; Model: NTEGRA, NT-MDT, Ireland). The grain size for TiAlN and AlCrN coatings was found 18 nm and 25 nm respectively. The details of the coating parameters and coating characterization have been reported in another paper (communicated).

Elements	C	Mn	Si	S	P	Cr	Mo	Fe
Nominal	0.15	0.3-0.6	0.5	0.03	0.03	1.9-2.6	0.87-1.13	Bal.
Actual	0.1658	0.3559	0.1159	0.001	0.020	2.6460	0.9027	Bal.

Table 1: Chemical composition (wt %) of T-22 Boiler Steel (ASTM code SA213-T-22).

2.2. Salt spray (Fog) testing:

The ASTM B117 Salt Fog test was used to evaluate the performance of the uncoated and nanostructured thin TiAlN and AlCrN coatings. The salt fog test is an accelerated corrosion test by which samples exposed to the same conditions can be compared. The samples are exposed to a salt fog generated from a 5% sodium chloride solution with a pH between 6.5 and 7.2 in salt fog testing set up (HSK 1000, Heraeus Votsch, Germini) as shown in Fig.1. The salt solution employed was prepared with NaCl analytical grade reagent with minimum assay 99.9 % supplied by Qualigens Fine Chemicals, Mumbai, India and deionised water. All the samples were placed in the salt fog chamber for 24 Hrs, 48 Hrs and 72 Hrs. Photographs were taken before and subsequent to exposure to document the surface conditions. Initial weight and dimensions were measured. The uncoated as well as the coated specimens were polished down to 1µm alumina wheel cloth polishing to obtain similar condition on all the samples before salt fog testing.

Figure 1: Experimental set-up for Salt spray (Fog) testing (a) Salt fog testing set up, (b) Salt fog chamber, (c) Interior view of chamber.

2.3. Analysis of the corroded specimens:

After exposure; samples were monitored and analyzed by using XRD and SEM/EDAX techniques. Visual examination was made after the completion of the tests and the macrographs of the corroded specimens were taken. Surface SEM analysis of the corroded specimens was conducted using Field emission scanning electron microscope (FEI Company, Quanta 200F) with EDAX attachment. EDAX analysis at few points of interest was taken. XRD analysis was carried out for the as coated specimens to identify the various phases present on their surfaces. The X-ray diffraction patterns were obtained by a Bruker AXS D-8 Advance Diffractometer (Germany) with CuKα radiation and nickel filter at 30 mA under a voltage of 40 kV. The specimens were scanned with a scanning speed of 2o/min in 2θ range of 20o to 120o and the intensities were recorded.

Before salt fog testing; the samples were cleaned in acetone, dried, weighed to an accuracy of 1×10-5 g using an electronic balance. After exposure; samples were monitored and analyzed by using XRD and SEM/EDAX techniques. Then all the samples were cleaned in running water not warmer than 38°C to remove salt deposits from the surface and then immediately dried with compressed air. The final weight was measured and then the weight loss per unit area was calculated.

3. Results and Discussion

All the uncoated and nanostructured thin TiAlN and AlCrN coated ASTM-SA213-T-22 boiler steel samples were placed in the salt fog chamber for 24 Hrs, 48 Hrs and 72 Hrs. Photographs were taken before and subsequent to exposure to document the surface conditions. Initial weight and dimensions were measured. After exposure; samples were monitored and analyzed by using XRD and SEM/EDAX techniques. Then all the samples were cleaned in running water not warmer than 38°C to remove salt deposits from the surface and then immediately dried with compressed air.

The macro morphologies of the uncoated and nanostructured thin TiAlN and AlCrN coated T-22 boiler steel exposed to salt fog test for 24 Hrs, 48 Hrs and 72 Hrs; are depicted in Fig.2. The uncoated T-22 boiler steel suffered severe corrosion in all three test conditions i.e. 24 Hrs, 48 Hrs and 72 Hrs (Fig.2.A). The brownish colored corrosion product on the surface of the samples and corrosion pits are visible. The nanostructured coated samples have shown resistance to the corrosion as compared to the uncoated T-22 boiler steel. The nanaostructured TiAlN coatings have shown negligible corrosion products in case of 24 Hrs study, but for 48 Hrs and 72 Hrs studies, these have shown the formation of some corrosion products (Fig.2.B). In case of nanostructured AlCrN coating, some corrosion products can be seen on the surface in all the three test conditions but still very less as compared to the uncoated T-22 boiler steel.

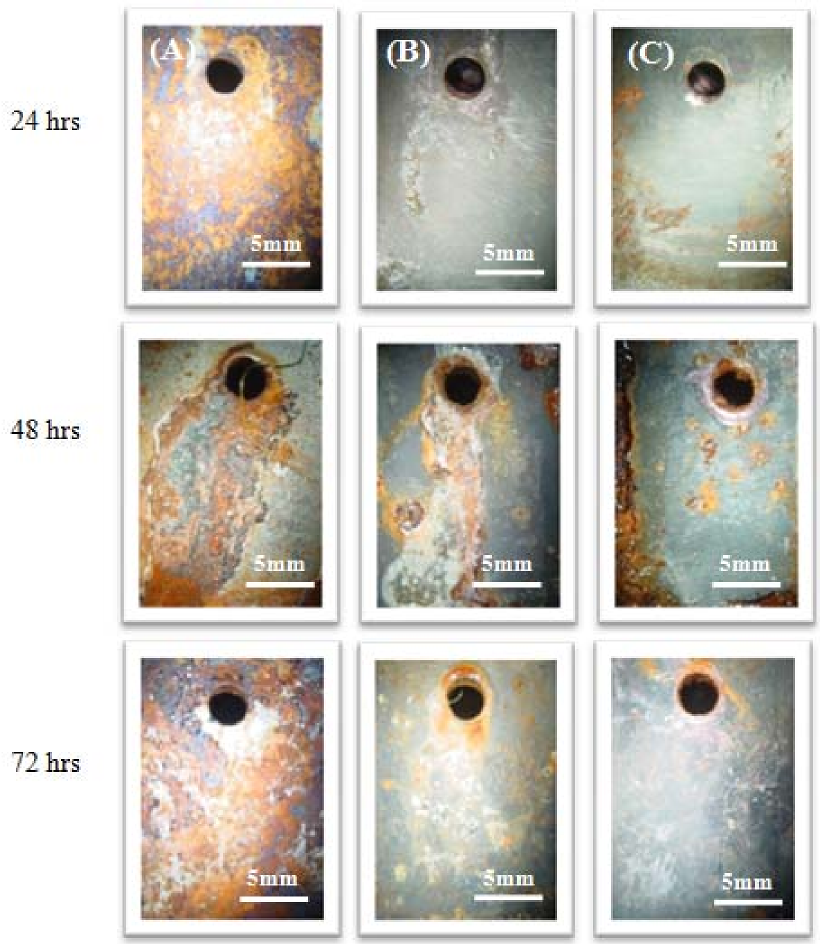

Figure 2: Surface macrographs of uncoated and coated ASTM-SA213-T-22 boiler steel subjected to salt-fog testing (5% NaCl) : (A) Uncoated T-22 boiler steel subjected to 24hrs, 48hrs and 72 hrs testing; (B) Nanostructured TiAlN coating subjected to 24hrs, 48hrs and 72 hrs testing; (C) Nanostructured AlCrN coating subjected to 24hrs, 48hrs and 72 hrs testing.

Figure.3 shows the surface SEM images of uncoated and nanostructured TiAlN and AlCrN coated T-22 boiler steel exposed to salt fog test for 24 Hrs. As can be seen in Fig.3(a), massive corrosion products were accumulated on the surface of uncoated T-22 boiler steel. The EDAX analysis at some locations of interest points out the presence of iron and oxygen on the corroded surface (Point 1 and 2 in Fig.3). In case of nanostructured thin TiAlN and AlCrN coatings; no corrosion products were visible (Fig.3.b & c). The EDAX point analysis (Point 3 to 6 in Fig.3) revealed the presence of the coating elements with negligible presence of Fe and O. So, in case of 24 Hrs test conditions; the nanostructured thin coatings have performed well and protected the substrate material.

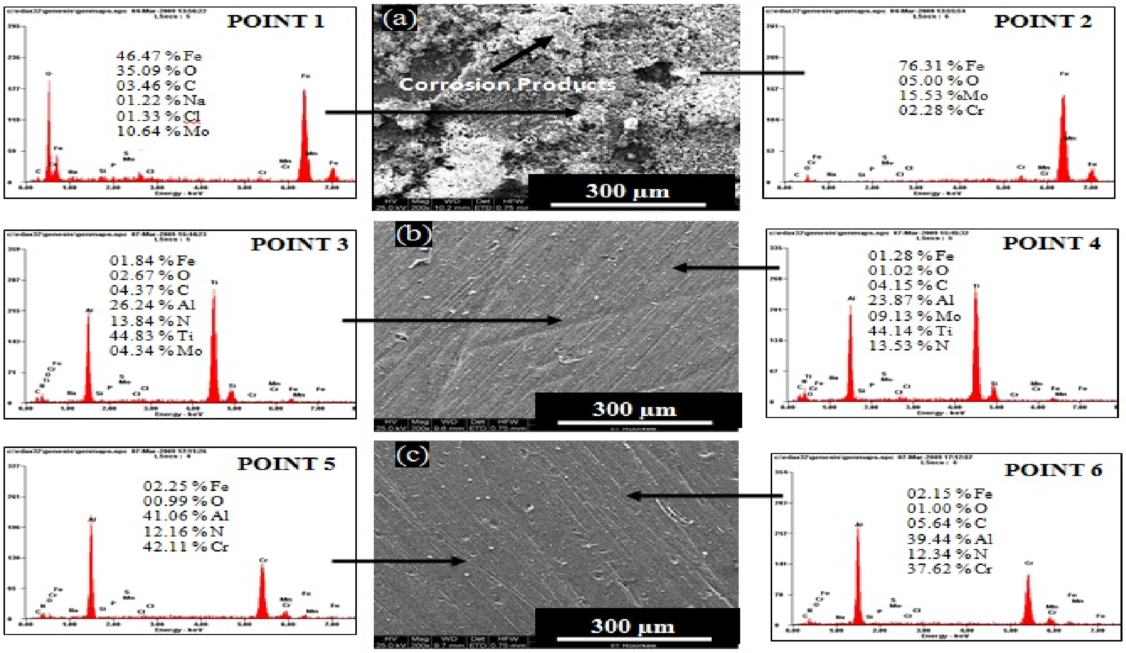

Figure 3: Surface macrographs of uncoated and coated ASTM-SA213-T-22 boiler steel subjected to salt-fog testing (5% NaCl) for 24 hrs: (a) Uncoated ASTM-SA213-T-22 boiler steel (b) Nanostructured TiAlN coating (c) Nanostructured AlCrN coating.

Figure.4 shows the surface SEM images of uncoated and nanostructured TiAlN and AlCrN coated T-22 boiler steel exposed to salt fog test for 48 Hrs. The uncoated T-22 boiler steel has shown severe corrosion as shown in Fig.4 (a). Corrosion cracks and corrosion products can be seen on the surface. The EDAX analysis shows the presence of Fe and O as the main elements along with some Mn, Cl and Na. As can be seen in Fig.4 (b & c), corrosion cracks were observed on the surface of as-deposited nanostructured TiAlN and AlCrN coatings after salt spray tests. Massive corrosion products were accumulated around the corrosion crevice. Obviously, severer corrosion would proceed in the as-deposited nanostructured thin coatings through the cracks, and cause coating cracking and fracture damage in the subsequent service at elevated temperatures. EDAX analysis (Point 3 and 4 in Fig.4) in case of nanostructured TiAlN coating indicates the products were composed of Fe and O. The corrosion products in case of nanostructured AlCrN coating were found rich in iron and oxygen with some amount of Al, Cr and Mn (Point 3 and 4 in Fig.4).

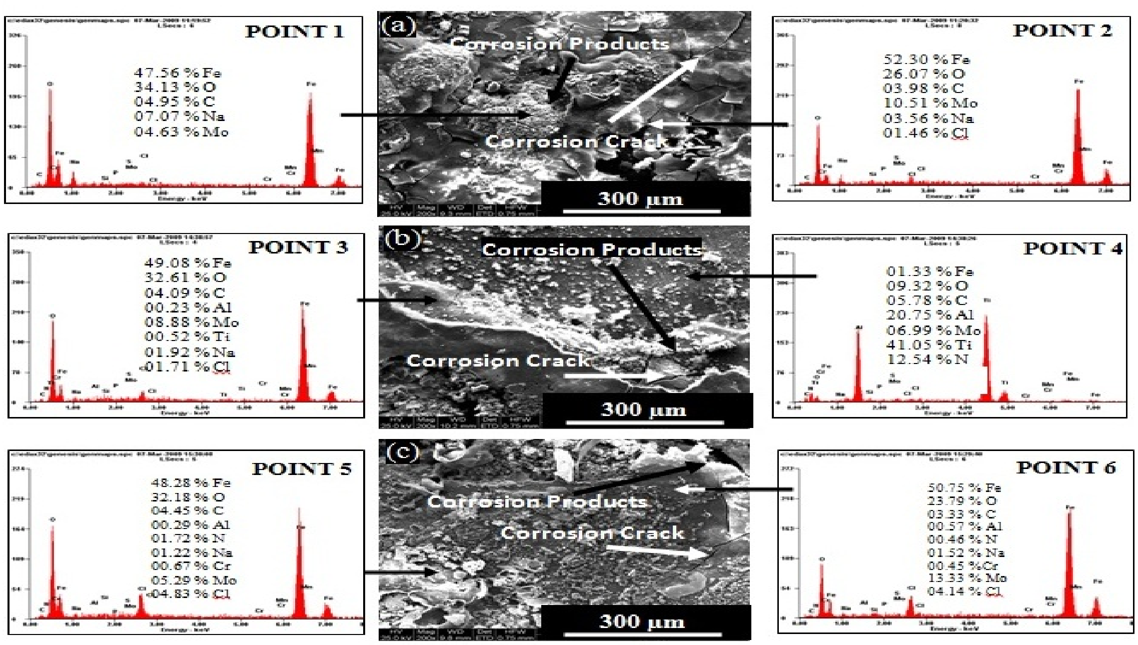

Figure 4: Surface macrographs of uncoated and coated ASTM-SA213-T-22 boiler steel subjected to salt-fog testing (5% NaCl) for 48 hrs: (a) Uncoated ASTM-SA213-T-22 boiler steel (b) Nanostructured TiAlN coating (c) Nanostructured AlCrN coating.

The surface SEM images of uncoated and nanostructured TiAlN and AlCrN coated T-22 boiler exposed to salt fog test for 72 Hrs; are shown in Fig.5. Massive corrosion products were accumulated on the surface in case of uncoated T-22 boiler steel after salt fog tests. EDAX analysis (Point 3 and 4 in Fig.5) in case of nanostructured TiAlN coating indicates the products were composed of Fe and O. In case of nanostructured thin AlCrN coating; EDAX point analysis (Point 5 in Fig.5) revealed the presence of Al and Cr as the main element in the un-corroded area of the surface and Fe and O rich corrosion products (Point 6 in Fig.5).

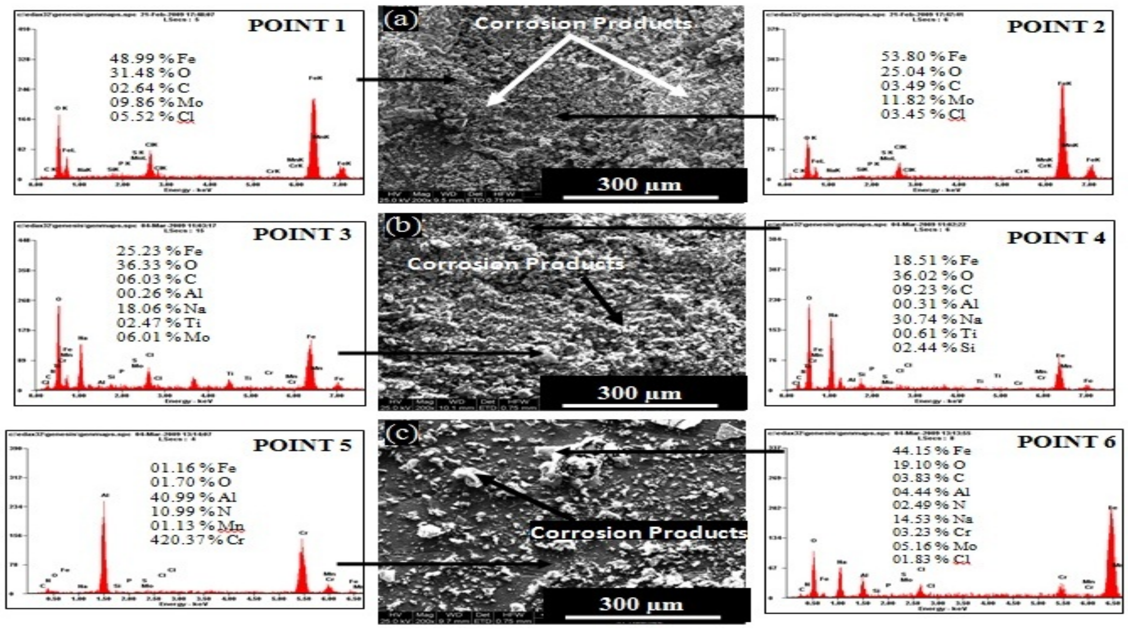

Figure 5: Surface macrographs of uncoated and coated ASTM-SA213-T-22 boiler steel subjected to salt-fog testing (5% NaCl) for 72 hrs: (a) Uncoated T-22 boiler steel (b) Nanostructured TiAlN coating (c) Nanostructured AlCrN coating.

XRD diffractograms for coated and uncoated ASTM-SA213-T-11 boiler steel subjected to salt fog tests for 24 Hrs, 48 Hrs and 72 Hr; are depicted in Fig.6 on reduced scale. As indicated by the diffractograms in Fig.6, Fe3O¬4 and with some minor peaks of Cr2O3 are the main phases present in the oxide scale of uncoated T-11 boiler steel. In nanostructured TiAlN coating, AlN, TiN and Fe3O4 are the main phases revealed with minor phases i.e. TiO2 and Al2O3. Further, the main phases identified for the nanostructured AlCrN coating are CrN, AlN along with Al2O3, Cr2O3 and Fe3O¬4. The formation of Fe3O¬4 in the scale of corroded specimens in salt spray tests is found to be in agreement with those reported by Panda, Bijayani et al., [8] and Vera et al., [9].

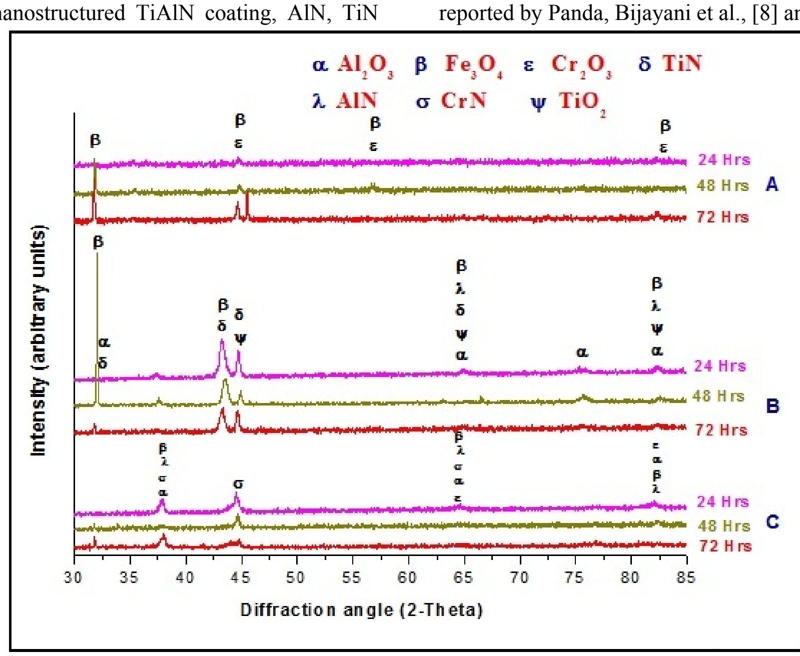

Figure 6: X-Ray Diffraction pattern of uncoated and coated ASTM-SA213-T-22 boiler steel subjected to salt-fog testing (5% NaCl) for 24 Hrs, 48 Hrs and 72 Hrs: (A) Uncoated T-22 boiler steel, (B) Nanostructured TiAlN coating, (C) Nanostructured AlCrN coating.

The weight loss measurements were carried out for the uncoated and nanaostructured thin TiAlN and AlCrN coated T-22 boiler steel exposed to the salt fog tests for 24 Hrs, 48 Hrs and 72 Hrs. Fig. 7, depicts the column chart showing the weight loss per unit area for the uncoated and coated T-22 boiler steel. It can be inferred from the plots that the uncoated T-22 boiler steel has shown maximum weight loss per unit area in all three test conditions i.e. 24 Hrs, 48 Hrs and 72 Hrs tests; as compared to the coated counterparts. Both the coatings have shown good protection to the substrate in terms of weight loss per unit area. it can be inferred from Fig.7 that the weight loss per unit area increases with the duration of the test for all the specimens. The weight loss per unit area in case of nanosructured thin TiAlN coating is less than as compared to the nanostructured AlCrN coating and uncoated boiler steel in all test conditions. It can be mentioned based on the present investigation that nanostructured thin TiAlN and AlCrN coatings can provide a very good corrosion resistance when exposed to the simulated marine environment i.e. salt fog test.

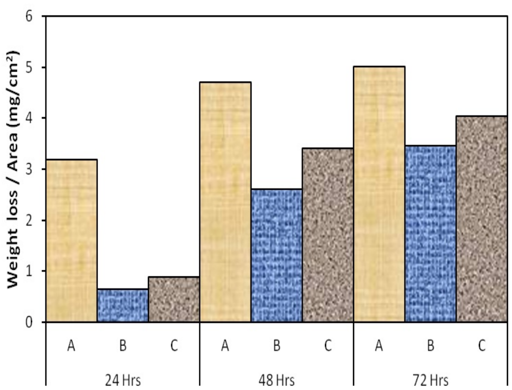

Figure 7: Column chart showing weight loss per unit area for the uncoated and coated ASTM-SA213-T-22 boiler steel subjected to salt-fog testing (5% NaCl) : (A) Uncoated T-22 boiler steel subjected to 24hrs, 48hrs and 72 hrs testing; (B) Nanostructured TiAlN coated T-22 boiler steel subjected to 24hrs, 48hrs and 72 hrs testing; (C) Nanostructured AlCrN coated T-22 boiler steel subjected to 24hrs, 48hrs and 72 hrs testing.

Salt spray corrosion is an electrochemical reaction process [7]. Generally, the corrosion resistance is influenced significantly by several factors, such as compositions, internal microstructure, and especially the surface condition. Bao et al., [7] have studied the corrosion behavior of as-deposited and pre-oxidized NiCoCrAlYSiB coatings by salt spray test. They have reported that an extra thin salt-containing moisture film would form due to deposition during salt spray test, and the film would adsorb and dissolve more oxygen. These active oxygen atoms would diffuse easily to reach the surface of a specimen. A continuous oxide layer could insulate active oxygen atoms from reacting with the underneath metallic coatings i.e. in case of pre-oxidized coating a thin layer of Al2O3 has developed and prevented the active oxygen to enter the substrate. On the contrary in case of as-coated coating, oxidation–reduction will occur easily as the metal confronts with the moisture film directly.

The proposed corrosion mechanism of the as-deposited coated specimen is as explained in Fig.8 which is similar to the one reported by Bao et al.,[7]. Micro-cracks got initiated by residual stress during deposition of coatings. The micro-cracks would be corroded easily and the solution would infiltrate into loose corrosion products and reach crack tip to sustain the internal corrosion, followed by crack propagation (Fig. 8.b and c). This process obeys the rules of crevice corrosion [7]. Acidity in the cracks increased significantly as neutralisation was not easily obtained by exchanging solution between inside and outside the cracks. An ascending acidity accelerates the corrosion attack and results in an unfavourable inner structure. When the acid solution flows across pores, corrosion will take place and enlarge a pore to a corrosion hole (Fig. 8.d).

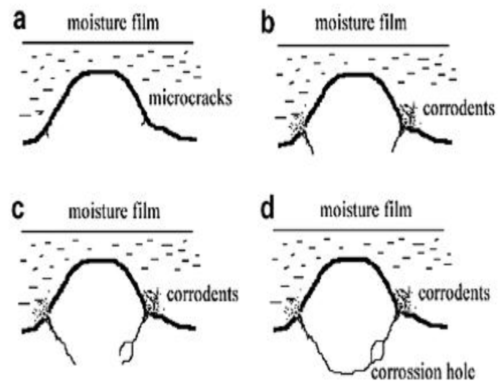

Figure 8: Corrosion evolution of the as-deposited coatings in salt spray test; a: initiation of corrosion micro-crack, b: cracks propagation, c: crack branching, d: formation of corrosion hole [7].

4. Conclusions

The corrosion behavior of the nanostructured thin (by physical vapor deposition process) TiAlN and AlCrN coatings on ASTM-SA213-T-22 boiler steel; has been analyzed by salt spray (Fog) tests (5.0 wt% NaCl). The following conclusions can be made:

- The uncoated T-22 boiler steel suffered severe corrosion in all three test conditions i.e. 24 Hrs, 48 Hrs and 72 Hrs. The nanostructured coated samples have shown resistance to the corrosion as compared to the uncoated T-22 boiler steel.
- It can be inferred from the weight loss per unit area plots that the uncoated T-22 boiler steel has shown maximum weight loss per unit area in all three test conditions i.e. 24 Hrs, 48 Hrs and 72 Hrs tests; as compared to the coated counterparts.
- The weight loss per unit area increases with the duration of the test. The weight loss per unit area in case of nanosructured thin TiAlN coating is less than as compared to the nanostructured AlCrN coating and uncoated boiler steel in all test conditions.
- It can be mentioned based on the present investigation that nanostructured thin TiAlN and AlCrN coatings can provide a very good corrosion resistance when exposed to the simulated marine environment i.e. salt fog test.

5. Acknowledgement

The authors wish to thank All India Council for Technical Education (A.I.C.T.E.), New Delhi, India for providing National Doctoral Fellowship (NDF) to Mr. Vikas Chawla (corresponding author) and grant under Nationally Coordinated Project (NCP).

References

[1] Pawlowski L., The Science and Engineering of Thermal Spray Coatings; Wiley; New York; 1995.

[2] J. P. Celis, D. Drees, M. Z. Huq, P. Q. Wu, M. De Bonte, Surf. Coat. Technol. Vol. 113, 1999, 165-181.

[3] Harpreet Singh, D. Puri and S. Prakash, Anti. Corros. Method Mater. Vol. 5 No.22, 2005, 84–95.

[4] Vikas Chawla, D. Puri, S. Prakash, Buta Singh, Manoj Singla; " a survey of the studies on hard TiAlN and AlCrN coatings" National Conference on advances in materials and manufacturing technology (AMMT-2007), Chandigarh, on 2007.

[5] M. Khandaker, Anwar Hossain, Said M. Easa, Mohamed Lachemi; Building and Environment; Vol. 44, 2009, 713-722.

[6] L. A. Dobrzanski, Z. Brytan, M. Actis Grande, M. Rosso; Journal of Materials Processing Technology, 192-193, 2007, 443-448.

[7] Z. B. Bao, Q. M. Wang, W. Z. Li, J. Gong, T. Y. Xiong, C. Sun, Corrosion Science, Vol. 50, 2008, 847-855.

[8] Bijayani Panda, R. Balasubramaniam, Gopal Dwivedi; Corrosion Science; Vol. 50, 2008, 1684-1692.

[9] R. Vera, M. Villarroel, A. M. Carvajal, E. Vera, C. Ortiz; Materials Chemistry and Physics, Vol. 114, 2009, 467-474.

JJMIE

Volume 5, Number 3, June 2011
ISSN 1995-6665
Pages 255 - 259

Jordan Journal of Mechanical and Industrial Engineering

A Two-stage Artifitial Neural Network Model to Predict the Shrinkage of a Polystyrene Matrix Reinforced with Silica Sand and Cement.

I. Jalham*

Industrial Engineering Dept, Faculty of Engineering & Technology, University of Jordan, Amman 11942 Jordan.

Abstract

Prediction of the shrinkage for the manufacturing purposes of composite materials is not an easy task. The use of existing mathematical and statistical tools may help in solving part of the problem.On the other hand, artificial network tools are of a great importance too. In this investigation, a two-stage Artifitial neural network was used to predict the amount of shrinkage. Using an experimentally measured values of the shrinkage under different material and processing parameters to judge about the relevance of the developed model, it was found that the two-stage Artifitial neural network approach is more capable of predicting the shrinkage than the analytical models because the latter lacks consideration of the materials and processing variables.

Keywords: Shrinkage; Composite; Polystyrene; Cooling rate; Regression

1. Introduction

Shrinkage is the change in size of the product due to thermal and other contractions. Its amount is dependent upon several factors such as the type of the used material, the type of the manufacturing process and the processing parameters. Moreover, the presence of the reinforcement, its volume fraction and size also affect shrinkage phenomenon especially when dealing with composite materials. As polymer processing requires temperature, shrinkage occuring due to thermal contraction has already been studied for homopolymers [Trznadel et al, 1992, Kozlov et al, 1998] and for composites [Beloshenko et al, 2000; Krueger et al, 2003]. Beloshenko et al [2000] studied the the influence of heating temperature and extrusion ratio on the shrinkage of the isostatic polypropylene-ultra-high-molecular polyethelene (PP-UHMPE) composite system. They concluded that the higher the temperature, the higher the shrinkage value while the higher the extrusion ratio, the higher the shrinkage until a ratio of 2 is reached. It was also observed in their work that the higher the content of the UHMPE in the system, the less the shrinkage value. Other factors such as the effect of light intensity on the shrinkage strain has been studied [Silikas et al, 2000]. It was found that the decrease in shrinkage strain values observed for low intensities. In our previous work [Jalham, 1999], a well-established method of manufacturing for a polystyrene matrix reinforced with Jordanian Silica Sand and cement was reported. The work in this field continued to cover the influence of material variables such as particle size (Z) and reinforcement content (S) in addition to the process parameters such as pressure (P) and cooling rate (C) and their interaction on the compressive load capacity of the manufactured composite [Jalham, 2003]. During the conduction of the experiments a shrinkage was observed among the specimens. To be able to predict the optimum size of the product, it was decided to study the effect of these materials and processing variables on the amount of shrinkage. A rough estimate was achieved using a multiple regression model [Jalham, 2004]. Although it gave better predictions than those using the rule of mixture (analytical approach), but not satisfied enough. To come to a better prediction, it was decided to use the two-stage Artifitial neural network approach model.

2. Theory

2.1. Analytical approach:

There are various methods to obtain composite properties. For example, the mechanics of materials method, the self consistent field method, the numerical technique method, and the variational calculus method [Meyers, 1999]. The latter focuses on the upper and lower limits of the properties and does not predict those properties directly. Only when the upper and the lower bounds coincide are particular properties determined. The relations of this technique are referred to as the "rule of mixtures". Thus a mathematical model to calculate the contraction in volume which expesses the shrinkage value can be developed as follows:

$$Vsc = Voc - \Delta Vc \tag{1}$$

Where Vsc is the volume of the composite after processing, Voc is the volume of the composite before

* Corresponding author. e-mail: jalham@ju.edu.jo

processing, and ΔVc is the volume difference of the composite before and after contraction.
Formula 1 can be rewritten as :

$$\Delta Vc = Voc - Vsc \quad (2)$$

To find the relative change of volume of the sample ($\Delta Vc/ Voc$ %), formula 2 should be divided by Voc resulting in

$$\Delta Vc/ Voc = 1 - Vsc/ Voc \quad (3)$$

According to Edrees et al [1999]:

$$Vsc = (1 - \Delta V/Vo)_m (1\text{-}f) Voc + Voc f \quad (4)$$

Where f is the volume fraction of the reinforcement and (1-f) is the volume fraction of the matrix. The subscript m denotes the matrix.
Substituting formula 4 in formula 3 gives the shrinkage value as a relative change of volume of the sample:

$$\Delta Vc/ Voc = 1 - [(1 - \Delta V/Vo)_m (1\text{-}f) + f] \quad (5)$$

$\Delta Vc/ Voc$ should be measured experimentally as a function of the material and processing variables and compared to the predictions of formula 5 above.

2.2. Two-stage ANN approach:

A neural network is an adaptable system that can learn relationships through repeated presentation of data and is capable of generalizing to new, previously unseen data. It is so powerful because it can learn any desired input-output mapping if they have sufficient numbers of processing elements in the hidden layers. The artificial neural network used in this current work is a supervised multi-layer feedforward network trained with a standard back propagation algorithm [Kong et al, 1998]. It Computes changes to the weights in the final layer first, reuses much of the same computation to compute changes to the weight in the pre-ultimate layer, and ultimately goes back to the initial layer. Its idea is to make a large change to a particular weight if the change leads to a large reduction in the error observed at the output nodes. The three-layer network with one hidden layer that was used in this investigation is shown in figure1. The multiplayer perceptron were trained with backpropagation algorithm. The equation to update the weights in momentum learning is [Kong et al, 1998]:

$$w_{ij}(n+1)=w_{ij}(n)+\eta\delta_i(n)x_j(n)+\alpha(w_{ij}(n)-w_{ij}(n-1)) \quad (1)$$

Where w_{ij} is the weight between nodes *i* and *j* at iteration *n*, $\delta_i(n)$ is the local error which can be directly computed from the instantaneous error between the desired response and the system response. At the output processing elements or as a weighted sum of errors at the internal processing elements, η is step size, and α is the momentum and is set to a value between 0.1 and 0.9.

The selection of training algorithm, stopping criteria and representative training set is the most important practical aspect related to training an ANN model. The mean square error of the test set was used as the stopping criteria and to evaluate the performance of the training. The work was accomplished by using the MATLAB software facilities. Unlike other ANN approaches [Hwwu et al, 1996; Kong et al, 1998], this approach used the output of the previous training to be as input to the next one which was called in this investigation as two-stage ANN approach.

3. Methodology

To study the effect of each of the material and processing variables on the shrinkage value, three levels of each variable were considered as in [Jalham, 2003] and presented in Table 1. Three samples for each level were manufactured, because of the limited supply of the polystyrene raw material. The manufacturing of the samples was conducted according to the proposed methodology in [Jalham, 1999] and the results were presented in the form of curves that relates the relative change of volume of the sample ($\Delta Vc/ Voc$ %) values that are measured experimentally as a function of each of the material and procssing variables. The samples were prepared in the form of cylinders of a diameter of 30 mm and a height of 30 mm.

Table 1: Levels of independent variables.

Variable	Units	Level		
		1	2	3
Processing Variables				
Pressure (P)	KN	4	5	6
Cooling rate(C)	°C /min	36	18	12
Materials Variables				
Sand percentage (S)	%	5	25	50
Sand Particle Size (Z)	Micron	60	75	85

As the purpose of this paper is to discover the capability of the two-stage ANN approach to predict the behavior of the polystyrene-base composites by comparing the results of the ANN predictions and the results of predictions by the regresion approach to some of the experimental results which were not used in the training of the network. The two-stage ANN methodology starts from the training of the ANN, shown in Figure 1, through the prediction of the behavior of the polystyrene matrix composite deformed under the same conditions and ending with using the output of the previous training to be as an input to the next stage of training. This approach helps in filtrating the data int the first stage before using it in the second one.

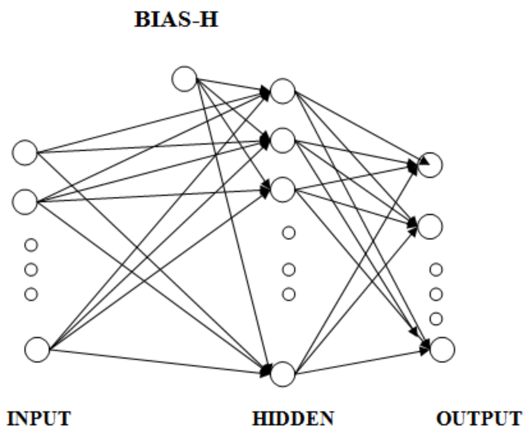

Figure1: The three–layer network with one hidden layer that was used in this investigation.

The preparation of the training data set is related to the way the output vary with inputs and availability of experimental data. If the output varies with inputs in different ways as shown in Fig2 (a & b), the training data used to generalise a model should be prepared differently. For the outputs which vary as in Fig (2b), it is necessary to optimise the training data used. To optimise the training process, Kong [Kong et al, 1998] proposed a way to select the most represantative data while in this investigation the output of the previous training were used to be as input to the next one which was called in this investigation as filtrated ANN approach.

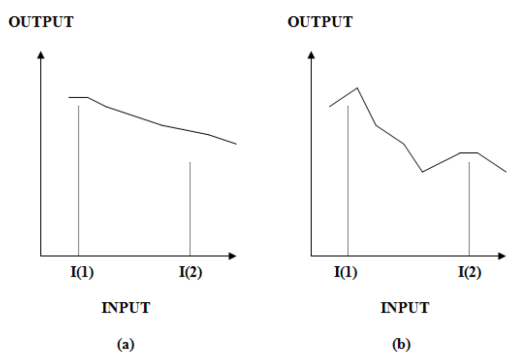

Figure 2: The different ways of output variation with the inputs.

4. Results and Discussions

The experimental results of this work are shown in figures 3-6. They show the effect of each of the materials and processing parameters and their interaction on the shrinkage value which was taken as the relative change of volume of the sample (ΔVc/ Voc %). Figure 3 shows the dependence of shrinkage value as a relative change of volume of the sample on the sand content and its interaction with the particle size of the reinforcement material. It can be observed that the higher the reinforcement content, the less the shrinkage value and for the same content of the reinforcement the higher the particle size, also the less the amount of the shrinkage. This is due to the increase of the amount of the incompressible reinforcement. A good agreement of these results with what have been repoted by Beloshenko et al [2000] was found.

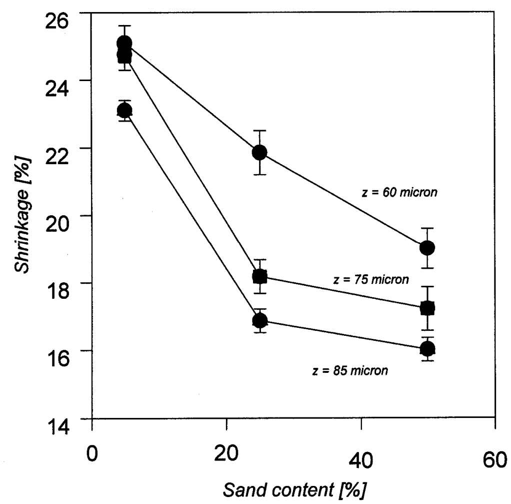

Figure 3: Dependence of the shrinkage of the samples as a relative change of volume on reinforcement content.

Figure 4 shows the dependence of shrinkage value on the pressure and its interaction with the cooling rate. It can be concluded from this figure that the higher the pressure, the higher the value of the shrinkage and for the same pressure the higher the cooling rate, the less the shrinkage. This is due to the increase of the degree of densification with the increase in the pressure during manufacturing. This is also in a good agreement with what have been repoted by Beloshenko et al [2000].

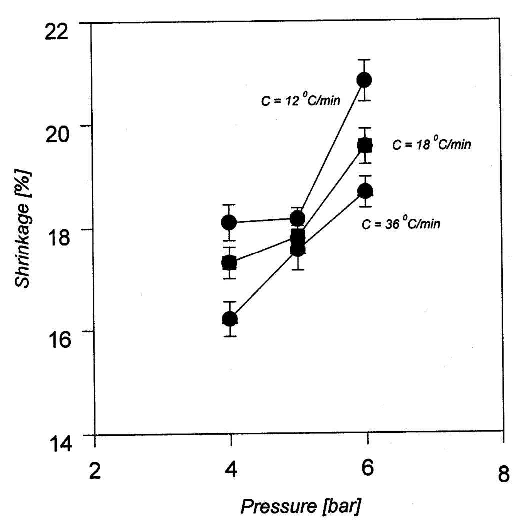

Figure 4: Dependence of the shrinkage of the samples as a relative change of volume on the pressure.

Figure 5 shows the dependence of shrinkage value on the cooling rate and its interaction with the sand content. It is clear that the higher the cooling rate, the less the value of shrinkage which is in a good agreement with the behaviour of homopolymers reported in [Trznadel et al, 1992, Kozlov et al, 1998] and for composites reported in [Beloshenko et al, 2000; Krueger et al, 2003]. This is due to the lower amount of time needed for solidification when using a high cooling rate processing.

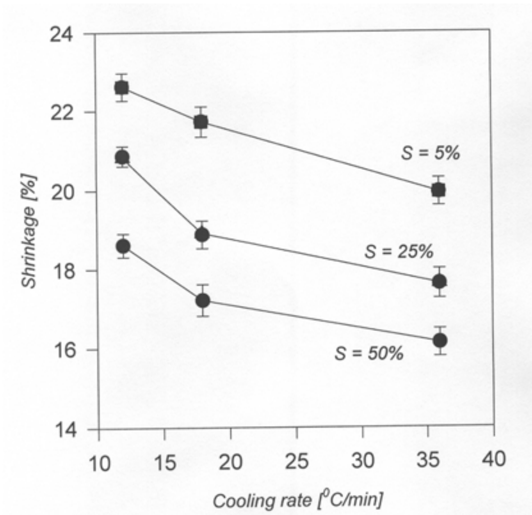

Figure 5: Dependence of the shrinkage of the samples as a relative change of volume on the cooling rate.

Figure 6 shows the dependence of shrinkage on the particle size and its interaction with the pressure vules. The figure indicates that the higher the particle size, the lower the shrinkage value although for the 85 micron particle size the 5 kN pressure shows lower shrinkage than at 5 and 6 kN. This shows that an optimum interaction of the parameters may exist when using a 5 kN pressure during processing.

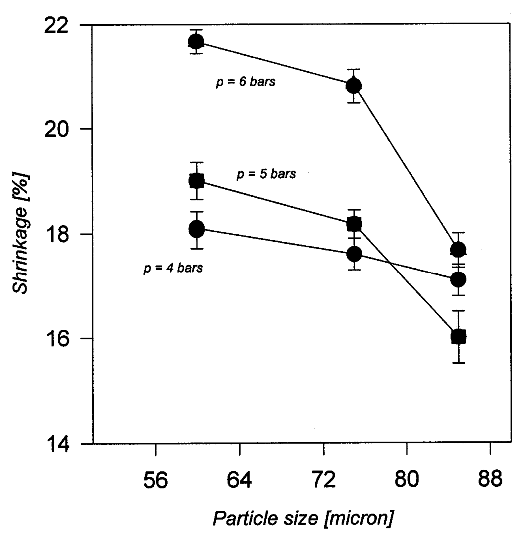

Figure 6: Dependence of the shrinkage of the samples as a relative change of volume on particle size.

It is of a great importance to find a model that may predict the value of shrinkage. This helps in reducing the number of the experiments and gives an idea about the amount of the material needed to produce an intended product. Based on the developed model above, formula 5 can be used to predict the shrinkage value. But the predictions using this formula may serve to predict the shrinkage value when the volume fraction of the reinforcement is the only variable. To be able to predict the shrinkage value when all the materials and processing values are taken into consideration, different approaches were used. In this investigation, analytical, multiple regression, and neural network approaches were of interest. MATLAB package was used as the main tool in this work. The shrinkage value was taken as the response variable and all other interactions where taken as the dependent variables.

It was decided to adopt the two-stage ANN approach because the relative error of the predicted results after the second training stage is better than after the primary stage of training and less than 5%.

A comparison between the model in formula 5, the regression model in [Jalham, 2004], and the experimental results are shown in figures 7-10. Figure 7 shows the results when the sand content is variable (S = 5, 25, 50 %) and the other variables were taken as constants with the following values: Z = 60 microns, P = 5 kN, C = 12 ^{o}C/min . The conditions for the calculations are presented under each figure. The relative change of volume of the polystyrene matrix ($\Delta V/Vo$) was measured experimentally to be 26% and this is constant for calculation conditions. Then the value $(1 - \Delta V/Vo)m$ will be 74% and used for the calculations of formula 5 results.

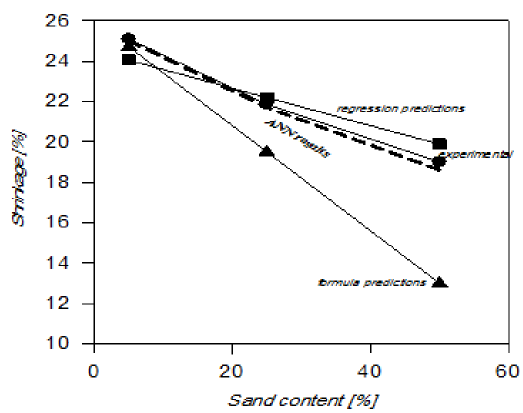

Figure 7: A comparison between the model in formula 5, the model in formula 6, and the experimental results when the sand content is variable (S = 5, 25, 50 %) and Z = 60 microns, P = 5 kN, C = 12 ^{o}C/min.

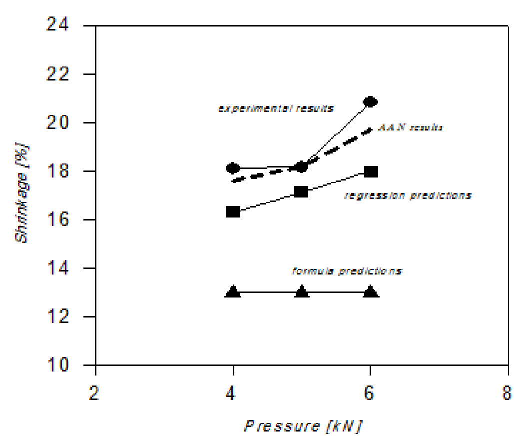

Figure 8: A comparison between the model in formula 5, the model in formula 6, and the experimental results when the pressure is variable (P = 4, 5, 6 kN) and Z = 75 microns, S = 50%, C = 12 ^{o}C/min.

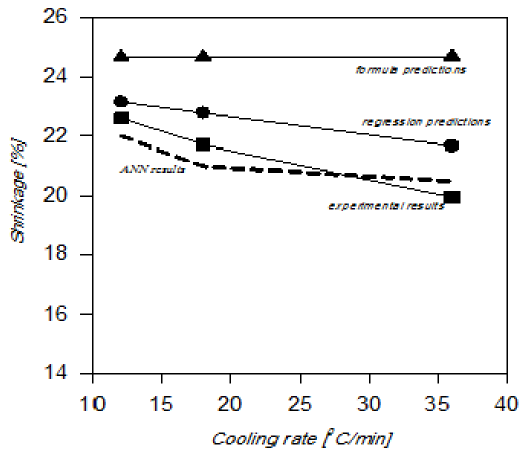

Figure 9: A comparison between the model in formula 5, the model in formula 6, and the experimental results when the cooling rate is variable (C = 12, 18, 36 C/min) and Z = 75 microns, P = 6 kN, S = 5%.

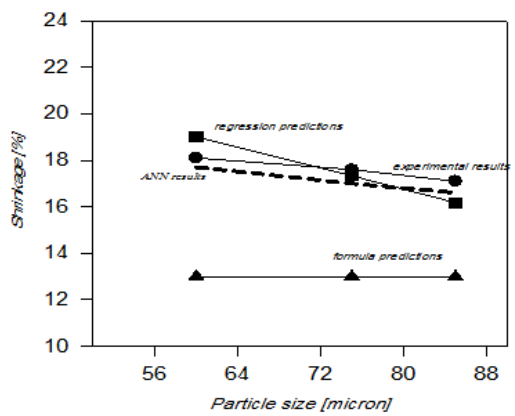

Figure 10: A comparison between the model in formula 5, the model in formula 6, and the experimental results when the particle size is variable (Z = 60, 75, 85 micron) and C = 12 C/min, P = 4 kN, S = 50%.

It is clear from these figures that the predictions using the two-stage ANN approach is better than using the multiple regression approach and better than using the analytical model developed (formula 5). This is because the model in formula 5 lacks the consideration of the conditions other than the reinforcement content.

5. Conclusions

As a result of this investigation, the following can be concluded :

- The higher the reinforcement content and the particle size, the less the shrinkage.
- The higher the pressure and the less the cooling rate, the higher the shrinkage.
- The two-stage ANN approach is better than using the multiple regression approach and better than using the analytical model.

References

[1] Beloshenko, V.A., Beygelzimer, Ya. E., and Varyukhin, V.N., Polymer, vol. 41, 2000, p 3837.

[2] Edrees, H.J. and Hendry, A., British Ceramic Transactions, vol.98, No.1, 1999, p 6.

[3] Hwwu Y. J., Pan and J.G. Lenard: steel Res., vol.67, 1996, p59.

[4] Issam S. Jalham, J. Dirasat, Engineering Sciences, vol. 26, No.2, 1999, p 241.

[5] Issam S. Jalham, The influence of processing and material parameters on the Compressive Load Capacity of a polystyrene matrix reinforced with Jordanian Silica Sand and Cement., accepted for publication in Emirates Journal for Engineering Research, 2003.

[6] Issam S. Jalham, J. Dirasat, Engineering Sciences, vol. 31, No.1, 2004, p 118.

[7] Kong L.X., P. D. Hodgson, and D. C. Collinson, ISIJ International, vol.38, 1998, No.10, pp1121-1129

[8] Kozlov, G.V., Beloshenko, Varyukhin, V.N., and Gazaev, M.A., J Appl. Mech. Tech Phys, vol 39, 1998, p 140.

[9] Krueger, Q.J., and King, J.A., Advances in polymer technology, vol.22, No. 2, 2003, p96.

[10] Meyers, M.A., and Chawla, K.K., “Mechanical behaviour of materials”, 1999, p 645.

[11] Silikas, N., Eliades, G., and Watts, D.C., Dental Materials, vol 16, 2000, p 292.

[12] Trznadel, M., and Kryszewski, M. , Macromol J Sci Rev Macromol Chem Phys, vol. 32, 1992, p 259.

JJMIE

Volume 5, Number 3, June 2011
ISSN 1995-6665
Pages 261 - 265

Jordan Journal of Mechanical and Industrial Engineering

Performance Analysis and Behaviour Characteristics of CVD (Semi Active) in Quarter Car Model

K. Kamalakannan*[a], A. ElayaPerumal[b], S. Mangalaramanan[c], K. Arunachalam[d]

[a]Faculty, Automobile Engineering, Hindustan University, India..
[b]Faculty Mechanical Engineering , Anna University, India..
[c]Section Head, Advanced Engineering, Ashok Leyland, India..
[d]Faculty Automobile Engineering –Anna University, Chennai , India..

Abstract

Semi-active suspension uses a special adaptive damper whose damping properties vary with road conditions under the influence of an electromagnet. The adaptive damper is used along with a sophisticated electronic circuit which constantly monitors the changing road conditions and adapts accordingly. The aim of this paper is to simulate and analyze a simple and low-cost semi active suspension system using 'MATLAB and SIMULINK' platform and establish its superiority, and also involves the development and simulation of a virtual quarter car model. Thereafter the graphical results obtained are analyzed. The model is developed using equations of motion involving stiffness, damping ratio and displacement. These equations are translated into a simple data flow circuit in the simulation software to obtain definite results in the form of graphical output .This paper aims at the development of a simpler and cheaper semi active suspension system which will allow its fitment in comparatively affordable cars.

Keywords: CVD (continuous Variable Damper); Semi Active; MATLAB; Suspension; SIMULINK

1. Introduction

In the interest of improving the overall performance of automotive vehicles in recent years, suspensions incorporating active components have been developed and the process moves to further developments and improvements.

SUSPENSION systems are classified in to three groups: Passive, Semi Active and Active suspension systems. Passive suspension system consists of an energy dissipating element, which is the damper, and an energy-storing element, which is the spring. Since these two elements cannot add energy to the system this kind of suspension systems are called passive, Figure 1 shows passive suspension system and Figure 2 shows semi active suspension, both differs in particular aspect (damper stiffness) which former is a fixed one and a secondary consists of a continuous variable. Sensors continuously monitor the operating conditions of the vehicle body, according to the base excitement the signals obtained by the sensors and prescribed voltage applied across the flow (Rheological Fluid)of the fluid in a shock absorber, the damping force can be controlled(Varied).Control strategy, the force in the actuator is modulated to achieve improved ride and handling. It should be noted, that the semi-active suspension system requires external power, of minimum requirement from the battery. It is greater advantage than active suspension for its higher power requirement, and also a considerable penalty in complexity, reliability, cost and weight.

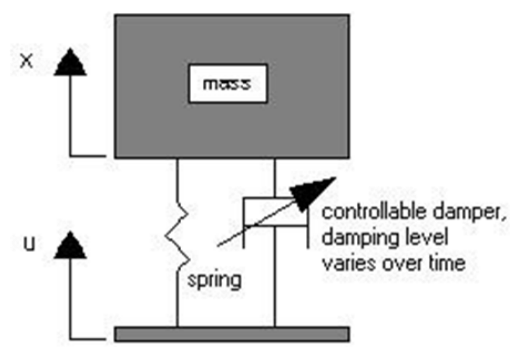

Figure 1: Passive Suspension.

Semi-active systems can only change the viscous damping coefficient of the shock absorber, and do not add energy to the suspension system. Though limited in their intervention (for example, the control force can never have different direction than that of the current speed of the suspension), semi-active suspensions are less expensive to design and consume far less energy.

In recent years, many investigators have predicted that with a semi active suspension it is possible to attain performance gains comparable to those possible with a fully active suspension. Semi active suspension control has been studied widely since Crossby and Karnopp [1] developed skyhook control system. The method by which the damper is controlled is one of the crucial factors that ultimately determines the success or failure of a particular semi active suspension. This study is an investigation into

* Corresponding author. e-mail: kamalakannan.ka@gmail.com

the effectiveness of a number of basic control strategies at controlling vehicle dynamics, particularly vehicle roll by Chalasani , R.M [2,3] .

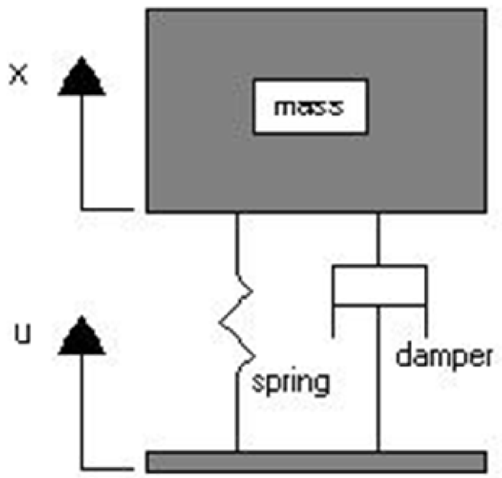

Figure 2: Semi active Suspension.

2. Basic Model of the Quarter Car Model

For the purpose of simulation and analysis of a semi active suspension system a quarter car model was taken into consideration .This is done to simplify the calculations involved in the modeling. The results obtained can then be scaled up and adjusted accordingly for the entire car. A quarter car as the name suggests comprises of the quarter portion of the car .It consists of a wheel, a variable damper and spring set.

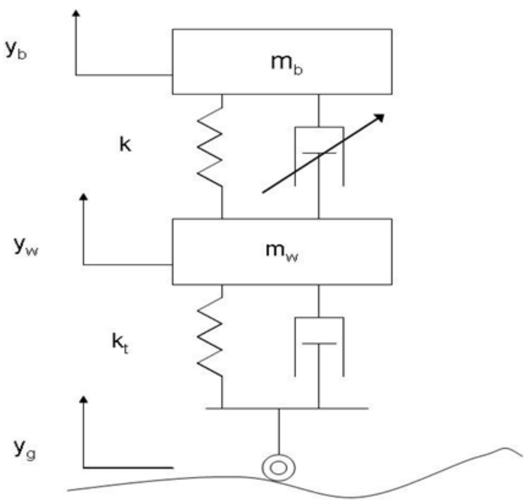

Figure 3: A Quarter car model of semi active suspension.

As shown in the Figure 3 the mass acting on the suspension system can be classified into sprung (m_b) and unsprung mass (m_W). The sprung mass comprises of the mass of the body which is damped by the suspension system (in case of quarter car model the value is 1/4th the total sprung mass value). The unsprung mass comprises the mass of the wheels, brakes, suspension components etc.

3. Simple Equation of Motion For Suspension System

$$K\,(y_W - y_B) + b\,(\dot{y}_W - \dot{y}_b) = m_b\ddot{y}_b$$

$$K_t\,(y_s - y_W) + b_t(\dot{y}_s - \dot{y}_W) +$$
$$K\,(y_b - y_W) + b\,(\dot{y}_b - \dot{y}_W) = m_W\ddot{y}_W$$

These equations can be further simplified and written as
$$f_k(\Delta) + f_b = m_b\ddot{y}_b$$

Where
$$\Delta = (y_W - y_b)$$

For passive suspension
$$f_b = f(\dot{\Delta})$$

Where
$$\dot{\Delta} = (\dot{y}_W - \dot{y}_b)$$

For semi active suspension
$$f_b = f(\dot{\Delta}, i)$$

Where
$$\dot{\Delta} = (\dot{y}_W - \dot{y}_b)$$
i = control current.

The above mentioned equation clearly depicts the difference between the variables that affect the shock damping force (fb) in both the cases .In case of a semi active suspension it also depends on the control current along with the velocity function .This clearly suggests that the damping force can be controlled by controlling the current input to the electromagnet around the damper.

4. Virtual Designing and Modeling

For the purpose of performance analysis the semi active suspension system's quarter model was developed. The basic model can be divided into the three sub parts for simplification of calculations, namely

- SEAT AND DRIVER
- SPRUNG MASS
- UNSPRUNG MASS

The model is based on equation of motion involving parameters like

- STIFFNESS
- DAMPING RATIO
- DISPLACEMENT
- MASS
- ACCELERATION
- VELOCITY

5. Equation of Motions

5.1. Equations for seat and driver:

$$M_{SE}\,\ddot{Z}_{SE} + K_{SE}\,(Z_{SE} - Z_S) + b_{SE}\,(\dot{Z}_{SE} - \dot{Z}_S) = 0$$

Or

$$\ddot{Z}_{SE} = \{- K_{SE}\,(Z_{SE} - Z_S) - b_{SE}\,(\dot{Z}_{SE} - \dot{Z}_S)$$

5.2. Equations for sprung mass:

$$M_S\,\ddot{Z}_S - K_{SE}\,(Z_{SE} - Z_S) - b_{SE}\,(\dot{Z}_{SE} - \dot{Z}_S) + K_S(Z_S - Z_U) + b_S(\dot{Z}_S - \dot{Z}_U) = 0$$

Or

$$\ddot{Z}_S = \{ K_{SE}\,(Z_{SE} - Z_S) + b_{SE}\,(\dot{Z}_{SE} - \dot{Z}_S) - K_S(Z_S - Z_U) - b_S(\dot{Z}_S - \dot{Z}_U)\}/M_S$$

5.3. Equations for unsprung mass

$$M_U\,\ddot{Z}_U - K_S\,(Z_S - Z_U) - b_S\,(\dot{Z}_S - \dot{Z}_U) + K_t(Z_U - Z_r) = 0$$

Or

$$\ddot{Z}_U = \{K_S\,(Z_S - Z_U) + b_S\,(\dot{Z}_S - \dot{Z}_U) - K_t(Z_U - Z_r)\}/\,M_U$$

These equations are combined in the simulation software in such a way that they form a feedback loop or in other terms any alterations in any of the values results in a change in the behavior of the system as a whole. These results are obtained in the form of graphs for each system separately depicting the effect of road input in the form of change in velocity and displacement from the mean position. These graphs are also dependent on the values of different constants as mentioned above. This property of the experimental model allowed the variation in damping coefficient (bs) of the suspension system, which differentiates semi active suspension system from passive suspension system, for which the damping coefficient is constant under all conditions.

6. Values of Parameters Used for Modeling

The values considered below are used only for the purpose of modeling and are reference values obtained from various related literature. A provision has been made within the model itself to make changes to these values to obtain corresponding graphs.

- M_{se} =90kg
- b_{se} =3000Ns/m
- K_{se} =8000N/m
- M_s =250kg
- b_s =2000Ns/m
- K_s =28000N/m
- M_u =40kg
- K_u = 12500N/m

7. Steps Involved in Modeling

After the initial calculations were done and parameters were established, the system was modeled using MATLAB and SIMULINK platform .The modeling was done in logical steps of the above mentioned equations ,were converted into a logical data flow circuit loop using predetermined logic boxes and connectors available in these platforms .Complete semi active suspension circuit consists of sub circuits like sprung mass circuit, seat and driver circuit and unsprung mass circuit.

As the damping coefficient of a semi active suspension varies with respect to the road conditions, a special sub circuit was developed for varying the damping coefficient with the change in road input.

8. A Complete Circuit of a Semi Active Suspension System

The figure below shows a complete circuit of a semi active suspension system:

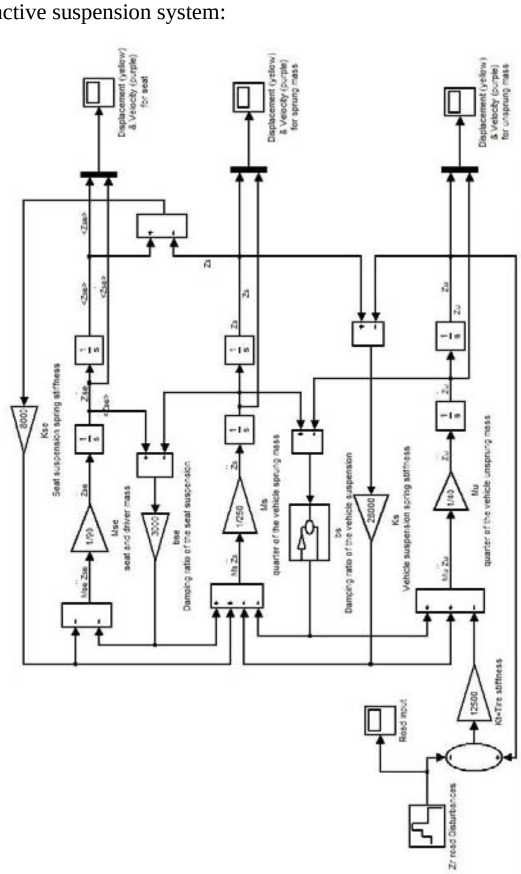

Figure 4: Complete Circuit of the Semi Active Suspension.

9. Simulation Parameters Considered in Modeling

Table .1: Simulation Parameters Varying with Zr.

Sl.No	Zr	Time Delay	bs
1	0.05	0	1500
2	0.1	80	3000
3	0.15	150	4500
4	0.07	230	2100
5	0.00	400	1200

The table given above shows the various parameters which were used for modeling for example the road input and its corresponding time delay and damping coefficient.

10. Simulation Results

The results are obtained in the form of graphs which consist of two variables with respect to time .These variables are velocity and displacement from the mean position the graph is in the form of an oscillating wave. These waves are almost similar in shape for the three parameters i.e. seat, sprung mass and unsprung mass but differ in amplitude and linearity. On the vehicle operation, payload varies from time to time. It is observed that a small mass makes the difference in peak harmonics. In practice, the excitation on the vehicle suspension depends on the road roughness, mass of the vehicle, inertia of the vehicle and vehicle speed.

11. Conclusion

The aim of this paper was to establish the superiority of a low cost semi active suspension model. From the results obtained it was concluded that the semi active suspension system offered superior damping properties over a wider load range. It also eliminated the need to compromise between ride comfort and handling which is a major drawback with the present passive suspension system. The low cost model developed will have a wider application in more economical vehicles making this technology available to everyone around the globe, which right now is restricted to a few expensive vehicles.

References

[1] D.C. Karnopp, M.J. Crosby, and R.A. Harwood, "Vibration Control Using Semi- Active Force Generators" ASME Journal of Engineering for Industry, Vol. 96, No. 2, 1975, 619-626.

[2] R.M. Chalasani, "Ride Performance Potential of Active Suspension Systems-Part I Simplified Analysis Based on a Quarter-Car Model," Proceedings of 1986 ASME Winter Annual Meeting, Los Angeles, CA,1986.

[3] R.M. Chalasani, "Ride Performance Potential of Active Suspension Systens-Part II: Comprehensive Analysis Based on a Full-Car Model," ASME Symposium on Simulation and Control of Ground Vehicles and Transportation Systems, AMD-Vol. 80, DSC-Vol. 2, 1986, 187-204.

[4] P. Barak, "Design and Evaluation of an Adjustable Automobile Suspension," Auto technologies Conference and Exposition, Vol. 98, Section 6, 1989.

[5] Lord Corporation Web Page; www. Rheonetic.com.

Appendix

Graphs for semi active suspension model

Seat and driver circuit

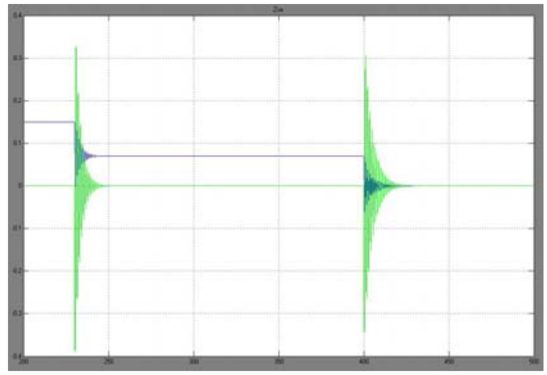

Figure 5: Seat and Driver Circuit Simulation.

The green line shows the velocity whereas the blue line shows the displacement of the seat and driver from the mean position and X axis in second (Actual Simulation).

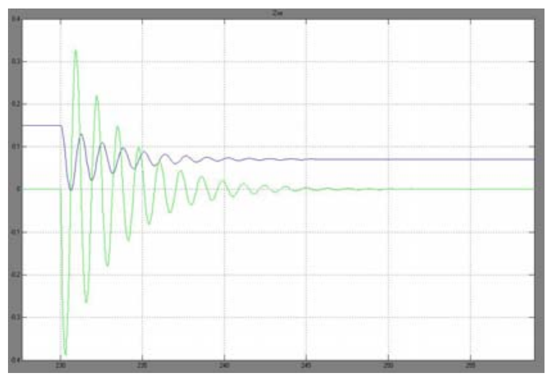

Figure 6: Zoomed view Seat and Driver Circuit Simulation.

Sprung mass circuit

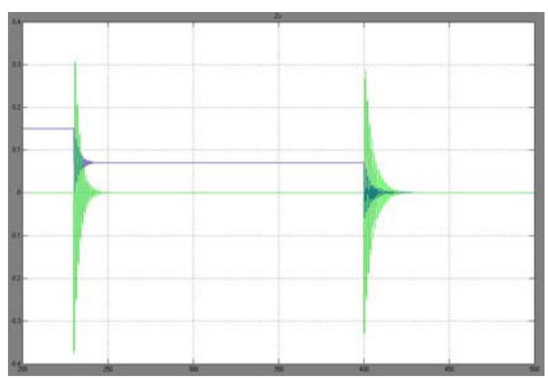

Figure 7: Sprung Mass Circuit Simulation.

The green line shows the velocity whereas the blue line shows the displacement of the sprung mass from the mean position. Although it is similar in shape to the seat and driver graph but the peak values clearly differ from each other in the two cases. This is because of the different values of the parameters involved. The most noticeable difference is the peak value of velocity.

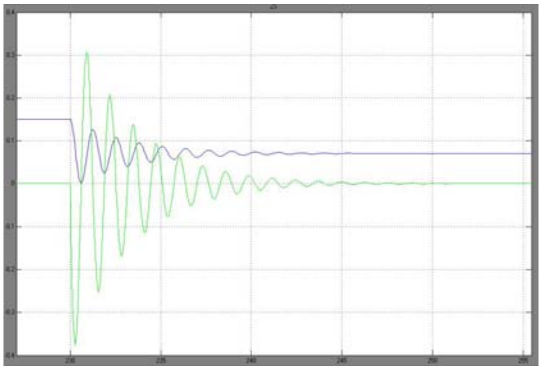

Figure 8: Zoomed View of Sprung Mass Circuit Simulation.

Unsprung circuit

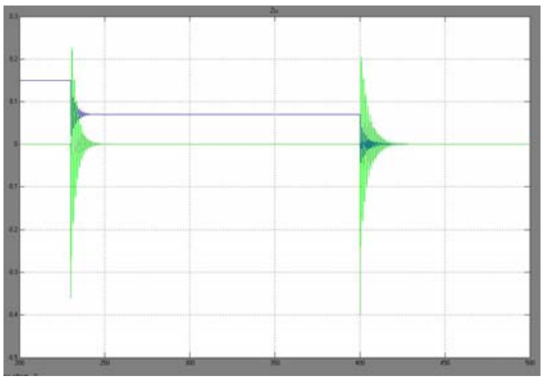

Figure 9: Unsprung Circuit Simulation.

The peak value of velocity is the least for this system when compared to the other two this shows that the unsprung mass gains the least velocity in any suspension system.

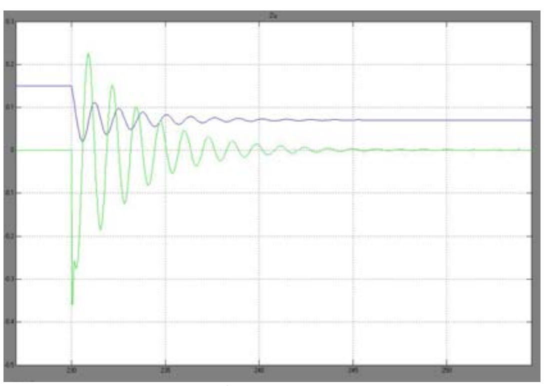

Figure 10: Zoomed View of Unsprung Circuit Simulation.

JJMIE

Volume 5, Number 3, June 2011
ISSN 1995-6665
Pages 267 - 272

Jordan Journal of Mechanical and Industrial Engineering

Drag Reduction in a Wing Model Using a Bird Feather Like Winglet

A. Hossain*[,a], A. Rahman[b], J. Hossen[b], P. Iqbal[a], N. Shaari.[a], G. K Sivaraj [a]

[a] *Department of Mechanical Engineering, Universiti Industri Selangor,Jln Timur Tambahan, 45600 Batang Berjuntai, Selangor Darul Ehsan, Malaysia*

[b] *Department of Mechanical Engineering, International Islamic University,Malaysia*

Abstract

This work describes the aerodynamic characteristic for aircraft wing with and without bird feather like winglet. The aerofoil used to construct the whole structure is NACA . Rectangular wing and this aerofoil have been used to compare the result with previous research using winglet. The model of the rectangular wing with bird feather like winglet has been fabricated using polystyrene before design using CATIA P3 V5R13 software and finally fabricated in wood. The experimental analysis for the aerodynamic characteristic for rectangular wing without winglet, wing with horizontal winglet and wing with 60 degree inclination winglet for Reynolds number 1.66×105, 2.08×105 and 2.50×105 have been carried out in open loop low speed wind tunnel at the Aerodynamics laboratory in Universiti Putra Malaysia. The experimental result shows 25-30 % reduction in drag coefficient and 10-20 % increase in lift coefficient by using bird feather like winglet for angle of attack of 8 degree.

Keywords: Winglet; Aerodynamic characteristics; External balance; Drag coefficient

Nomenclature

α	Angle-of-attack
D	Drag force
L	Lift force
ρ_∞	Air density
S	Reference area
V_∞	Free stream velocity
a_0	Lift slope
C_D	Drag coefficient
C_L	Lift coefficient
d	Diameter of sphere
$[K_{ij}]$	Coefficient matrix
$\{F_i\}$	Load matrix
$\{L_i\}$	Signal matrix

1. Introduction

One of the primary obstacles limiting the performance of aircraft is the drag that the aircraft produces. This drag stems from the vortices shed by an aircraft's wings, which causes the local relative wind downward (an effect known as downward) and generated a component of the local lift force in the direction of the free stream. The strength of this induced drag is proportional to the spacing and radii of these vortices. By designing wings which force the vortices farther apart and at the same time create vortices with large core radii, one may significantly reduce the amount of the drag the aircraft induces [1]. Airplanes which experience less drag require less power and therefore less fuel to fly an arbitrary distance, thus making flight, commercial and otherwise, more efficient and less costly. Vortices at the wing tip can cause crash in aircraft. This is when a big aircraft goes in front of a small aircraft; this big aircraft which has larger vortices can cause the small aircraft to loose control and crash. In airport to minimize the separation rule, an aircraft of a lower wake vortex category must not be allowed to take off less than two minutes behind an aircraft of a higher wake vortex category. If the following aircraft does not start its take off roll from the same point as the preceding aircraft, this is increased to three minutes. One promising drag reduction device is winglet. For a number of years many investigations have been carried out to prove the possible benefits of modifying wing tip flow. Tip devices have become a popular technique to increase the aerodynamic performances of lifting wings [2-3]. The idea behind all the devices described is to diffuse the strong vortices released at the tip and optimize the span wise lift

* Corresponding author. e-mail: altab75@unisel.edu.my

distribution, while maintaining the additional moments on the wing within certain limits. The design of a winglet is very complex. It requires the same aerodynamic characteristics as a wing and its chord wise position on the tip of the wing require special care to optimize its efficiency and to prevent detrimental flow interactions with the wing [4]. According to A.J. Bocci [5] winglets show greater efficiency when there is high loading near the tips of the wing and it is more efficient than a wing tip extension producing the same bending moment at the root. It enables to increase the aircraft efficiency. However, the winglet efficiency depends on the lift produced by the wing and strong aerodynamic interference can be found at the concave junction between the wing and the winglet. A group of biologists at the Technical University of Berlin has worked and demonstrated the effectiveness of multiple slotted wings or wing grid. They have shown how these features could have evolved naturally in birds through gradual increases in wing effectiveness. This theory has been emulated in an aircraft optimization algorithm developed by Kroo and Takai [6]. The new design approach "WING-GRID", developed from the observation of storks, results in revolutionary new options for aircraft wings and application to practical any aircraft can reap solid benefits [7-9]. Winglets have become a popular method of altering the trailing tip vortex system from an aircraft wing and thus improve the aircraft performance. A winglet is a device used to improve the efficiency of aircraft by lowering the lift-induced drag caused by wingtip vortices. A winglet provides an innovative method of achieving the vortex arrangement described above. The concept involves constructing wings whose tips are small extension in the form of a smaller aerofoil section placed at any angle. Because the vortices shed by the wing are strongest at the tips of the wing, the addition of the wing tip surfaces can reduce and diffuse the strength of these vortices, thus reducing the overall vortex drag of the aircraft. Two bird feather like winglets have been used with the aircraft model wing to do the experiment with the wind tunnel in Aerodynamics Laboratory of Aerospace Engineering Department, Universiti Putra Malaysia. The longitudinal aerodynamic characteristics of aircraft wing with two-winglet configurations have been the subject of this research work.

The study on the enhanced performance of the aircraft models is also given by incorporating elliptical and circular winglets. An interaction matrix method has also been presented to revalidate the calibration matrix data provided by the manufacturer of the six-component external balance. The calibration of free stream velocity and flow quality in the test section has been established and documented in the earlier published paper [10].

2. Methodology

2.1. Wind tunnel, model details and Instrumentation:

An aircraft model's wing with two sets of bird feather like winglets have been designed and fabricated using wood for testing aerodynamic characteristic in subsonic wind tunnel in Aerodynamic Laboratory, University Putra Malaysia. The NACA 653-218 airfoil has been used for the whole structure of wing, winglet and adapter. The winglet design is shown in Figure 1. The aircraft model has a span of 0.66 m and a chord of 0.121 m as shown in Figure 2. The tests were carried out with free-stream velocities of 21.36 m/s, 26.76 m/s, and 32.15 m/s respectively with and without winglet of different configurations. The ambient pressure, temperature and humidity were recorded using barometer, thermometer, and hygrometer respectively for the evaluation of air density in the laboratory environment. Figure 3 shows a photograph of the aircraft model wing with bird feather like winglet without adapter in the test section in wind tunnel.

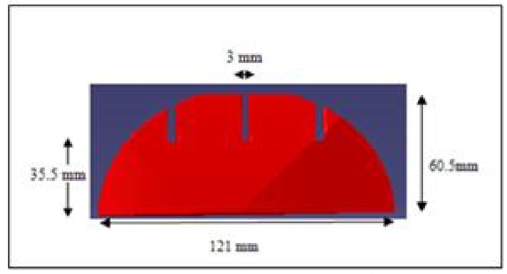

Figure 1: Geometry Characteristic of Bird Feather like Winglet from Top View.

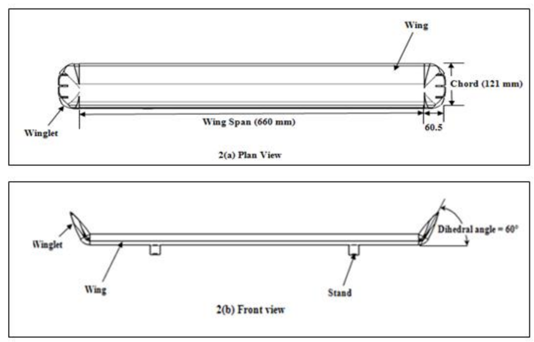

Figure 2: Rectangular Wing with Winglet Inclination using Adapter.

Figure 3: Aircraft model wing with bird feather like winglet.

Longitudinal tests were carried out at angle of attack ranging from 0 degree to 14 degree with an increment of 2 degree. During the test the pitching moment, lift and drag forces were measured using the six-component external balance and the coefficients of lift, drag and moment are obtained using the Eqs. (1-3) [11-12] given below, Coefficient of lift is defined as

$$C_L = \frac{L}{\frac{1}{2}\rho_\infty V_\infty{}^2 S} \quad (1)$$

Coefficient of drag is defined as

$$C_D = \frac{D}{\frac{1}{2}\rho_\infty V_\infty{}^2 S} \quad (2)$$

Coefficient of pitching moment is defined as

$$C_M = \frac{M}{\frac{1}{2}\rho_\infty V_\infty{}^2 Sc} \quad (3)$$

Calibration of the six-component balance has been done to re check the calibration matrix data provided by the manufacturer. The relationship between signal readings, Li and the loads, Fi applied on the calibration rig are given by the following matrix equation, the detailed procedure of calibration is explained elsewhere [13]

$$\{L_i\} = [K_{ij}]\ \{F_i\} \quad (4)$$

Where, $[K_{ij}]$ is the coefficient matrix, $\{L_i\}$ is the signal matrix, and $\{F_i\}$ is the load matrix.

3. Results and Disscussion

Wind-tunnel measurements using the aircraft model without winglet and with winglet of different configurations were carried out at Reynolds numbers 1.66x105, 2.08x105 and 2.5x105. The measured values for the lift coefficient, drag coefficient, pitching moment coefficient and lift and drag ratio for the various Reynolds number are given in Table 1 to 4 and detail calculations have been performed as per the procedure explained in [10].

Table 1: Lift Coefficient over Angle of Attack.

Winglet Configuration	Reynolds Number (10^5)	Angle of attack α: 0	4	8	12	14
Without winglet	1.66	0.228	0.594	0.804	0.725	0.666
	2.08	0.256	0.605	0.787	0.721	0.589
	2.5	0.308	0.677	0.88	0.797	0.735
Winglet in horizontal (0 degree)	1.66	0.405	0.678	0.85	0.68	0.572
	2.08	0.433	0.668	0.915	0.81	0.722
	2.5	0.414	0.725	0.972	0.83	0.759
Winglet 60 degree inclined	1.66	0.442	0.787	0.993	0.812	0.78
	2.08	0.456	0.817	0.956	0.876	0.75
	2.5	0.481	0.803	0.99	0.854	0.828

Table 2: Drag Coefficient over Angle of Attack.

Winglet Configuration	Reynolds Number (10^5)	Angle of attack α: 0	4	8	12	14
Without winglet	1.66	0.088	0.105	0.156	0.216	0.258
	2.08	0.0849	0.1029	0.152	0.236	0.289
	2.5	0.0667	0.0878	0.136	0.191	0.218
Winglet in horizontal (0 degree)	1.66	0.0616	0.065	0.103	0.175	0.193
	2.08	0.0546	0.0576	0.0936	0.145	0.164
	2.5	0.0534	0.0554	0.085	0.117	0.131
Winglet 60 degree inclined	1.66	0.076	0.0935	0.118	0.16	0.193
	2.08	0.0642	0.0907	0.104	0.152	0.171
	2.5	0.052	0.071	0.091	0.139	0.159

Table 3: Pitching Moment Coefficient over Angle of Attack.

Winglet Configuration	Reynolds Number (10^5)	Angle of attack α: 0	4	8	12	14
Without winglet	1.66	-0.086	-0.098	-0.12	-0.32	-0.373
	2.08	-0.091	-0.125	-0.197	-0.425	-0.502
	2.5	-0.113	-0.143	-0.27	-0.55	-0.643
Winglet in horizontal (0 degree)	1.66	-0.294	-0.373	-0.524	-1.075	-1.12
	2.08	-0.319	-0.404	-0.577	-0.983	-1.1
	2.5	-0.353	-0.424	-0.613	-1.045	-1.207
Winglet 60 degree inclined	1.66	-0.385	-0.486	-0.686	-1.207	-1.47
	2.08	-0.406	-0.531	-0.709	-1.103	-1.28
	2.5	-0.481	-0.549	-0.704	-1.09	-1.24

Table 4: Lift/Drag Ratio over Angle of Attack.

3.1. Drag coefficient versus angle of attack:

Figure 4 for Reynolds number 1.66 × 105 shows that without winglet the drag coefficient is higher than the winglet with 0 degree and 60 degree inclined position for all angle of attack. The drag coefficient is very high for wing without winglet for Reynolds number 2.08 × 105 compare with using winglet. Although 60 degree inclined winglet drag coefficient is little bit higher than horizontal winglet, it is more efficient to use inclined winglet because it will give more lift force. For all configurations the drag will be the highest at 14 degree because the flow separation is high at that angle. Overall from the Fig. 4, it can be concluded that by using winglet the drag force can be reduced.

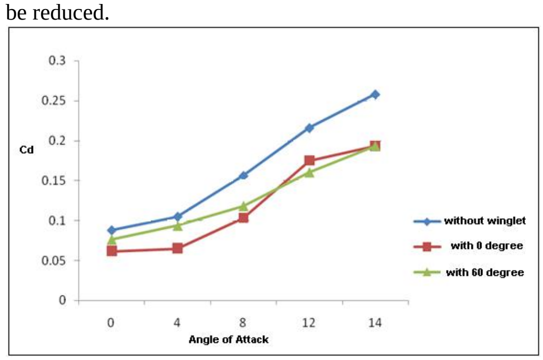

Figure 4.a: Drag coefficients for the Aircraft wing model (Reynolds number 1.66×10^5)

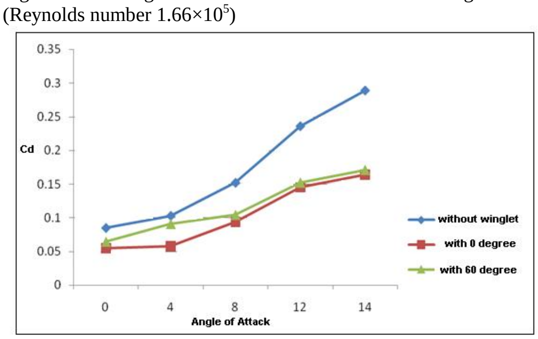

Figure 4.b: Drag coefficients for the Aircraft wing model (Reynolds number 2.08×10^5).

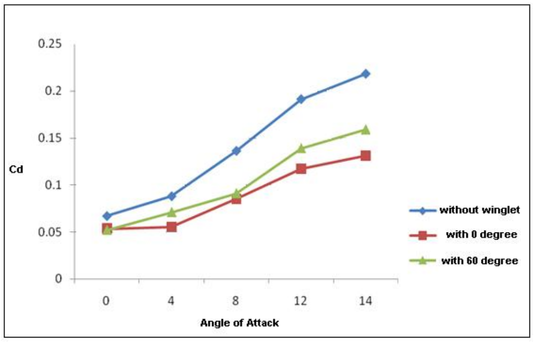

Figure 4.c: Drag coefficients for the Aircraft wing model (Reynolds number 2.50×105).

3.2. Lift coefficient versus angle of attack:

The coefficient of lift versus angle of attack for the aircraft model with and without winglet studied in the present investigation are shown in Figure 5 for different Reynolds number. For all graph, the lift increases with the addition of angle and reach maximum lift is at angle of attack of 8 degree then it is reduced with the addition of angle of attack. So it can be concluded that lift coefficient for using winglet is higher than without winglet.

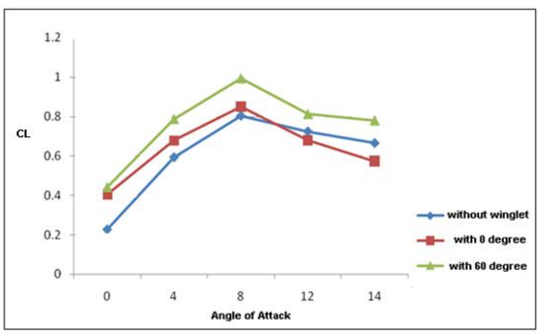

Figure 5.a: Lift coefficients for the Aircraft wing model (Reynolds number 1.66×10^5).

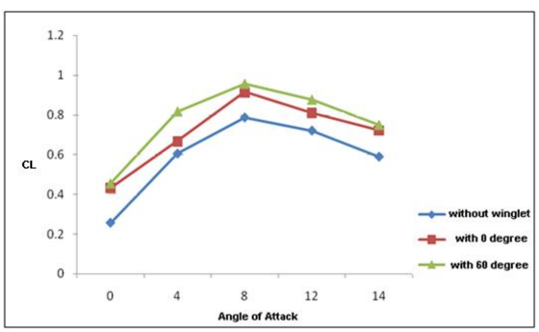

Figure 5.b: Lift coefficients for the Aircraft wing model (Reynolds number 2.08×10^5).

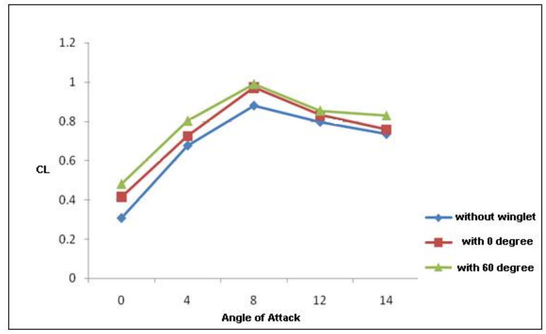

Figure 5.c: Lift coefficients for the Aircraft wing model (Reynolds number 2.50×10^5).

3.3. Pitching moment coefficient versus angle of attack:

The coefficient of pitching moment versus angle of attack for the aircraft model with and without winglet studied in the present investigation are shown in Figure 6 for different Reynolds number. Pitching moment coefficient for 60 degree inclined winglet is lowest for all three Reynolds number. The pitching moment decreases with the increase of angle of attack and finally minimum at angle of attack of 14 degree. The pitching moment coefficient decreases rapidly with the increase in angle of attack to a certain value and then it decreases more rapidly with the increase of attack. This is because the increasing of separation flow over the wing surface at that angle of attack.

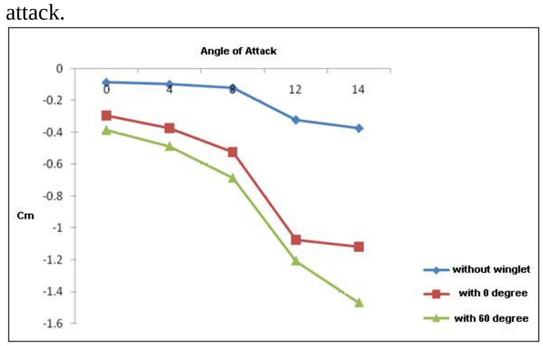

Figure 6.a: Pitching moment coefficients for the wing model (Reynolds number 1.66×10^5).

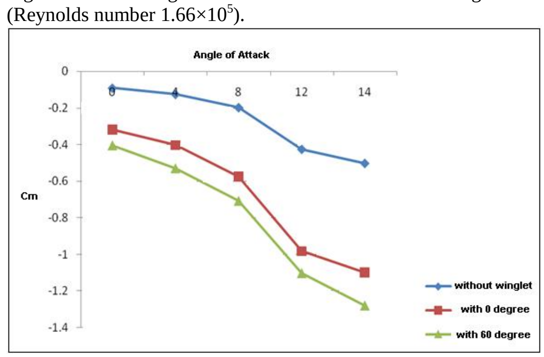

Figure 6.b: Pitching moment coefficients for the wing model (Reynolds number 2.08×10^5).

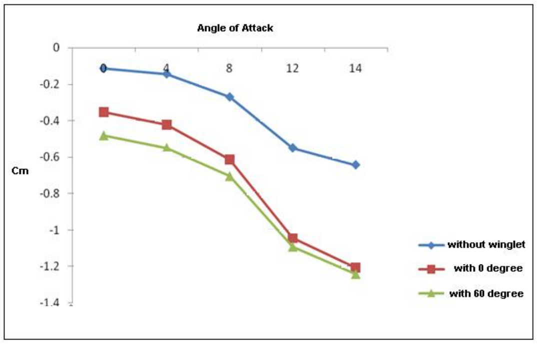

Figure 6.c: Pitching moment coefficients for the wing model (Reynolds number 2.50×10^5).

3.4. Lift/Drag aatio versus angle of attack:

The lift/drag ratio or lift/drag coefficient over angle of attack is the outcome of the study made in the previous sections. Lift/drag ratio or lift/drag coefficient over angle of attack has been shown in Figure 7 for different Reynolds number in this observation. The lift and drag ratio increases with the increase of angle of attack and reach maximum at 4 degree.

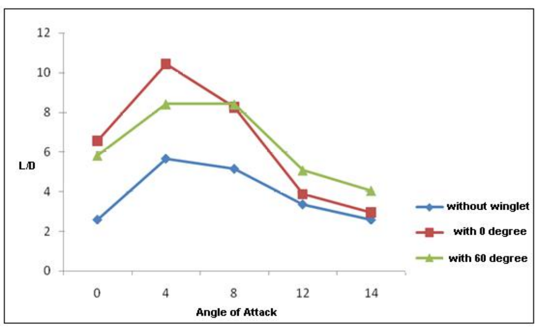

Figure 7.a: Lift/Drag ratio for the wing model (Reynolds number 1.66×10^5).

From the figure it is observed that the ratio decreases with further addition of angle of attack. The maximum value of lift / drag ratio is found as 10.43, 11.6 and 13.09 for wing with horizontal winglet at angle of attack of 4 degree. From the experimental results it can be concluded that that winglet performs better compared to without winglet.

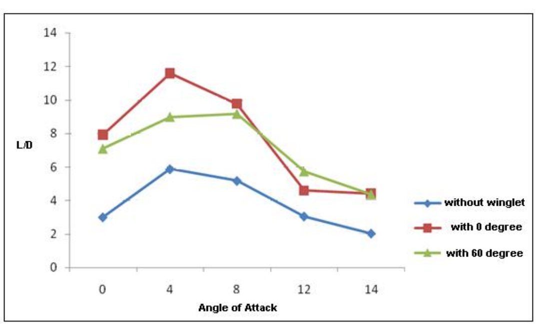

Figure 7.b: Lift/Drag ratio for the wing model (Reynolds number 2.08×10^5).

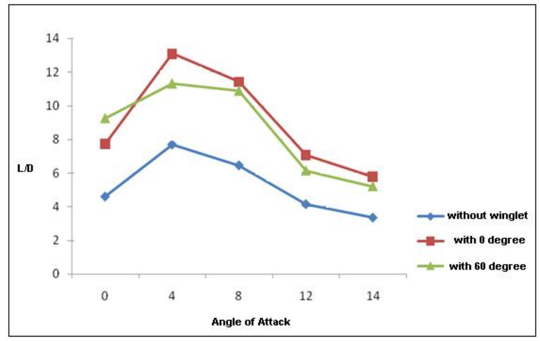

Figure 7.c: Lift/Drag ratio for the wing model (Reynolds number 2.50×10^5).

.

3.5. Performance comparisons between the present and previous works:

The experimental results of the present works can be explained by comparing with the results obtained from the previous works related to the different types of winglets [13-15]. The tests at the Universiti Putra Malaysia [13] were run in three different configurations: without winglet (Configuration 0), winglets of elliptical shaped installed at 00 angle (Configuration 1), winglets of elliptical shaped installed at 600 angle (Configuration 2), winglets of circular shaped installed at 00 angle (Configuration 1), and winglets of circular shaped installed at 600 angle (Configuration 2). They investigated that at the maximum Reynolds number of 2.50×105 elliptical shaped winglet (Configuration 1 and 2) provided the largest increase of lift curve slope, ranging from 1% to 6% increases and at the same time drag decreased more for these two configurations ranging from 24.6% to 28% decrease, giving an edge over other configurations as far as L/D for the elliptical winglet of configuration 1 and 2 was considered. Tests at the Georgia Institute of Technology [14] were also run in three different configurations: without winglet (Configuration 0), winglets installed at 00 angle (Configuration 1), and winglets installed at +200, +100, 00, -100, -200 angle (Configuration 2). They showed that flat plate winglets set at zero degrees (Configuration 1) increased lift curve slope by 10% for the maximum Reynolds number of 2.90×105. They also showed that configuration 2 provided the largest increase of lift curve slope, ranging from 15% to 22% increase with the decrease of drag ranging from 15% to 20%. Compare to the previous works done by the ref. [13-14], it is observed that the present works on bird feather like winglet shows good performance with the reduction of 25-30 % drag coefficient as well as 10-20 % increase in lift coefficient by using winglet for angle of attack of 8 degree.

4. Conclusion

Following are the conclusions drawn from this investigation

- From the drag coefficient and lift coefficient graph it is clearly shown that using bird feather like winglet will increase lift force and reduce drag force.
- This winglet design is capable to reduce induced drag force and convert wing tip vortices to additional thrust which will save cost by reducing the usage of

fuel, noise level reduction and increase the efficiency of the aircraft engine.
- The experiment result shows 25-30 % reduction in drag coefficient and 10-20 % increase in lift coefficient by using winglet for angle of attack of 8 degree.

5. Acknowledgment

The authors are grateful to Universiti Industri Selangor for overall facilities and Universiti Putra Malaysia for using the Wind Tunnel.

References

[1] McCormick, B.W., Aerodynamics of V/STOL Flight. Academic Press, London, 1967.

[2] R. T. Whitcomb, “A Design Approach and Selected Wind-Tunnel Results at High Subsonic Speeds for Wing-Tip Mounted Winglets”. NASA TN D-8260, 1976.

[3] R. T. Whitcomb, “Methods for Reducing Aerodynamic Drag”. NASA Conference Publication 2211, Proceedings of Dryden Symposium, Edwards, California, 1981.

[4] Chandrasekharan, M. Reuben, Murphy, R. William, Taverna, P. Frank, and Boppe, W. Charles “Computational Aerodynamic Design of the Gulftream IV Wing”. AIAA-85-0427, 1985.

[5] A.J. Bocci, “Wing W4 fitted with a winglet: winglet design and preliminary test results”, Aircraft Research Association, ARA/M-230, 1981.

[6] I. Kroo, M. Takai, “A Quasi-Procedural Knowledge-Based System for Aircraft Design”, AIAA Paper AIAA-88-6502, 1988.

[7] M. D. Maughmer, S. S. Tmothy, S. M. Willits. “The Design and Testing of a Winglet Airfoil for Low-Speed Aircraft”. AIAA Paper 2001-2478.

[8] J. J. Spillman,, H. Y.Ratcliffe, A. McVitie “Flight experiments to evaluate the effect of wing-tip sails on fuel consumption and handling characteristics”. Aeronautical Journal, 1979, 279-281.

[9] La. U. Roche , S. Palffy, “WING-GRID, a Novel Device for Reduction of Induced Drag on Wings,” Proceedings of ICAS 96, Sorrento, 1996.

[10] A. Hossain , R. A. Prithvi, A. Rahman, A. A. Jaafar, and A.K.M.P. Iqbal “Analysis of Aerodynamic characteristics of an Aircraft model with and without winglet”, Jordan Journal of Mechanical and Industrial Engineering (JJMIE), Vol. 2, No. 3, 2008, 143-150,.

[11] Bertin, J. J. Aerodynamics for Engineers. New Jersey, Prentice-Hall, Inc. Page-98, 2002.

[12] Anderson, J. D. Introduction to Flight. McGraw-Hill Companies, Inc., United States of America, 2005.

[13] R. A. Prithvi, A. Hossain, A. A. Jaafar, P. Edi, T. S. Younis, and M. Saleem, “Drag Reduction in Aircraft Model using Elliptical Winglet”. Journal of IEM, Malaysia, Vol. 66, No. 4, 2005.

[14] M. J. Smith, N.Komerath, R. Ames, O. Wong, and J. Pearson, “Performance Analysis of a Wing with Multiple Winglets”. AIAA Paper-2001-2407, 2001.

[15] A. Hossain, A. Rahman, J. Hossen, A.K.M. P. Iqbal, and SK. Hasan, “Application of Fuzzy Logic Approach for an Aircraft Model with and without Winglet”. International Journal of Mechanical, Industrial and Aerospace Engineering, Vol. 4, No. 2, 2010, 78-86.

JJMIE

Volume 5, Number 3, June 2011
ISSN 1995-6665
Pages 273 - 280

Jordan Journal of Mechanical and Industrial Engineering

Design of Photovoltaic Water Pumping System and Compare it with Diesel Powered Pump

M.Abu-Aligah*

Jordan Petroleum Refinery Company (JPRC), Irbid LPG Filling Station Hall, PO Box 3396 Amman 11181, Jordan

Abstract

In locations where electricity is unavailable, other means are necessary to pump water for consumption. One option is a photovoltaic (PV) pumping system. Advantages of PV pumping systems include low operating cost, unattended operation, low maintenance, easy installation, and long life. These are all important in remote locations where electricity may be unavailable.
So far, in the development of this research, the focus has been to estimate the available radiation at a particular location on the earth's surface and then analyzed the characteristics of a photovoltaic generator and a photovoltaic network. The purpose of this research is to examine all the necessary steps and key components needed to design and build a pump using photovoltaic system.

Keyword: Design load; Site condition; Annual radiation; Life Cycle Costs; Break-even point; Battery capacity

1. Introduction

Most of the increase in the area of irrigated land in the world has been through the increasing use of engine-driven pumps. However, the increasing price of oil-based fuel has reduced the margin to be gained by farmers from irrigation, since food prices have generally been prevented from rising in line with energy costs. Despite present short-term fluctuations in oil prices, conventional oil-based engine-driven power sources and mains electricity are expected to continue to increase in the longer term. If we are to decrease our dependence on imported oil, we have to find methods for energizing irrigation pumps that are independent of imported oil or centralized electricity.

Solar radiation as a source of energy is. Of course, the epitome of the clean. sustainable energy technology. except for residues possibly arising out of the manufacture of solar component (e.g. semiconductors), solar technology have very low environmental impacts. The environmental impacts of solar system in operation are very low and the source is, for us inexhaustible.

The designer should specify components in the following order:

- Choose place and mounting method for modules, select modules.
- Estimate of the electricity Demand.
- Estimate the overall system losses.
- Prepare full list of parts and tools to order.

Small Comparison between Solar PV & Diesel and gasoline pumps:

Table 1: Comparison between Solar PV & Diesel and gasoline pumps.

Type	Advantages	Disadvantages
Solar PV	Unattended operation	High capital costs
	Low maintenance	Water storage is require for cloudy periods
	Easy installation	Repair often require skilled technicians
	Long life	
Diesel and Gasoline Pumps	Quick and easy to install	Fuel supplies erratic and expensive
	Low capital costs	High maintenance costs
	Widely used	Short life expectancy
	Can be portable	Noise and fume pollution

2. Components of the System

2.1. Photovoltaic panels:

A solar-powered water pumping system is made up of two basic components. The first component is the power supply consisting of photovoltaic (PV) panels (Figure.1). The smallest element of a PV panel is the solar cell.

* Corresponding author. e-mail: Mohammad.Abu-Aligah@Jopetrol.com.jo

Figure 1: Photovoltaic (PV) panels.

Each solar cell has two or more specially prepared layers of semiconductor material that produce direct current (DC) electricity when exposed to light. This DC current is collected by the wiring in the panel. It is then supplied either to a DC pump, which in turn pumps water whenever the sun shines, or stored in batteries for later use by the pump.

Manufacturers normally rate voltage (volts) and current (amps) output from PV panels under peak power conditions. Peak power (watts=volts x amps) is the maximum power available from the PV panel at 1000 W/m² solar irradiance (amount of sunshine) and a specified temperature, usually 25 C (77 F). Typical output from a 60-watt PV panel is shown in Table 2. The amount of DC current produced by a PV panel is much more sensitive to light intensity striking the panel than is voltage generated. Roughly speaking, if you halve the light intensity, you halve the DC current output, but the voltage output is reduced only slightly.

Table 2: Typical output from a 60-watt, 12-volt photovoltaic panel.

Maximum power	60 watts
Maximum power voltage	16.9 volts
Maximum power current	3.55 amps

Individual PV panels can be wired in series or parallel to obtain the required voltage or current needed to run the pump. The voltage output from panels wired in series is the sum of all the voltages from the panels.

For example, the maximum voltage output from two of the 12-volt PV panels wired in series is 33.8 volts. Thus, a 24-volt DC pump requires a minimum of two, 12-volt panels wired in series. The current (amps) output from these same panels wired in series is equal to the current (amps) output from an individual panel, 3.55 amps.

The voltage and current output from panels wired in parallel is the exact opposite of series-wired panels.

For panels wired in parallel, the current (amps) output is the sum of all the currents (amps) from the panels and the voltage is equal to the voltage output from an individual panel.

2.2. Solar (DC) water pumps:

The other major component of these systems is the pump. Solar water pumps are specially designed to use solar power efficiently. Conventional pumps require steady AC current that utility lines or generators supply. Solar pumps use DC current from batteries and/or PV panels. In addition, they are designed to work effectively during low-light conditions, at reduced voltage, without stalling or overheating.

Although wide ranges of sizes are available, most pumps used in livestock-watering applications are low volume, yielding 7-15 liters of water per minute. Low-volume pumping keeps the cost of the system down by using a minimum number of solar panels and using the entire daylight period to pump water or charge batteries. Some solar pumps are fully submersible, while others are not. The use of submersible pumps eliminates potential priming and freezing problems. Most solar water pumps are designed to use solar power most efficiently and operate on 12 to 36 volts DC.

Many solar pumping systems use positive displacement pumps that seal water in cavities inside the pump and force it upward. Their design enables them to maintain their lift capacity all through the solar day at the slow, varying speeds that result from varying light conditions. Positive displacement pumps include piston and jack pumps, diaphragm, vane and screw pumps.

Centrifugal-type pumps that impart energy to the water using a rotating impeller are typically used for low-lift or high-volume systems. Centrifugal pumps start gradually and their flow output increases with the amount of current. For this reason, they can be tied directly to the PV array without including a battery or controls. However, because their output drops off at reduced speeds, a good match between the pump and PV array is necessary to achieve efficient operation.

Pumps, because of their mechanical nature, have certain well-defined operating properties. These properties vary between types of pumps, manufacturers and models. The amount of water that a solar pumping system will deliver over a given period of time (usually measured in liters per minute (LPM) or liters per hour (LPH)) depends upon the pressure against which the pump has to work. The system pressure is largely determined by the total vertical pumping distance (the vertical distance between the water source and the watering tank) referred to simply as elevation head. It is roughly equal to an increase of one bar for every 10.28 meters of elevation head. Simply put, as the vertical pumping distance increases, the amount of water pumped over a given period of time decreases. When system friction losses and discharge pressure requirements (if any) are added to elevation head, the total system head can be determined. Pump manufacturers publish information that describes how each pump will perform under varying operating conditions. The expected flow rates and minimum recommended solar panel sizes for a typical 24-volt, positive-displacement, diaphragm-type submersible pump are shown in Table 3. The choice of pump depends on water volume needed, efficiency, price and reliability.

Table 3: Estimated flow rates in liters per minute for a typical positive-displacement, 24-volt diaphragm type pump.

Total head (meter)	Flow Rate (liter/min)	Current in ampere
0	14.00	1.6
3.048	13.20	1.7
6.096	12.80	2.0
9.144	12.50	2.2
12.192	12.10	2.4
15.24	11.70	2.6
18.288	11.35	2.9
21.336	10.98	3.1
None Shaded areas- Two 53-watt panels in series. Shaded areas – Two 70-watt panels in series.		

2.3. Pump controller:

The primary function of a pump controller in a battery-coupled pumping system is to boost the voltage of the battery bank to match the desired input voltage of the pump. Without a pump controller, the PV panels' operating voltage is dictated by the battery bank and is reduced from levels, which are achieved by operating the pump directly off the solar panels. For example, under load, two PV panels wired in series produce between 30 to 34 volts, while two fully charged batteries wired in series produce just over 26 volts. A pump with an optimum operating voltage of 30 volts would pump more water tied directly to the PV panels than if connected to the batteries. In the case of this particular pump, a pump controller with a 24-volt input would step the voltage up to 30 volts, which would increase the amount of water pumped by the system.

3. Solar-Powered Water Pumping System Configurations

There are two basic types of solar-powered water pumping systems, battery-coupled and direct-coupled.

A variety of factors must be considered in determining the optimum system for a particular application.

3.1. Battery-coupled solar pumping systems:

Battery-coupled water pumping systems consist of photovoltaic (PV) panels, charge control regulator, batteries, pump controller, pressure switch, tank, and DC water pump (Figure.2). The electric current produced by PV panels during daylight hours charges the batteries, and the batteries in turn supply power to the pump anytime water is needed. The use of batteries spreads the pumping over a longer period of time by providing a steady operating voltage to the DC motor of the pump. Thus, during the night and low light periods, the system can still deliver a constant source of water for livestock.

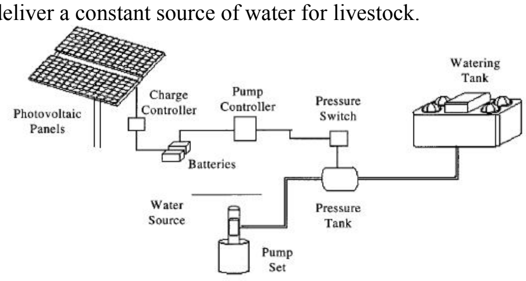

Figure 2: Battery-coupled water-pumping systems.

The use of batteries has its drawbacks. First, batteries can reduce the efficiency of the overall system because the operating voltage is dictated by the batteries and not the PV panels. Depending on their temperature and how well the batteries are charged, the voltage supplied by the batteries can be one to four volts lower than the voltage produced by the panels during maximum sunlight conditions. This reduced efficiency can be minimized with the use of an appropriate pump controller that boosts the battery voltage supplied to the pump.

3.2. Direct-coupled solar pumping system:

In direct-coupled pumping systems, electricity from the PV modules is sent directly to the pump, which in turn pumps water through a pipe to where it is needed (Figure.3). This system is designed to pump water only during the day. The amount of water pumped is totally dependent on the amount of sunlight hitting the PV panels and the type of pump. Because the intensity of the sun and the angle at which it strikes the PV panel changes throughout the day, the amount of water pumped by this system also changes throughout the day. For instance, during optimum sunlight periods (late morning to late afternoon on bright sunny days) the pump operates at or near 100 percent efficiency with maximum water flow. However, during early morning and late afternoon, pump efficiency may drop by as much as 25 percent or more under these low-light conditions.

During cloudy days, pump efficiency will drop off even more. To compensate for these variable flow rates, a good match between the pump and PV module(s) is necessary to achieve efficient operation of the system.

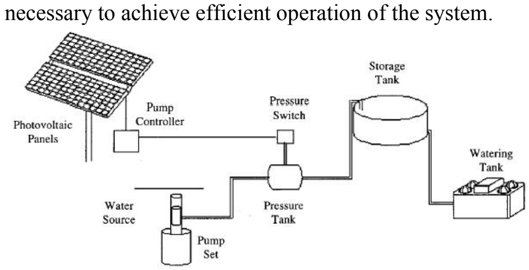

Figure 3: Direct-coupled pumping systems.

Direct-coupled pumping systems are sized to store extra water on sunny days so it is available on cloudy days and at night. Water can be stored in a larger-than-needed watering tank or in a separate storage tank and then gravity-fed to smaller watering tanks. Water-storage capacity is important in this pumping system. Two to five days' storage may be required, depending on climate and pattern of water usage. Storing water in tanks has its drawbacks. Considerable evaporation losses can occur if the water is stored in open tanks, while closed tanks big enough to store several days water supply can be expensive. In addition, water in the storage tank may freeze during cold weather.

4. System Sizing

Before choosing the final components, the system should be roughly sized to allow viewing of approximate component sizes. Later, the components must be sized again by a detailed electrical and mechanical design. The purpose of this chapter is to provide simple tools to roughly estimate the needed system size before contacting a PV specialist.

The approach is to estimate the required component size by making assumptions about the efficiency of all key components and by using monthly average weather data. To make the procedure easier, a set of worksheets (#1--#5) has been prepared for the different steps.

4.1. Specification of site conditions (worksheet #1):

Define the site and weather station location (latitude, longitude) and the monthly average values of the global irradiance on the horizontal surface (kWh/m2) and the annual average as well as the minimum and maximum monthly average ambient temperatures.

Main factors affecting the solar availability are the orientation (tilt and azimuth angel) and the possible shading caused by the surrounding. By multiplying the horizontal radiation values with monthly tilt azimuth angle factor, the monthly radiation values on the module surface can be estimated. This monthly factor is presented for different location for horizon shadowing levels of 0, 20 and 45 degrees.

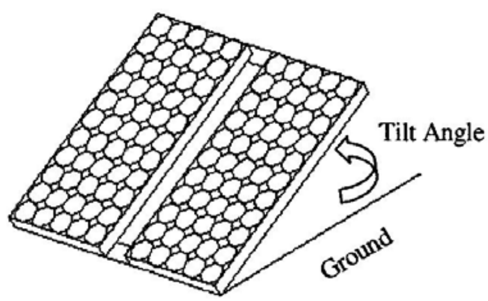

Figure 4: Solar panel tilt angle (Summer Use: tilt angle = 25 degrees, Winter Use: tilt angle = 45 degrees).

Worksheet #1: Define site condition and solar availability.

Shadow: 0, 20° horizon shading, Tilted: 45° angle due south.

4.2. Estimation of the electricity demand (worksheet #2):

The very first step in designing a PV system must be careful examination of the electrical loads. The reasons are twofold:

- Obviously, the sizing of the system components is dependent on the electricity and power demand. For stand-lone systems, his is crucial.
- Oversized systems resulting from a poor load analysis and the idea of staying on the 'safe side' increase the system costs. This is particularly demanding in a field where poor economics are major drawback, which still is the case for PV.

The second reason also leads to the important issue of minimizing loads without decreasing the user's comfort.

4.2.1. Solar pump sizing:

$$HE = V \times H \times \rho w \times g / (3.6 \times 106) \quad (1)$$

Where:

HE : hydraulic energy (kWh/day)
V : volume (m³/day)
ρw : water density ≈ 1000 (Kg/ m³)
g : gravity ≈ 9.82 m/s2

$$Ppv = HE / ((S / \text{days of operation}) \times F \times E) \quad (2)$$

Where:

Ppv	: is the nominal power of PV at standard test condition (STC) in (kW)
S	: is the annual solar radiation of the PV array (kWh/m²)
F	: array mismatch factor = 0.85 on average.
E	: daily subsystem efficiency = 0.25 - 0.40 typically

Table 4: Define site condition and solar availability (Worksheet #1).

System: "Amman" PV		
System Location:	Latitude:31.57 N°	Longitude:35.57 E°
Insulation Location:	Latitude: 31.57 N°	Longitude: 35.57 E°

Month	Location		Array Plane						
	Ambient Temperature (C°)	Horizontal Radiation	*	Tilt, azimuth Shadow factor	=	Radiation			
		kWh/m²day	*	fraction	=	kWh/m²day	*	=	kWh/m²
January	10	3	*	1.4	=	4.2	31	=	130.2
February	12	3.8	*	1.3	=	4.94	28	=	138.32
March	18	4.6	*	1.2	=	5.52	31	=	171.12
April	22	5.8	*	1	=	5.8	30	=	174
May	27	7	*	0.9	=	6.3	31	=	195.3
June	31	7.5	*	0.9	=	6.75	30	=	202.5
July	34	7.7	*	0.9	=	6.93	31	=	214.83
August	36	7.3	*	1	=	7.3	31	=	226.3
September	28	5.8	*	1.1	=	6.38	30	=	191.4
October	19	4.3	*	1.3	=	5.59	31	=	173.29
November	17	3.4	*	1.3	=	4.42	30	=	132.6
December	11	2.8	*	1.5	=	4.2	31	=	130.2

Table 5: Estimation of the electricity Demand (Worksheet #2)

Load Description	AC Or DC	AC Load	Inverter Efficiency	DC Load W	Duty Cycle h/day	Duty Cycle Day/Week	Daily Load Wh/day	Nominal Volt	Ah-load Ah/day
-------	---	----	---------	-----	-----	------	----------	------	-----
Water pump	DC	----	-------	250	5	4	(250*4*5)/(7) = 714.28	24	29.761
------	---	---	-------	----	-----	-------	---------	------	-----
------	---	---	-------	----	----	------	---------	------	------
				Maximum DC load =∑ 250 W			Total Daily load =∑ 714.28 Wh/day		Total load =∑ 29.761 Ah/day

Design load (Total load)	≈ 30	Ah/Day
Design peak Current Draw (Maximum DC load / Nominal voltage)	≈ 11	A
Annual load Energy (Total daily load*week in operation (≈38 weeks per year) *7/1000)	≈ 192.9	kWh

4.3. Sizing of grid-connect system (worksheet #3):

The optimum size of grid-connect system also depends on a number of external factors such as : the investment cost of the system, the available budget, governmental subsidies, the energy payback policy of the local utility, and the amount of PV energy directly used by the building. It must be remembered that because of the variable nature of PV power it is seldom used to decrease the peak load demand of the building.

In practice, the nominal size of the PV array should be chosen based on the load size and the budget. The require PV module area APV (m²) can be calculated from the chosen nominal PV power using the formula:

$$APV = Ppv / \eta pv \quad (3)$$

Where:

ηpv : is the efficiency of the modules at STC

The annual energy production of the system can be calculated using the formula below:

$$Epv = \eta Bos * Kpv * Ppv * S \quad (4)$$

Where:

Kpv : is a decreasing factor (~0.9), which takes into account phenomena such as modules temperature, dust, array imbalance, circuit losses etc.

ηBos : is the balance of system efficiency, depend on inverter efficiency or wiring losses.

Table 6: Sizing of grid-connect system (Worksheet #3).

Chosen PV array Power Ppv (kW)	/	PV efficiency ηpv	=	PV array area APV (m²)
2	/	0.15	=	13.33

Chosen PV array Power Ppv (kW)	×	Annual radiation on PV array Worksheet #1 S (kWh/m²)	×	BOS efficiency ηBos	×	Kpv	=	Annual produced energy PV energy Epv (kWh)
2	×	2080.06	×	0.8	×	0.9	=	2995.2864

Annual produced PV energy Epv (kWh)	/	Annual load Energy Worksheet #2 (kWh)	=	PV Load ratio	Directly used PV Energy
2995.2864	/	192.9	=	15.52	0.3 --- 0.5

Chosen PV array Power Ppv (kW)	×	Optimum inverter efficiency	=	Inverter nominal power (kW)
2	×	0.75 --- 0.9	=	1.5 - -- 1.8

Average inverter efficiency	×	Wiring losses	=	BOS efficiency ηBos
0.85	×	1-0.1 = 0.9	=	0.765

4.4. Sizing of battery (worksheet #4):

Battery sizing is the capability of a battery system to meet the load demand with no contribution from the photovoltaic system. For a stand-alone photovoltaic system, the principal goal of battery storage is to ensure that the annual minimum photovoltaic system energy output equals the annual maximum load energy input. The photovoltaic system must also maintain a continuous energy supply at night and on cloudy days when there is little or no solar energy available. The amount of battery storage needed will depend on the load energy demand and on weather patterns at the site. Having too much energy and storage capacity will increase cost, therefore there must be a trade-off between keeping the cost low and meeting the energy demand during low-solar-energy periods.

Table 7: Sizing battery (Worksheet #4).

Design load Worksheet #2 Ah/Day	×	Day of autonomy (Day)	/	Max depth of discharge	=	Usable battery Capacity Ah
30	×	2	/	0.3	=	200

Operating Temp = 25 Discharge rate = 24× Day of autonomy (number of days a battery system will provide a given load without being recharged by the photovoltaic array) = 48 h

Usable battery Capacity Ah	/	Usable Friction of Capacity available	=	Design battery Capacity Ah
200	/	0.95	=	211

4.5. Sizing of array an components (Worksheet #5):

The next step is to size the PV array and the other system components. This is done with the help of worksheet #5. For PV array sizing, the month with lowest radiation on the array plane is chosen as the design month (from worksheet #1).

Dividing the average daily load of the design month by the average daily solar radiation & the system component efficiencies. Yield the necessary PV array size (kW). The efficiencies to be taking into account are the wiring efficiencies, charge regulator efficiency and battery efficiency.

Table 8: Sizing of array components (Worksheet #5).

Operating season (months)	February ------- October

Design month daily load kW/day	/	Lowest radiation on PV array Worksheet #1 kWh/m²day	/	Wiring losses	/	Charge regulator efficiency	/	Battery efficiency	=	Design PV array power kWp
0.98	/	4.94	/	0.9	/	0.85	/	0.9	=	0.289

Design PV array power Wp	×	PV array sizing safety factor	=	PV array power Wp
289	×	1.3	=	376

Design PV array power Wp	/	Nominal voltage V	=	Design array current A
376	/	24	=	15

The design array current is greater than the peak load current.

PV array power Ppv kWp	/	PV efficiency ηpv	=	PV array area Apv m²
0.376	/	0.15	=	2.51

5. A Cost and reliability comparisons between solar and diesel powered pumps

There are very distinct differences between the two power sources in terms ofcost and reliability. Diesel pumps are typically characterized by a lower first costbut a very high operation and maintenance cost.

Solar is the opposite, with ahigher first cost but very low ongoing operation and maintenance costs.

In terms of reliability, it is much easier (and cheaper) to keep a solar-powered System going than it is a diesel engine. This is evident in field where dieselengines lie rusting and unused by the thousands and solar pumps sometimes runfor years without anyone touching them.

The first cost of solar is often daunting to donors and project implementers who are tempted to stretch their budgets as far as possible to reach the greatestnumber of beneficiaries by using a low first-cost option.

But most would probably agree that "quantity over quality" is not a good value if the higher quantity option is not likely to be giving good service five years down the road and if beneficiaries are going to be stuck with interventions they cannot afford to sustain over time.

Solar pumping has had clear advantages for a number of years but the differences are becoming more striking in a world of rapidly escalating fuel costs.

Not only will some of the world's poorest people not be able to afford fuel for their pumps, but living at the end of remote supply chains, they may not even be able to get it in the first place as world demand overtakes supply.

In this example, model choices for a Pumping system that is designed to pump 790 liters per hour from a total Depth (head) of around 30 meters. It compares a solar array of 1900 watts against a 4 kW diesel generator. Both power an equivalent pump of approximately 1 Horsepower = 746 watts, several simulations were performed to gauge the effect of the price of fuel and the fuel efficiency of the diesel generators. These and other parameters are listed below:

Key program inputs:

1) Fuel cost:
   - Case 1: $1.20 per liter.
   - Case 2: $1.70 per liter.
2) Fuel efficiency (consumption) of diesel generator:
   - Case 1: 0.3 liters per kilowatt generated.
   - Case 2: 0.7 liters per kilowatt generated.
3) Solar resource: Annual average of 4.6 peak sun hours per day.
4) Real annual interest rate: 5%.
5) System life: 20 years.

Key program outputs:

1) Initial capital cost: "first cost" for each option – assumes same pump costs
2) Operation cost/year: Average operation and maintenance costs per year. Does not include pump Replacement costs, which would be same for both.
3) Net Present Cost: The present value of the cost of installing and operating the system over the lifetime of the project (also referred to as lifecycle cost).
4) $ Per kilowatt: The cost per kilowatt of electricity per each option.

Simulation 1: "Worst case" for solar: Fuel cost: $1.20 per liter. Consumption rate: 0.3 liters per kilowatt.

Table 9: Simulation 1 Cost comparison for solar and diesel water pumps.

	Initial Capital	Operating cost/year	Total NPC(Net Present Cost)	$ per kWh
PVP (Photo-Voltaic Pumping) Option	$12,300	$335	$16,472	$0.66
DP (Diesel Pumping) Option	$2,000	$4,854	$62,494	$2.48

Simulation 2: "Best case" for solar: Fuel cost: $1.70 per liter. Consumption rate: 0.7 liters per kilowatt.

Table 10: Simulation 2 Cost comparison for solar and diesel water pumps.

	Initial Capital	Operating cost/year	Total NPC	$ per kWh
PVP Option	$12,300	$335	$16,472	$0.66
DP Option	$2,000	$12,525	$158,094	$6.27

We can see from these simulations that solar ranges from one tenth to one fourth (1/10-----1/4) the Net Present Cost of the diesel option.

5.1. Life cycle costs:

Figure.5 shows a comparison for solar and diesel water pumps that includes a range of pumping heads (10m to 200m) and a range of daily flow rates (3,000 – 50,000 liters). The life cycle costs (LCC) were calculated over a 20-years period taking into account upfront cost, operating costs, maintenance costs, and replacement costs.

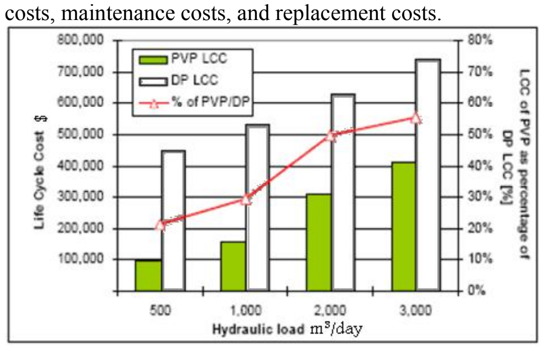

Figure 5: life cycle cost as function of the hydraulic load.

5.2. The break-even point:

Figure.6 shows the break-even point for a single case – a pumping system with an output of 10,000 liters per day from a head of 80 meters. The study also states that for pumping systems having a hydraulic load of 1,000 or less, the break-even point is less than 2.5 years.

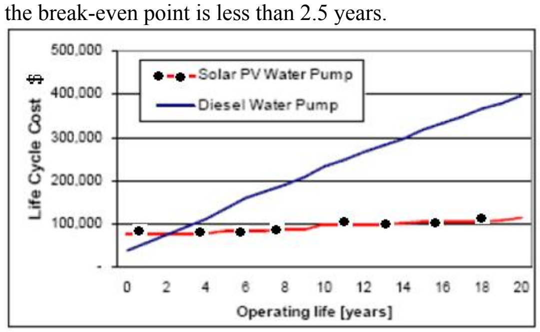

Figure 6: Typical years to break-even graph for PV pump vs. a diesel pump.

6. Conclusion

The output of a solar pumping system is very dependent on good system design derived from accurate site and demand data. It is therefore essential that accurate assumptions are made regarding water demand/pattern of use and water availability including well yield and expected drawdown.

With a solar pump, energy is not available on demand, and the daily variation in solar power generation necessitates the storage of a surplus of water pumped on sunny days for use on cloudy days, solar energy needs to be reserved in the form of either electricity in batteries of lifted water in a storage tank. The suitability of solar power for lifting water to irrigate plants is undeniable because of the complementary between solar irradiance and water requirements of crops. The more intensively the sun is shining the higher is the power to supply irrigation water while on the other hand on rainy days irrigation is neither possible nor needed.

Water pumping has long been the most reliable and economic application of solar-electric (photovoltaic, or PV) systems. Most PV systems rely on battery storage for powering lights and other appliances at night or when the sun is not shining. Most PV pumping systems do not use batteries – the PV modules power the pump directly.

Instead of storing energy in batteries, water is pumpedinto storage reservoirs for use when the sun is not shining. Eliminating batteries from the system eliminates about 1/3 of the system cost and most of the maintenance.

Without batteries, the PV pumping system is very simple. It consists of just three components: the solar array, a pump controller and the pump. The only moving part is the pump. The solar modules are warranted to produce for 20-25 years. The expected life of most controllers is 5-10 years. Pump life can vary from 5 - 10+ years (and many are designed to be repaired in the field). Unless the pump or controller fails, the only maintenance normally required is cleaning the solar modules every 2- 4 weeks! This task obviously can be done cheaply by non-skilled local labor.

References

[1] Roy Barlow, Bernard McNelis and Anthony Derrick: "Solar Pumping. An introduction and update on the technology, performance, costs and economics". IT Publications, 1993

[2] Peter Fraenkel. " Water Pumping Devices". ITDG Publishing, 1997.

[3] Jeff Kenna and Bill Gillett: "Solar Water Pumping". IT Publications, 1985.

[4] U.R.S. Rentch: "Solar Photovoltaic for Irrigation Water Pumping".SKAT, St. Gallen, 1982.

[5] Jeff Kenna and Bill Gillett: "Solar Water Pumping, Groundwater and Water lines" Vol.20, No.2, 2001.

[6] M. Belarbi, K. Haddouche, A. Midoun "Modeling and simulation of photovoltaic solar panel" *WREEC* 2006.

[7] M. Chikh, A. Mahrane, A. Chikouche, "A proposal for simulation and performance evaluation of stand-alone PV systems". Proc. 23th EPVSEC, Valence, Spain, 2008,

[8] E. Worrell, S. Ramesohl, G. Boyd, "Advances in energy forecasting models based on engineering economics". Annual Review of Environmental Resources, Vol. 29, 2004, 345-81.

[9] S. B. Kjaer, J. K. Pedersen, and F. Blaabjerg, "A review of single-phase grid-connected inverters for photovoltaic modules", IEEE Transactions on Industry Applications, Vol. 41, No. 5, 2005, 1292–1306.

[10] Odeh, I., Yohanis, Y.G., and Norton B. "Economic viability of photovoltaic water pumping Systems", Journal of Solar Energy, Vol. 80, 2006, 850–860.

Appendix

1. PV modules Characteristics

Table 11: Characteristics of two type (12, 24 V) 1000 W/m²-PV module.

ELECTRICAL (1000 W/m², 25 °C cell, AM 1.5)		
Nominal Voltage (V_0)	12 V	24 V
Maximum Power (P_{max})	150 W_p ± 5 %	
Short-circuit current (I_{sc})	8,9 A	4,45 A
Open circuit voltage(V_{oc})	21,6 V	43,2V
Maximum power current (I_{max})	8,7 A	4,35 A
Maximum power voltage (V_{max})	17,3 V	34,6 V

Figure.7 schematically shows a characteristic I-V curve of a photovoltaic module together with the generated power curve and two different working points, A and B.

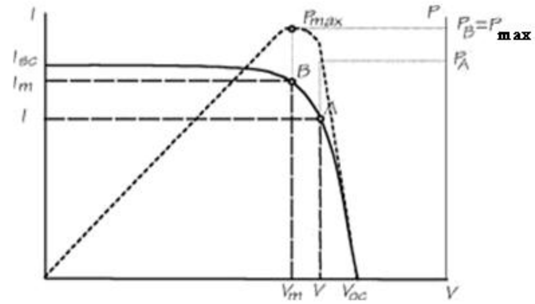

Figure 7: Characteristic I-V curve and generated power curve.

It can be seen that the closer to the maximum power voltage we can make the photovoltaic module work, the greater will be the power we shall obtain from it.

To summarize, depending on solar radiation, the temperature of the cells and of the equipment to which connected, a photovoltaic module will generate a certain current at a certain working voltage, the product of which will set the power generated by the module. Under normal conditions, a photovoltaic module with mono-crystalline silicon cells is likely to produce more current and/or voltage than that specified under standard conditions. In these cases, the values of Isc and Voc may be multiplied by a factor of 1.25, and components such as fuses, conductors and controllers must be adapted to the photovoltaic generator's output.

2. Battery Specifications

A photovoltaic system designer must consider the following when specifying a properly sized and installed battery storage system for a stand-alone photovoltaic system:

- Days of autonomy
- Battery capacity
- Rate and depth of discharge
- Life expectancy
- Environmental conditions
- Price and warranty

The percentage of a battery's rated amp-hour capacity that has been used is called the depth of discharge. Battery life (number of daily cycles) versus depth of discharge (in percent of battery capacity) is shown for a lower cost sealed battery in Figure 8.

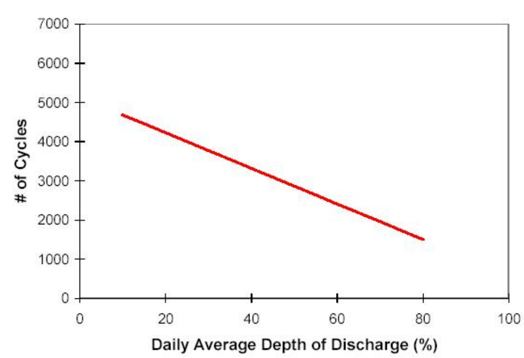

Figure 8: Cycle Life vs. Depth of Discharge.

JJMIE
Jordan Journal of Mechanical and Industrial Engineering
Volume 5, Number 3, June 2011
ISSN 1995-6665
Pages 281 - 284

Energy and Exergy Use in the Utility Sector of Jordan during 2007-2010

A. Al-Ghandoor*[,a], J.O. Jaber[b], I. Al-Hinti[c]

[a] Department of Industrial Engineering, Hashemite University, Zarqa, Jordan
[b] Faculty of Engineering Technology, Al-Balqa' Applied University, Amman, Jordan
[c] Department of Mechatronics Engineering, German Jordanian University, Amman, Jordan

Abstract

In this study, an analysis of energy and exergy utilization in the utility sector of Jordan by considering the sectoral energy and exergy flows for the years 2007-2011 has been conducted based on real data obtained from main generators in Jordan. The overall energy and exergy efficiencies, for the entire utility sector, are found to be in the range of 35.1 to 38.1%. It is expected that the results of this study will be helpful in developing highly applicable and productive planning for future energy policies, especially for the power sector.

Keywords: Energy; Exergy; Efficiency; Utility Sector; Jordan

1. Introduction

In this day and age, the search for optimum utilization of energy resources is becoming increasingly important. This is due to the alarming depletion rates of high quality energy carriers, finite natural resources, the rapid growth in population and industrialization, and the associated increase in energy demand and consumption. Over the past few years, concern about energy consumption in Jordan has taken a new dimension. The annual fuel bill has been rapidly increasing over the past few years due to population and economic growth combined with consecutive increases in oil prices. In 2010, Jordan's consumption of primary energy amounted to 7.357 million Ton Oil Equivalent (TOE) [1]. Nearly 97% of this consumption came in the form of imports of crude oil, natural gas and petroleum products.

The present paper is among a series of practical articles, by authors, aimed to model various sectors and applications by employing insightful energy and exergy analysis [2-5]. Thus, the prime objective of the present study was oriented towards determining energy and exergy losses and related efficiencies as first step to understand influence and weight of different factors in the Jordanian utility sector. As Jordan is considering and in the process of implementing the updated national energy strategy, with more emphasis on energy efficiency policies in different sectors, it is believed that this investigation will provide a scientific judgment and insight to general performance of main generators and possible future improvements for energy policy implementation within the utility sector and may be useful to engineers and scientists working in the field of energy, in Jordan and some neighbouring countries.

2. Electricity Generation in Jordan

Figure 1 shows the percentage of electrical energy by type of generation in 2010 [6]. It is obvious that almost all generated power came out from thermal power plants and combined cycle power plants ranked first with sharing ratio exceeding 50% of total generated power. This was followed by steam power plants and gas turbines. Others, which represents only 0.5%, include wind, biogas and hydro power units. The electricity sector ranked first in primary energy consumption with a percentage of 44.4% of the total energy consumed in 2010 compared to 40.7% during 2007 [6].

In 2010, the installed capacity was about 3,273 MW. The system's peak load, in 2010, was 2,670 MW compared with 2,320 MW in 2009 with a growth rate of 15.1%. The peak load always occurs late in the summer, i.e. during the July-September period. This is due to the excessive use of air-conditioning and ventilation systems as a result of the dry climate and high temperatures, as well as being the holiday season for tourists and many returning Jordanians, who normally work abroad.

The interconnected system in Jordan consists of the main generating power stations, 132 kV and 400 kV transmission network. This transmission network interconnects the power stations with the load centres and different areas in the kingdom. The system also includes the 230 kV, 400 kV tie lines with Syria and 400 kV tie line with Egypt. The distribution networks serve about 99.9% of the total population in Jordan. In addition to that, the electrical power system in Jordan includes some private power stations, which are synchronized with the rest of the power stations in the integrated network and there are a few private power stations, which are not connected with the interconnected network and serve only their owners.

* Corresponding author. e-mail: gandoor2002@yahoo.com

Before 2003, HFO was the dominant fuel used because the two main power stations, i.e. Aqaba and Hussein, are conventional thermal plants employing Rankine steam cycle and fired by such an inexpensive fuel. However, since 2003, imported natural gas from Egypt replaced HFO in Aqaba power station and in early 2006 replaced diesel fuel at Rehab and Asamrah power plants. The dominant role of steam turbines, diesel-fuel fired gas-turbines, and combined cycle power plants is leading to increase dependence on imported oil: less than 8% of the electrical-power generation, at present in Jordan, arises from the exploitation of the indigenous domestic natural gas from the Risha field.

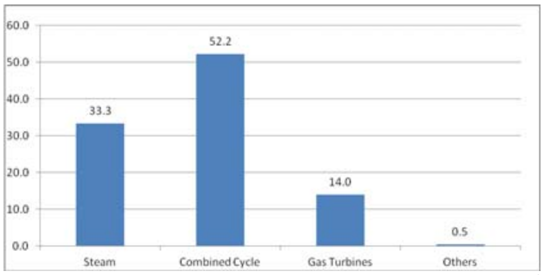

Figure 1: Generated electrical energy in Jordan by type of generation in 2010 (%).

3. Methodology

In order to compare the quality levels of various energy carriers, e.g. fuels, it is necessary to determine the equivalents of each energy quantity at a particular grade level. This can be done by using exergy concept, which overcomes the limitations of the first law of thermodynamics and is based on both the first and second laws of thermodynamics [7-8]. An exergy analysis can identify the locations of energy degradation and rank them in terms of their significance [9]; this knowledge is useful in directing the attention of process design, researchers and practicing engineers to those components of the system being analyzed that offer the greatest opportunities for improvement. Furthermore, exergy analysis has been used to analyze energy utilization on the national level, and for various sectors of the economy, in order to better understand energy utilization efficiency. This approach was first used by [10] who applied it to the overall U.S. economy in 1970. Since then, it has been adopted by several researchers for other countries such as Japan [11], Canada [12], and Brazil [13]. A summary of exergy analyses for different countries can be found in Ertesvag [14]. The concept has been also applied to cross-country analysis of some industrial segments [15-19, 5], residential sector [20, 2], transportation sector [21-24, 4], agricultural sector [25-26, 3], and utility sector [27-29]. The purpose of this section is to discuss the main mathematical relations necessary to conduct energy and exergy analyses in the utility sector.

3.1. Exergy calculation:

By describing the use of energy resources in society in terms of exergy, important knowledge and understanding can be gained, and areas identified where large improvements could be obtained by applying efficient technology, in the sense of more efficient energy-resource conversions. In principle, the exergy of matter can be determined by bringing it to the dead state by means of reversible processes. The basic formulas used in exergy analysis modelling for this study are given below.

3.1.1. Exergy of fuel:

The specific exergy of the fuel at environmental conditions reduces to chemical exergy, which can be written as:

$$\varepsilon_f = \gamma_f H_f \quad (1)$$

Where   is the fuel specific exergy,   the exergy grade function, and Hf the higher heating value of the fuel. Table 1 shows higher heating value, chemical exergy, and fuel exergy grade function of different fuels considered in this study [8, 10, 19, 30]. As shown, in Table 1, all values of the exergy grade function are very close to unity. Consequently, the common practice in such cases is to assume that the exergy of the fuel is approximately equal to the higher heating value [31-32].

Table 1: Higher heating value, chemical exergy, and exergy grade function for different fuels (at 25^{o}C and 1 atm) [8, 10, 19, 30].

Fuel	H_f (kJ/kg)	ε_f (kJ/kg)	γ_f (ε_f /H_f)
Diesel	39,500	42,265	1.070
HFO	40,600	40,194	0.990
Natural Gas	55,448	51,702	0.930

3.1.2. Exergy of electricity:

From the definition of exergy, electricity, We, is identical to the physical work exergy, EWe:

$$E^{We} = W_e \quad (2)$$

3.2. Energy and exergy efficiencies:

Energy efficiency (first law efficiency) is the ratio of energy contained in useful products of a process to energy contained in all input streams, while exergy efficiency (second law efficiency) is the ratio of exergy contained in the useful product to the exergy contained in all input streams. Energy efficiency (η) and exergy efficiency (ψ) are defined as:

$$\eta = \left(\frac{\text{energy in products}}{\text{total energy input}}\right) \times 100\% \quad (3)$$

$$\psi = \left(\frac{\text{exergy in products}}{\text{total exergy input}}\right) \times 100\% \quad (4)$$

Energy, η_e , and exergy, ψ_e , efficiencies for electricity generation through fossil fuels, mf, can be expressed as follows:

$$\eta_e = (W_e / (m_f H_f)) \times 100\% \quad (5)$$

$$\psi_e = (E^{We} / (m_f \varepsilon_f)) \times 100\% = (W_e / (m_f \gamma_f H_f)) \times 100\% = \eta_e \quad (6)$$

Therefore, exergy efficiency for electricity generation process can be taken as equivalent to the corresponding energy efficiency [32].

4. Results and Discussion

As stated previously, electricity is mainly produced by means of thermal power plants in addition to small portions produced by using available renewable sources. Figure 2 shows an illustrative presentation of electricity production in Jordan. In order to simplify the analysis of energy and exergy efficiencies for this sector, energy consumption and electric production flows are analyzed, for three power plants namely steam, combined cycle, and gas turbines that consume most of fuels, i.e. 99.5%, supplied to the utility sector.

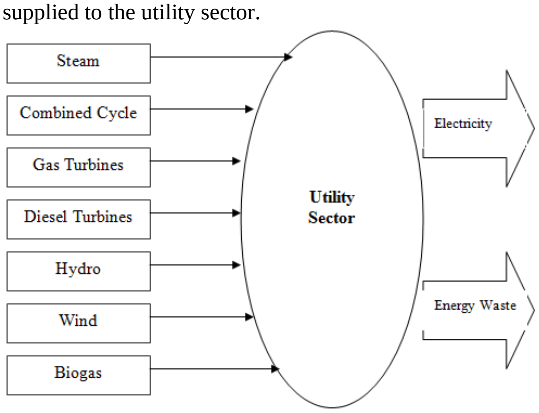

Figure 2: An illustrative presentation of the electricity production in Jordan.

Real data, from the field, have been obtained by compiling and analyzing scattered data collected from electricity generation companies for a period spanned from 2007 to 2010; this forms a unique point in this study by developing data that are not published elsewhere. Table 2 summarizes the collected data.

Table 2: Total primary energy consumption and electricity generation according to type of generator during the period 2007-2010.

	Primary Energy Consumption (1000 toe)	Electricity Generation (GWh)			
		Steam	Combined Cycle	Gas Turbines	Others
2007	3026	6525	5061	949	74
2008	3275	5726	5043	2664	74
2009	3430	5424	5393	3123	69
2010	3270	4824	7561	2028	73

As clearly can be seen from Table 2, the share of combined cycle power plants, fired by imported natural gas, has been increased by almost 12% during the period of study. This will have a dramatic effect on the performance of the utility sector, in Jordan, since it has the highest efficiency as compared with other available thermal technologies of power generation.

The analysis has been carried out based on input and output energies and exergies given in Table 2. Energy and exergy efficiencies for each year have been determined by using equations 5 and 6, considering energy grade function as unity. Table 3 shows both of energy and exergy efficiencies for the whole electricity generation sector.

Table 3: Calculated energy and exergy efficiencies during 2007-2010 (%).

Year	Overall Efficiency (%)
2007	35.8
2008	35.5
2009	35.1
2010	38.1

In general, for the utility sector, several investigators have come up with the same results that the energy and exergy efficiencies for similar activities are almost identical for the utility sector. This result indicates that inefficiencies in this sector are not caused by mismatch in the input-output quality levels but rather by the presently available techniques used for conversion processes. Substantial improvements in this sector are expected to be difficult to obtain and will involve major changes in the conversion methods [32].

For comparison purposes, energy and exergy efficiencies for main generating plants for year 2010 are indicated in Figure 3. It is obvious that combined cycle units have the highest values. This should attract the attention of planners and policy makers to upgrade all existing power plants based on gas turbines to operate as combined cycle in the near future. Moreover, future expansion in power generation projects should be limited to combined cycle plants, especially when fired with natural gas. Such trend has the extra advantage of reducing total gaseous emissions, including greenhouse gases, from the power sub-sector [33].

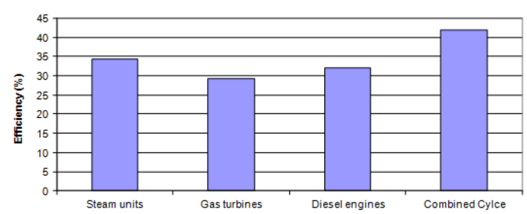

Figure 3: Energy and exergy efficiencies of power plants of the utility sector in Jordan for the year of 2010.

5. Conclusion

In this study, energy and exergy efficiencies of the Jordanian utility sector were determined for period spanning from 2007 to 2010. Calculated exergy efficiency of the utility sector is same as its corresponding energy efficiency since for fossil fuels energy, which is the prime energy source for electricity production in Jordan, the exergy grade function is almost unity. The average overall energy and exergy efficiencies are found to be about 38.1% in 2010.

The calculated efficiencies over the studied period can be considered as an important tool for policy makers, energy planners and operators to get deeper insight into the performance of the utility sector. Furthermore, such results could provide important guidelines for future research work since large energy and exergy losses, which are reported in this study, should be taken as a challenge by the society, concerned governmental institutions and generators to achieve sustainability goals.

References

[1] Ministry of Energy and Mineral Resources (MEMR), 2011. Annual Report 2010. Amman, Jordan.

[2] A. Al-Ghandoor, I. Al-Hinti, B. Akash, E. Abu-Nada, “Analysis of energy and exergy use in the Jordanian urban residential sector”. International Journal of Exergy Vol. 5, 2008, 413-428.

[3] A. Al-Ghandoor, J. O. Jaber "Analysis of energy and exergy utilization of Jordan’s agricultural sector”. International Journal of Exergy Vol. 4, No.6, 2008, 413-428.

[4] J. O Jaber, A. Al-Ghandoor, S. A. Sawalha. “Energy analysis and exergy utilization in the transportation sector of Jordan”. Energy policy Vol. 36, 2008, 2995-3000.

[5] A. Al-Ghandoor, M. Al-Salaymah, Y. Abdallat, M. Rawashdeh. “Energy and exergy utilizations of the Jordanian SMEs Industries”. Energy Conversion and Management (Accepted for publication).

[6] National Electricity Power Company (NEPCO), 2011. Annual Report 2010, Amman, Jordan.

[7] Moran, M., Availability analysis: a guide to efficient energy use. Prentice-Hall, INC: New Jersey, 1982.

[8] Szargut, J., Morris, D., Steward, R. Exergy analysis of thermal, chemical, and metallurgical processes. Hemisphere Publishing Corporation: New York, 1988.

[9] Moran, M., Shapiro, H., Fundamentals of engineering thermodynamics. John Willey & Sons, INC: NewYork , 2000.

[10] G. Reistad, “Available energy conversion and utilization in the United States”. Journal of Energy Power Vol. 97, 1975, 429-434.

[11] G. Wall, “Exergy conversion in the Japanese society”. Energy. Vol. 15, 1990, 435-444.

[12] M. Rosen, “Evaluation of energy utilization efficiency in Canada using energy and exergy analysis”. Energy Vol. 17, 1992, 339-350.

[13] R. Schaeffer, R. Wirtshafter, “An exergy analysis of the Brazilian economy: from energy production to final energy use”. Energy Vol. 17, 1992, 841-855.

[14] I. Ertesvag, “Society exergy analysis: a comparison of different societies”. Energy Vol. 26, 2001, 253-270.

[15] S. Ozdogan, M. Arikol, “Energy and exergy analyses of selected Turkish industries”. Energy Vol. 20, 1995, 73-80.

[16] I. Dincer, M. Hussain, I. Al-Zaharnah, “Energy and exergy use in the industrial sector of Saudi Arabia”. Proc. Instn Mech. Engrs, Part A: J. Power and Energy 217, 2003, 481-492.

[17] M. G. Rasul, W. Widianto, B. Mohanty, “Assessment of the thermal performance and energy conservation opportunities of a cement industry in Indonesia.” Applied Thermal Engineering Vol. 25, 2005, 2950-2965.

[18] M. Oladiran, J.P. Meyer. Energy and exergy analyses of energy consumptions in the industrial sector in South Africa. Applied Energy Vol. 84, 2007, 1056-1067.

[19] Z. Utlu, A. Hepbasli. “A review and assessment of the energy utilization efficiency in the Turkish industrial sector using energy and exergy analysis method”. Renewable and Sustainable Energy Reviews Vol. 11, 2007, 1438-1459.

[20] R. Saidu, H. Masjuki, M. Jamaluddin, “An application of energy and exergy analysis in residential sector of Malaysia”. Energy Policy, Vol. 35, 2007, 1050-1063.

[21] I. Dincer, M .M. Hussain, I. Al-Zaharnah, “Energy and exergy utilization in transportation sector of Saudi Arabia”. Applied Thermal Engineering, Vol. 24, 2004, 525-538.

[22] Z. Utlu, A. Hepbasli, “Assessment of the energy utilization efficiency in the Turkish transportation sector between 2000 and 2020 using energy and exergy analysis method”. Energy Policy Vol. 34, 2006, 1611-1618.

[23] X. Ji, G. Q. Chen, “Exergy analysis of energy utilization in the transportation sector in China”. Energy Policy, Vol. 34, 2006, 1709-1719.

[24] V. Ediger, U. Camdali, “Energy and exergy efficiencies in Turkish transportation sector, 1988-2004”. Energy Policy Vol. 35, 2007, 1238-1244.

[25] I. Dincer, M. Hussain, I. Zaharnah,“Energy and exergy utilization in agricultural sector of Saudi Arabia”. Energy Policy Vol. 33, 2005, 1461-1467.

[26] Z. Utlu, A. Hepbasli, “Assessment of the energy and exergy utilization efficiencies in the Turkish agricultural sector”. International Journal of Energy Research Vol. 30, 2006, 659-670.

[27] I. Dincer, M. M. Hussain, I. Al-Zaharnah “Energy and exergy use in the utility sector of Saudi Arabia”. Desalination Vol. 169, 2004, 245-255.

[28] R. Saidur, M. A. Sattar, H. H. Masjuki, H. Abdessalam, B. S. Shahruan “Energy and exergy analysis at the utility and commercial sectors of Malaysia”. Energy Policy Vol. 35, 2007, 1956-1966.

[29] Z. Utlu, A. Hepbasli, “Assessment of the Turkish utility sector through energy and exergy analyses”. Energy Policy Vol. 35, 2007, 5012-5020.

[30] Petchers N, Combined heating, cooling and power handbook: technologies and application. The Fairmont Press, INC: Lilburn, GA. , 2003.

[31] M. Rosen, Dincer I. , “Sectoral energy and exergy modeling of Turkey”. ASME-J. Energy Resources Technol. Vol. 119, 1997, 200-204.

[32] I. Dincer, M .M. Hussain, I. Al-Zaharnah “Analysis of sectoral energy and exergy use of Saudi Arabia”. International Journal of Energy Research Vol.28, 2004, 205-243.

[33] J.O. Jaber, A. Al-Sarkhi, B. Akash, M. Mohsen, “Medium-range planning economics of future electrical power generation”. Energy Policy, Elsevier Science Journal, Vol. 32, 2004, 357-366.

المملكة الأردنية الهاشمية

الجامعة الهاشمية

المجلة الأردنية
للهندسة الميكانيكية والصناعية

JJMIE

مجلة علمية عالمية محكمة

http://jjmie.hu.edu.jo/

ISSN 1995-6665

المجلة الأردنية للهندسة الميكانيكية والصناعية

مجلة علمية عالمية محكمة

المجلة الأردنية للهندسة الميكانيكية والصناعية: مجلة علمية عالمية محكمة أسستها اللجنة العليا للبحث العلمي، وزارة التعليم العالي والبحث العلمي، الأردن، وتصدر عن عمادة البحث العلمي والدراسات العليا، الجامعة الهاشمية، الزرقاء، الأردن.

ترسل البحوث إلى العنوان التالي:

رئيس تحرير المجلة الأردنية للهندسة الميكانيكية والصناعية

عمادة البحث العلمي والدراسات العليا

الجامعة الهاشمية

الزرقاء - الأردن

هاتف : 00962 5 3903333 فرعي 4147

Email: jjmie@hu.edu.jo

Website: www.jjmie.hu.edu.jo